

The Development of a Kinesthetic Feedback System for Lower-Limb Prosthetic  
Use

McNiel-Inyani Keri

A thesis submitted in partial fulfillment of the requirements for the degree of

Master of Science

Department of Mechanical Engineering

University of Alberta

© McNiel-Inyani Keri, 2019

## **Abstract**

Limb amputation affects many individuals worldwide, with the majority of amputations occurring in the lower extremity. In addition to losing structure and motor function with amputation, the body loses important sensory organs and information required to optimize performance (e.g., ambulation). Specifically, the loss of proprioception (spatial awareness of limbs) and kinesthesia (sense of limb movement) has profound implications for individuals using lower-limb prostheses. This lack of sensory feedback may result in decreased balance, which may lead to falling, and a decreased quality of life. The kinesthetic illusion (KI), a phenomenon whereby mechanical vibration administered to the musculotendinous region of a limb may illicit a perception of limb movement, offers a method in which intuitive movement information might be relayed to prosthesis users. The body of work focusing on kinesthetic feedback attempts a somatotopic approach to restore kinesthetic sensations in individuals with transhumeral amputations that have undergone targeted reinnervation (TR); a surgical technique where the sensory and motor nerves formerly innervating amputated limbs are reinnervated to new muscle and skin sites. To date, no work has been published on restoring movement sensations for individuals with lower-limb amputations.

The objectives of this thesis were to (1) perform an exploratory study to determine whether it is possible to provide kinesthetic feedback to lower-limb prosthesis users who have not undergone TR, using the KI; and (2) developing a low-cost wireless inertial measurement unit-based system (WibS) which can track the movement of a single-axis prosthetic knee, to bridge the movement of a prosthesis to actuators responsible for administering the KI. Accomplishing the two objectives

will then allow demonstration of the ability to close the sensory feedback loop for a participant with lower-limb amputation as a proof of concept.

To accomplish the objectives, the following methods were implemented. The explorative study was achieved by using a vibration motor to identify sites on the residual limb which elicit strong and consistent movement percepts. Motion capture (mocap) and a 5-point Likert scale was used for quantifying both kinematics and the strengths of the experienced movement percepts respectively. To satisfy the second objective, a movement sensor comprised of a microcontroller, Bluetooth radio, inertial measurement unit, and battery with corresponding circuitry was developed. Computing the joint angle of a prosthetic knee was achieved using two movement sensors. This joint angle computation was validated through comparison with a commercial inertial measurement (cIMU) system and mocap using the root-mean-square error (RMSE) with two motion profiles (Gaussian and sinusoidal) and three velocities (60, 120, 180 degrees/second) chosen based on the properties of gait. Moreover, a benchtop system, comprised of two WlBS and a threshold-based controller, was used in a case study to test the developed system's ability to elicit movement percepts.

Through the exploratory study, 4 out of 9 participants spontaneously reported movement percepts about their phantom knee or ankle. Out of the 4, half the participants experienced movement percepts in the direction characteristic of the KI. The other half experienced a sensation like the patellar reflex (i.e., a singular outward jerk of the knee). The remaining participants experienced a variety of sensations related to stimulation of cutaneous receptors. Results for the developed movement sensor showed that, the sensor can track a gaussian motion profile with a RMSE less than 1 degree when compared to both the cIMU and mocap system at all tested velocities. For cyclic motion, the RMSE is within 2 (cIMU) and 8 degrees (mocap) at velocities up to 120

degrees/second, with greater error at faster velocities. These results suggest that, the developed sensor may be able to provide reliable movement detection during typical walking speeds for prosthesis users. Lastly, a participant with an above-knee lower-limb amputation that can experience the KI, as determined through the exploratory study, participated in a proof of concept demonstration. The benchtop system was successful in eliciting movement percepts on the participant by reliably detecting the movement of the single-axis robotic system and activating the vibration motor appropriately with no false triggers.

Altogether, this work takes the first steps toward clinical translation of the KI for users of a lower-limb prosthesis. This approach has the potential to restore lost sensation and improve the quality of life for many prosthesis users.

## **Preface**

This thesis includes an adapted version of Chapter 4 that was accepted as a podium manuscript and winner of the best student paper at the 2018 IEEE Life Sciences Conference on (IEEE LSC 2018, October 2018). I was responsible for the hardware development, graphical user interface and software development, validation study design, data collection, data analysis, and manuscript production. Ahmed Shehata and Quinn Boser were responsible for guidance during the developmental process and contributed to manuscript revisions. Albert Vette and Jacqueline Hebert were the supervisory authors and contributed to study design, device development, and manuscript production.

The MATLAB code used to calculate human joint angles in Chapter 3 and 5 (Appendix B) was developed by Quinn Boser; I was responsible for minor modifications regarding the Cardan angle extraction (last function in Appendix B). My original work includes the exploratory study in Chapter 3, movement sensor development and validation in Chapter 4, integration study in Chapter 5 and conclusion in Chapter 6.

The research outlined in this thesis received ethics approval from the Health Research Ethics Board of the University of Alberta: “Physiologically Relevant Prosthetic Limb Movement Feedback for Upper and Lower Extremity Amputees”, HREB Pro00063695.

## Acknowledgments

With sincere gratitude, I would like to thank all of those that have provided support during my Master of Science in Mechanical Engineering. Throughout the past two and a half years, your influence has greatly impacted my development as researcher, academic and human being.

Firstly, I would like to thank my co-supervisors, Dr. Albert Vette and Dr. Jacqueline Hebert. Both have been incredibly supportive, sympathetic and accommodating to my needs which I truly appreciate. Albert, thank you for introducing me to the Bionic Limbs for Improved Natural Controls (BLINC) lab. I really appreciate your patience, understanding and commitment during my studies. Jacqueline, thank for accepting me into your interdisciplinary team of researchers and clinicians. The BLINC lab has provided a unique environment for growth in many areas beyond academics (e.g., community outreach) which have supplemented my studies. Additionally, I really appreciate your ability to accommodate and combine my various interests into a single coherent project. Your clinical expertise, guidance and encouragement were invaluable to the completion of this project. Thank you both for showing strong dedication to your roles as supervisors, I am very grateful. Thank you!

To my lab mates and co-workers at the BLINC lab, thank you for fostering an incredibly supportive, productive and fun work environment. Specifically, I would like to thank Katherine Schoepp, Michael (Rory) Dawson and Jonathon Schofield for their enormous support throughout the past two years; the three of you have gone above and beyond to ensure my success, this I am very grateful for. In addition to this, I would like to thank Katherine for being a mentor beyond the lab in various community settings; Katherine, I have learned so much from our time together. I would also like to thank Ahmed Shehata, Quinn Boser, James Austin, Dylan Brenneis, Alex Kearney, Heather Williams, Thomas (Riley) Dawson and the rest of the members of the BLINC lab for their support, interesting discussions, and good company. The BLINC lab is an exceptionally talented group of people, and I have learned so much from your diverse expertise.

I would like to also acknowledge the various professors, students and other labs or groups who have contributed to my graduate experience including the Neuromuscular Control & Biomechanics Laboratory (NCBL) – my second home, Sensory Motor Adaptive Rehabilitation Technology

(SMART) group, Action in Complex Environments Laboratory (ACELab), the Rehabilitation Robotics lunch group and the Telerobotic and Biorobotic Systems (TBS) lab.

Lastly, I would like to thank my family and friends. Mom and dad, I truly appreciate your support and encouragement in a pursuit of further education. Although the journey is far from completion, I know you will continue to stand by my side. Finally, thank you to all those whom I call friends, although I cannot mention everyone here, I am very appreciative of your friendship and the support that comes with it. I would apologize for boring many of you with a flood of nerdy rants, but I regret nothing!

This work was supported in part by the U.S. Department of Defense, Award number: W81XWH-15-1-0575. PI: Paul Marasco, Cleveland Clinic Lerner Research Institute; Sub PI: Jacqueline Hebert, University of Alberta. Project title: Physiologically relevant prosthetic limb movement feedback for upper and lower extremity amputees.

# Table of Contents

<b>ABSTRACT .....</b>	<b>II</b>
<b>PREFACE .....</b>	<b>V</b>
<b>ACKNOWLEDGMENTS .....</b>	<b>VI</b>
<b>TABLE OF CONTENTS.....</b>	<b>VIII</b>
<b>LIST OF FIGURES.....</b>	<b>XII</b>
<b>LIST OF TABLES .....</b>	<b>XVIII</b>
<b>1. INTRODUCTION .....</b>	<b>1</b>
1.1 PROBLEM DEFINITION .....	1
1.2 OBJECTIVES.....	2
1.3 OUTLINE OF THESIS .....	3
<b>2. LITERATURE REVIEW .....</b>	<b>4</b>
2.1 OVERVIEW.....	4
2.2 LOWER-LIMB PROSTHESES DESIGN.....	5
2.2.1 <i>Current Lower-Limb Protheses Design</i> .....	5
2.2.2 <i>Passive Components in Lower-Limb Protheses</i> .....	6
2.2.2.1 <i>Passive Foot-Ankle Systems</i> .....	6
2.2.2.2 <i>Passive Knee Systems</i> .....	7
2.2.3 <i>Active Components in Lower-Limb Protheses</i> .....	8
2.2.3.1 <i>Active Foot-Ankle Systems</i> .....	8
2.2.3.2 <i>Active Knee Systems</i> .....	8
2.2.4 <i>Concluding Remarks on Lower-Limb Prosthesis Technologies</i> .....	9
2.3 GAIT AND LOWER-LIMB PROSTHESES.....	9
2.3.1 <i>The Gait Cycle</i> .....	9
2.3.1.1 <i>Phases of the Gait Cycle</i> .....	10
2.3.2 <i>Analysis of Gait for Users of Lower-Limb Protheses</i> .....	12
2.3.2.1 <i>Gait of individuals with Transfemoral (Above-Knee) Amputation</i> .....	13
2.3.2.2 <i>Gait of Individuals with Transtibial (Below-Knee) Amputation</i> .....	13
2.3.3 <i>Concluding Remarks on Gait and Lower-Limb Protheses</i> .....	14
2.4 INERTIAL MEASUREMENT UNITS FOR TRACKING LOWER-LIMB MOVEMENT.....	15
2.4.1 <i>Kinematics and Constraints</i> .....	16
2.4.2 <i>Sensor Fusion Techniques</i> .....	16

2.4.3	<i>Issues in IMU-Based Movement Tracking</i>	17
2.4.4	<i>Tracking Lower-Limb Movement</i>	17
2.4.5	<i>Differences in Tracking Prosthetic and Human Single-Axis Joints</i>	19
2.4.6	<i>Concluding Remarks on Inertial Measurement Unit-Based Lower-Limb Movement Tracking</i>	19
2.5	<b>SENSORY FEEDBACK MECHANISMS IN RELATION TO PROSTHESES</b>	20
2.5.1	<i>Sensorimotor Integration</i>	20
2.5.1.1	<i>Cutaneous Receptors</i>	20
2.5.2	<i>Sensory Feedback</i>	22
2.5.2.1	<i>Sensory Substitution</i>	23
2.5.2.2	<i>Modality Matched</i>	26
2.5.2.3	<i>Somatotopic Matching</i>	26
2.5.2.4	<i>The Kinesthetic Illusion</i>	28
2.5.3	<i>Concluding Remarks on Prosthetic Sensory Feedback Mechanisms</i>	33
<b>3.</b>	<b>KINESTHETIC ILLUSION IN INDIVIDUALS WITH LOWER-LIMB AMPUTATION</b>	<b>35</b>
3.1	<b>INTRODUCTION</b>	35
3.2	<b>METHODS</b>	36
3.2.1	<i>Participants</i>	36
3.2.2	<i>Experimental Setup</i>	36
3.2.3	<i>Experimental Protocol</i>	37
3.2.3.1	<i>Percept Mapping</i>	38
3.2.3.2	<i>Illusion Quantification</i>	38
3.2.4	<i>Experimental Data Processing and Analysis</i>	42
3.3	<b>RESULTS</b>	43
3.3.1	<i>Percept Mapping</i>	44
3.3.1.1	<i>Participants that Experienced the Kinesthetic Illusion</i>	44
3.3.1.2	<i>Remaining Participants and Other Sensations</i>	50
3.4	<b>DISCUSSION</b>	54
3.4.1	<i>Limitations</i>	59
3.4.2	<i>Conclusions</i>	60
<b>4.</b>	<b>DEVELOPMENT AND VALIDATION OF A WIRELESS SENSOR FOR TRACKING SINGLE-AXIS PROSTHESES MOVEMENT</b>	<b>61</b>
4.1	<b>INTRODUCTION</b>	61
4.2	<b>METHODS</b>	61
4.2.1	<i>Development of a Wireless Sensor for Tracking Single-Axis Movement</i>	61
4.2.1.1	<i>Hardware Design</i>	61

4.2.1.2 Software Design .....	64
4.2.1.3 Prosthetic Knee Joint Angle Detection Algorithm .....	66
4.2.1.4 Technical Validation of the Wireless IMU-Based System .....	69
4.3 RESULTS .....	72
4.3.1 <i>Gaussian Movement</i> .....	72
4.3.2 <i>Sinusoidal Movement</i> .....	74
4.3.3 <i>Results Summary</i> .....	76
4.4 DISCUSSION .....	77
4.4.1 <i>System Performance</i> .....	77
4.4.2 <i>Practical Use of the Movement Sensor</i> .....	78
4.4.2.1 <i>Limitations</i> .....	79
4.5 CONCLUSIONS .....	79
<b>5. INTEGRATION OF A KINESTHETIC FEEDBACK MECHANISM: A CASE STUDY .....</b>	<b>81</b>
5.1 INTRODUCTION .....	81
5.2 METHODS .....	82
5.2.1 <i>Triggering Systems for the Vibratory Actuator</i> .....	82
5.2.1.1 <i>Wired System</i> .....	82
5.2.1.2 <i>Wireless System</i> .....	83
5.2.2 <i>Controller Design</i> .....	84
5.2.3 <i>Real-Time Filter Design</i> .....	86
5.2.3.1 <i>Filter Selection</i> .....	86
5.2.3.2 <i>Filter Design</i> .....	86
5.2.4 <i>Experimental Setup</i> .....	87
5.2.5 <i>Experimental Protocol</i> .....	90
5.2.6 <i>Data Processing and Analysis</i> .....	90
5.3 RESULTS .....	91
5.3.1 <i>System Performance</i> .....	91
5.3.2 <i>Mapping and Illusion Quantification</i> .....	92
5.4 DISCUSSION .....	95
5.4.1 <i>System Performance</i> .....	96
5.4.2 <i>System Induced Movement Percepts</i> .....	96
5.4.3 <i>Practical Use of the Sensory Feedback System</i> .....	98
5.4.3.1 <i>Socket Integration</i> .....	98
5.4.3.2 <i>Further Development</i> .....	99
5.5 CONCLUSION .....	99

<b>6. CONCLUSIONS .....</b>	<b>100</b>
1.1 FUTURE DIRECTIONS .....	101
<b>REFERENCES.....</b>	<b>104</b>
<b>APPENDIX A [ETHICS].....</b>	<b>133</b>
A.1. CONSENT FOR RELEASE OF CONTACT INFORMATION .....	133
A.2. PARTICIPANT INFORMATION LETTER AND CONSENT FORM .....	134
A.3. PARTICIPANT INFORMATION SHEET .....	139
<b>APPENDIX B [MOTION CAPTURE JOINT ANGLE CALCULATIONS] .....</b>	<b>140</b>
B.1. MATLAB CODE FOR DETERMINING ILLUSION KINEMATICS .....	140
<b>APPENDIX C [MOVEMENT SENSOR DEVELOPMENT] .....</b>	<b>143</b>
C.1. HARDWARE .....	143
C.2. ARDUINO CODE FOR SENSOR ACQUISITION AND RN42 BLUETOOTH RADIO TRANSMISSION .....	146
C.3. SOFTWARE .....	149
C.4. C# CODE FOR THE MOVEMENT SENSORS GRAPHICAL USER INTERFACE .....	150
<b>APPENDIX D [MOVEMENT SENSOR VALIDATION] .....</b>	<b>159</b>
D.1. DELSYS TRIGNO .....	159
D.2. C# CODE FOR DELSYS TRIGNO TCP/IP COMMUNICATION .....	160
D.3. C# CODE FOR THREE DEGREE OF FREEDOM ROBOTIC ARM.....	161
<b>APPENDIX E [MOVEMENT SENSOR INTEGRATION] .....</b>	<b>164</b>
E.1. HARDWARE.....	164
E.2. SOFTWARE.....	165
E.3. C# CODE FOR VIBRATORY ACTUATOR TRIGGERING SYSTEM.....	165

## List of Figures

Figure 2.1: Common components used in lower-limb prostheses. Lower-limb prosthetic devices are comprised of key components including sockets, rotators, knee joints, shanks, and the ankle/foot units.....	5
Figure 2.2: Generally, an inertial measurement unit is comprised of accelerometers and gyroscopes capable of monitoring changes in the individual axis of the device. Note: The X's, which are enclosed by a yellow area, indicate a rotation arrow entering the page. ....	15
Figure 2.3: The mechanisms in which sensory feedback is communicated to prosthesis users can be partitioned into three subgroupings: substitution, modality matched and somatotopic matching. ....	23
Figure 3.1: Users of prosthetic devices initiate muscle contractions and resulting movements of the residual limb are transferred to the socket interface to biomechanically control the movement of the prosthesis. This is an open-loop control system that does not communication the state of a prosthesis to user's in a functional or intuitive fashion. ....	35
Figure 3.2: Vibrasense VB200 vibratory system. (a) the controller of the vibratory actuator, which allows for change of vibration parameters (frequency, amplitude); (b) the hand-held segment or vibrator actuator that produces the vibration; and (c) the tactor head contacting the participant's limb. ....	37
Figure 3.3: The anterior lateral view of the residual limb of P1 (left thigh): the numbers (written in red ink) represent the center of areas that, when stimulated, resulted in perception of knee flexion. Site 1 represents the location with the most consistent movement percept; this was the site used for determining the illusion kinematics. ....	45
Figure 3.4: The movement percepts (knee flexion) of participant P1, as demonstrated by the participant's intact limb (captured by mocap plates), are plotted, with similar trajectories color-coded. The movement percepts of participant P1 can be generally described as an inverted sigmoidal curve. Red trajectories occurred across trials, but mostly for earlier trials. Blue trajectories mostly occurred for middle trials, demonstrating a quicker movement percept with	

greater flexion range. Finally, black trajectories occurred for two later trials and presented longer, slower movement percepts with smaller range of knee flexion. The participant indicated the first eight trials reached a terminal flexion angle, unlike the remainder of trials which would have continued to indicate movement if the vibration had not been terminated. .... 46

Figure 3.5: The lateral view of the residual limb of participant P4 (right leg): the numbers represent the center of areas which, when stimulated, resulted in movement percepts. Sites 6/7 and Site 8 are located anterior and posterior of the participant’s fibula, respectively; Site 9 is located on the participant’s gastrocnemius. Sites 7 and 8/9 represent locations where the participant experienced movement percepts of ankle dorsiflexion coupled with inversion and eversion, respectively. Site 8 represents the location with the strongest movement percept and used for determining the illusion kinematics. Site 6 corresponded to sensation on the heel. Note: image is blurred to mask identifying information. .... 47

Figure 3.6: The anterior (a) and medial (b) views of the residual limb of participant P4: Stimulation of Site 4 and Site 5 generated a sensation as if “someone cupped [the] ankle and started squeezing”. .... 48

Figure 3.7: The successful movement percepts (ankle dorsiflexion) of participant P4 are plotted, with similar trajectories color-coded. Both red and blue trajectories occurred for earlier trials, whereas other blue trajectories and black trajectories occurred for later trials in an alternating manner. Sigmoidal curves can be used to describe some of the movement percepts for earlier trials (red). Movement percept for later trials (blue and black) are better described by either a square root or logarithmic curve. The participant indicated the perceived movement would have continued in two of the blue trials (7 and 9), whereas the remaining trials had reached a terminal flexion angle. .... 49

Figure 3.8: The anterior view of participant P2’s residual limb (right leg): the numbers represent the center of areas which, when stimulated, produced unique sensations. Vibration at Site 1 produced a sensation in the phantom knee similar to the patellar reflex. Through continual stimulation, the sensation ceased and was replaced by a tingling sensation. Stimulation of Sites 3 and 6 resulted in a tingling sensation on that phantom foot which was described as a “waving back and forth”. Vibrations on Site 3 were ultimately stopped as they resulted in painful sensations for

the participant. Stimulating Sites 2, 4, and 7 produced a static tingling sensation concentrated on the phantom foot. Vibration on Site 5 produced a similar vibration on the phantom calf bone... 51

Figure 3.9: The lateral view of participant P3’s residual limb (right leg): the numbers represent the center of areas which, when stimulated, produced unique sensations. Vibration at Site 3 produced a sensation in the phantom knee similar to the patellar reflex. Through continual stimulation, the sensation ceased and was replaced by a tingling sensation. The remaining sites produced tingling sensations on various segments of the phantom limb..... 52

Figure 4.1: The system is comprised of an Arduino Pro Mini microcontroller (center), a Bosch BNO05 inertial measurement unit (bottom right), an RN42 Bluetooth module (top right), a lithium-ion battery, and a boost converter (left of the microcontroller)..... 62

Figure 4.2: Enclosure for the wireless inertial measurement unit-based system. The dimensions and placement of the electronics within the enclosure are shown above. .... 64

Figure 4.3: Graphical user interface (GUI) for data collection. (a) outlines the entrance GUI, which is used to enter information about the device and trial, as well as establish a connection with the movement sensors; (b) is the second layer of the GUI and is released after a secure connection to the movement sensors is established. This interface allows for the monitoring and logging of data. The angles between two connected, wireless modules are shown in the three plots. The calibration status of each inertial measurement unit is also shown on this page..... 66

Figure 4.4: The global coordinate frame for the two movement sensors is shown on the left. Two movement sensors are placed proximally and distally of the knee joint on a prosthetic leg (a). A calibration procedure is performed once the prosthesis is in full extension, to align the coordinate frames of both movement sensors with the relevant axis of rotation of the prosthesis according to the recommendations by the International Society of Biomechanics (b). The movement of the prosthetic knee is determined by extracting Cardan angles from the relative orientation between the two movement sensors (c)..... 67

Figure 4.5: A five degree of freedom robotic arm was used as a platform to test the ability of the movement sensors to monitor single-axis movements. The three degrees of freedom used by the robot arm are marked in the figure by the three purple arrows between (a) and (b). The X’s, which

are enclosed by a yellow area, indicate a rotation arrow entering the page. Two movement sensors were used for the validation, each sensor was attached to a commercial inertial measurement unit system and a motion capture plate, containing four markers each. The movement sensors were then placed on a stationary section of the robotic arm (a) and a location capable of moving about the three axes of the movement sensors (b). ..... 70

Figure 4.6: The results for the individual axis of the wireless inertial measurement unit-based (WibS) versus the commercial inertial measurement unit (cIMU) and motion capture (mocap) systems for the Gaussian profile. In each plot, the dotted lines represent angles from the WibS, the solid lines angles from the cIMU system, and the dashed lines angles from the mocap system. These lines are difficult to identify in the figure due to their good agreement. Results for individual axes (X, Y, Z) are structured in rows. The columns represent the tested speed. Isolated WibS movements about each axis were within a degree of agreement with both the cIMU and mocap systems. The movement of both stationary axes of the WibS were within a quarter of a degree relative to the cIMU and mocap systems. .... 73

Figure 4.7: The results for the individual axis of the wireless inertial measurement unit-based system (WibS) versus the commercial inertial measurement unit (cIMU) and motion capture (mocap) systems for the sinusoidal profile. In each plot, the dotted lines represent angles from the WibS, the solid lines angles from the cIMU system, and the dashed lines angles from the mocap system. Results for individual axes (X, Y, Z) are structured in rows. The columns represent the tested speed. At the two lower speeds, isolated WibS movements about each axis were within two and eight degrees of agreement with the cIMU and mocap systems, respectively. At the fastest speed, the root mean square error increased to six and fourteen degrees of disagreement relative to the cIMU and mocap systems, respectively. WibS movement for both stationary axes was within one degree relative to the cIMU and mocap systems. .... 75

Figure 5.1: The kinesthetic illusion is currently administered manually. Activation of the actuator responsible for delivering the illusion is not connected to the movement of the prosthetic device. .... 81

Figure 5.2: The WIbS can be used to track the movement of the prosthetic device. This tool can be used to close the sensory feedback loop by activating the KI through a more intuitive and functional manner. .... 82

Figure 5.3: In the wired system, signals are received over the air (Bluetooth) from the WIbS. These signals are then run through the joint angle computation algorithm and the threshold-based controller before activating the vibratory actuator through serial communication..... 83

Figure 5.4: Similar to the wired system, the wireless system receives signals over the air (Bluetooth) from the WIbS. These signals are then run through the joint angle computation algorithm and the threshold-based controller before activating the vibratory actuator through a wireless signal. .... 84

Figure 5.5: To infer movement, the controller determines whether the magnitude of the difference between successive joint angles is greater than a predefined sampling frequency dependent threshold. This controller is used to activate or deactivate the actuator responsible for administering the kinesthetic illusion. .... 85

Figure 5.6: The participant was shown his unattached prosthesis with the WIbS attached proximally and distally of the knee joint. He was informed that movement of the prosthesis, as detected by the wireless modules, was responsible for triggering the vibratory actuator. The participant was unaware, however, that the robotic arm was used instead..... 88

Figure 5.7: The participant was seated with a vibratory actuator pressed into his residual limb (a). A clamp was used to fix the vibratory actuator to a site eliciting strong and consistent movement percepts as determined through a mapping procedure identical to that described in Chapter 3, Section 3.2.3. The vibratory actuator was driven by the single-axis movement of a robotic limb detected by the WIbS (b). This robotic limb was used for repeatability and consistency across the trials..... 89

Figure 5.8: (a) and (b) outline the delay introduced by each compartment of the wired and wireless systems, respectively. Both systems impede signal flow from the movement sensor to the Vibrasense by less than 100 milliseconds. However, the internal transients of the Vibrasense introduce a repeatable delay of roughly 700 milliseconds..... 92

Figure 5.9: The anterior lateral view of P1’s residual limb: The numbers were used as handles to represent the center of areas that, when stimulated, resulted in movement percepts. Site 3 represents the location with the most consistent movement percept; this was the site used for determining the illusion kinematics. .... 94

Figure 5.10: The experienced movement percepts (knee flexion) of participant P1, as demonstrated by the participant’s intact limb (captured by mocap plates), are plotted with similar trajectories color-coded. The movement percepts of participant P1 can be generally described as an inverted sigmoidal curve. The blue trajectories represent rapid knee flexion, red trajectories represent minimal and slow knee flexion, and black trajectories are between these extremes. The participant indicated that only five trials (1, 4, 5, 8 and 10) experienced a terminal knee flexion angle; the remainder of trials would have continued to indicate phantom movement if the vibration had not been terminated. .... 95

## List of Tables

Table 2.1: Summary of cutaneous mechanoreceptors and their attributes .....	21
Table 3.1: Summary of participant information. ....	36
Table 3.2: Time intervals and information provided to participants to experience movement sensations. ....	43
Table 3.3: Summary of other sensations not related to the kinesthetic illusion. ....	53
Table 4.1: Movement profiles and applied parameters. ....	71
Table 4.2: Accuracy and repeatability results for the Gaussian movement profile. ....	74
Table 4.3: Accuracy and repeatability results for the sinusoidal movement profile. ....	76

# 1. Introduction

## 1.1 Problem Definition

Individuals living with limb loss can be found across the globe. In 2005, more than 1.6 million individuals with limb amputation were living in the United States of America [1]; this number is anticipated to double by 2050 [1]. In developing countries, amputation often occurs in younger individuals and is predominately a result of trauma, infection, or uncontrolled diabetes mellitus [2]. In developed countries, amputations are usually a result of vascular problems affecting the elderly [3], [4]. The majority of extremity amputations occur in the lower limbs [1], [5]. In addition to losing structure and motor function, the body loses important sensory organs and information required to optimize performance (e.g., during ambulation). As a result, lower limb loss can drastically decrease the quality of life of the individuals affected [6]–[8].

Mobility has been shown to have a positive correlation with the overall quality of life for individuals with lower-limb amputation [6]. However, restoration of walking for individuals with lower-limb amputations is highly dependent on balance [9]. Balance is dependent on the vestibular [10], visual [10], somatosensory [10], proprioceptive and kinesthetic senses [11]. Amputation results in loss of somatosensory, proprioceptive and kinesthetic feedback [12], [13]. In particular, the loss of proprioception (spatial awareness of limbs) and kinesthesia (sense of limb movement) has profound implications for lower-limb prosthesis users [14], [15]. The inability to distinguish when the lower limbs are moving is highly disruptive to gait [16]. This lack of sensory feedback may result in decreased balance which may lead to falling, abnormal gait, greater dissatisfaction, and decreased quality of life [6]. Therefore, prostheses capable of providing users with a relative sense of the limb replacement's movement could improve mobility and contribute to an improved quality of life for prosthesis users.

The majority of work focusing on the restoration of sensation for individuals with amputations has been directed towards individuals with upper limb amputation [17]–[22]; however, individuals with lower limb amputations could also potentially benefit from the use of sensory feedback. Commercial sensory feedback systems for prosthesis users do not exist; however, a variety of sensory feedback systems for use in prosthetic devices have been proposed in the research

literature. Sensory feedback systems can be divided into three subgroups: those using substitution, modality matching, or somatotopic matching. Sensory substitution communicates the state of a prosthesis to users through sensory channels not physiologically representative of what a healthy limb would experience [23]. Modality-matched feedback mechanisms are those in which communicated stimuli are matched in terms of the type of sensation, i.e., touch to the prosthesis is felt as touch to some area of the skin [17]. Somatotopic methods deliver feedback such that individuals with amputations can sense the stimulus as though it were applied to the same corresponding location of their missing limb.

Touch and pressure sensory feedback, delivered through sensory substitution, is the most commonly used feedback approach reported in the literature [17], [23]–[26]. Compared to touch and force feedback, there has been very little work on restoring kinesthetic (movement) sensations. However, targeted reinnervation (TR), a surgical technique where the sensory and motor nerves formerly innervating amputated limbs are reinnervated to new muscle and skin sites, has been used as a technique for relaying both tactile and kinesthetic somatotopic feedback to prosthesis users [22], [24], [27], [28]. These studies utilized the kinesthetic illusion (KI), a phenomenon whereby mechanical vibration administered to the musculotendinous region of a limb may illicit a perception of limb movement, as a method in which somatotopic movement information was relayed to prosthesis users with TR proximal upper-limb amputations [18], [29]. Vibration-induced movement percepts for upper-limb prosthesis users have been shown to: produce perceptions of complex hand grip movements, improve the efficiency of reach and grasp movements and establish a sense of agency (ownership) over movements [29]. As previously mentioned, the quality of life for individuals with lower-limb amputation is correlated with stability during ambulation; this stability is highly dependent on sensory feedback, in particular, kinesthetic feedback [11], [13]. To date, no work has been completed on restoring movement sensation for individuals with lower-limb amputations.

## 1.2 Objectives

This thesis aims to set up the necessary methodology for exploration of the KI in individuals with lower-limb loss and to take the first steps towards clinical translation of the KI as a feedback mechanism in lower-limb prosthetic devices. The specific objectives of this thesis were to: (1) perform an exploratory study to determine whether it is possible to provide kinesthetic feedback

to individuals using a lower-limb prosthesis who have not undergone TR, using the KI; and (2) develop a low-cost wireless sensor, using inertial measurement units, capable of tracking the single-axis movement of a lower-limb prostheses. Accomplishing these two critical objectives could allow prosthetic joint movement to drive actuators that close the sensory feedback loop for prosthesis users in an intuitive and functional manner, by bridging the movement of a prosthesis to actuators responsible for administering the KI.

### 1.3 Outline of Thesis

The second chapter of this thesis provides a review of the general areas of research and development pertaining to lower-limb prosthetic devices. Existing prosthesis design, lower-limb prosthetic gait, sensor technologies, sensory feedback, and the KI are discussed. In the third chapter, the KI is explored in individuals with non-TR lower-limb amputations. The outcome of this exploration showcases the promise of KI in relaying movement feedback to individuals with lower-limb amputation. The third chapter also highlights the challenges and variability that must be overcome before the KI can be implemented into practical systems. The intuitive use of any feedback mechanism utilizing the KI will require movement of the prostheses to properly trigger activation of the feedback system. The fourth chapter therefore outlines the design and validation of an inexpensive wireless movement sensor that is based on inertial measurement units, for the purpose of tracking the single-axis movement of a prosthetic knee. Results from the fourth chapter indicate the developed movement sensor can reliably track single-axis movement of a prosthetic knee during the range of activities commonly performed by lower-limb prosthesis users. Specifically, the results indicate that the developed sensor may be able to provide robust movement detection during walking or jogging, but not during running or sprinting. In the fifth chapter, the wireless movement sensor is implemented in a benchtop system to elicit movement sensations in a prosthesis user, using the KI. Through the benchtop system, the movement sensor's capability to close the sensory feedback loop is verified, through use of the device to successfully elicit movement percepts in a person with a lower-limb amputation. Although the benchtop system is capable of eliciting movement sensations in prosthesis users, there remains considerable work in socket integration prior to clinical translation. The final chapter provides concluding remarks and opportunities for future exploration.

## 2. Literature Review

### 2.1 Overview

Individuals with intact limbs rely on biological sensors embedded within their anatomy to understand their body and its interaction with the environment. These biological sensors transmit information pertaining to a multitude of sensations including force, temperature and movement [10], [30]. Similar to individuals with intact limbs, prosthesis users may benefit from the use of sensory feedback in understanding and interacting with their environment. As indicated in the previous chapter, the majority of work focusing on the restoration of sensation for individuals with amputations has been directed towards individuals with upper limb amputations [18], [20]–[22], [24], [29], [31]–[37]; however, individuals with lower-limb amputations could also benefit from the use of sensory feedback. The quality of life for individuals with lower-limb amputation is correlated with stability during ambulation, and this stability is highly dependent on sensory feedback, in particular, movement feedback [10], [11], [13]. This chapter reviews three major areas in the prosthetic literature relevant to the restoration of movement feedback for individuals using lower-limb prosthetic devices: (1) lower-limb prosthetic design and gait, (2) sensing technologies relevant to prosthetic design, and (3) sensory feedback mechanisms in relation to prostheses. In the first section, current lower-limb prosthetic socket systems and above and below-knee componentry capable (active) and incapable (passive) of net power generation are discussed. Some of the more advanced prosthetic, microcontroller-based systems are capable of monitoring the movement of the prosthesis, which is instrumental to the development of a movement feedback system. The first section also provides a foundation for exploring gait deviations lower-limb prosthesis users may exhibit by highlighting the limitations of prosthetic componentry during ambulation. The second section briefly compares the gait cycle and gait kinematics of individuals with intact limbs to those with above and below-knee amputation, while emphasizing common gait deviations prosthesis users may face. An understanding of potential gait deviations of prosthesis users will aid in developing technologies capable of tracking these movements. The next section explores inertial measurement units (IMUs) as a sensing technology capable of tracking single-axis movement of a prosthetic device. Sensing technologies capable of reliably tracking the movement of a lower-limb prosthesis are essential in the development of intuitive feedback systems, which operate based on the movement of the prosthesis. Finally, the current

sensory feedback mechanisms available to prosthesis users are explored, with an emphasis on techniques which hold promise for reliably relaying movement feedback to prosthesis users.

## 2.2 Lower-Limb Prostheses Design

### 2.2.1 Current Lower-Limb Prostheses Design

Prostheses are constructed from several key components (Figure 2.1). These components consist of various combinations of sockets and commercially available prosthetic links, such as rotators, knee joints, ankles and feet [38]. Sockets are the interface between an individual's residual limb and the prosthesis components. Generally, sockets are designed for support and load transmission during weight-bearing (stance) and suspension during the swing phase of gait. Although there are general principles for socket design, each socket is generally custom-fit for the individual based on limb anatomy and patient characteristics.

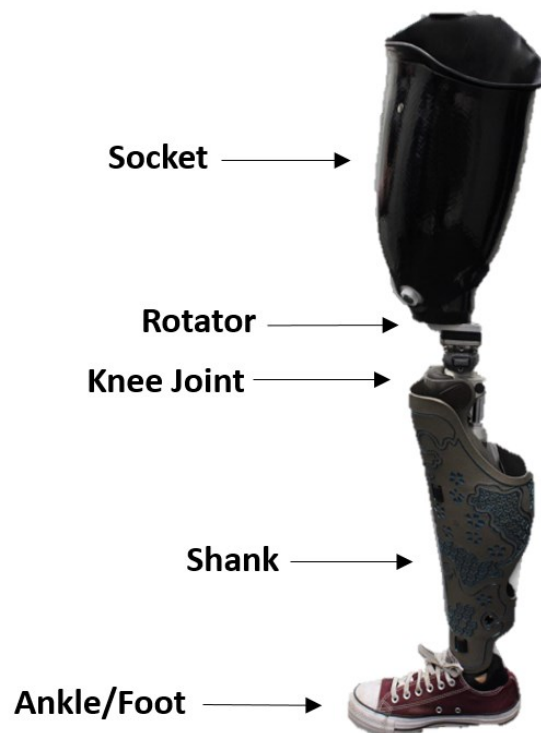


Figure 2.1: Common components used in lower-limb prostheses. Lower-limb prosthetic devices are comprised of key components including sockets, rotators, knee joints, shanks, and the ankle/foot units.

## 2.2.2 Passive Components in Lower-Limb Prostheses

While recent technological advancements have resulted in the commercialization of externally powered lower-limb systems, most components in lower-limb prostheses are passive systems. Passive systems are incapable of introducing power into the movement of the prosthetic joint to aid users of lower-limb prosthesis during ambulation.

### 2.2.2.1 Passive Foot-Ankle Systems

The solid ankle cushion heel (SACH) foot is the most basic prosthetic foot available [39]. The foot, containing no moving parts, provides good shock absorption for moderate activity levels. Due to minimal plantarflexion at heel strike, the SACH foot relies on a cushioned heel wedge to dissipate energy in early stance [39]. Flexible toes positioned at the keel of the foot approximate forefoot dorsiflexion, providing compliance during the stance to swing transition [39]. Major drawbacks of the SACH foot include potential deterioration of the heel wedge over time.

Dynamic foot-ankle systems (also called energy-return systems) absorb and return energy to users in various segments of the stance phase of gait to improve gait efficiency. The flexibility of the keel is of great benefit to gait. Increased foot compliance results in increased step length, decreased impact force at heel strike, and reduced gait asymmetry for individuals with unilateral transtibial amputations [40].

Expanding on the energy-return systems, hydraulic foot-ankle designs utilize hydraulic componentry to allow tuning of ankle resistance in plantarflexion and dorsiflexion. Lower resistance allows for increased ankle movement and improved adaptation to uneven terrain, whereas higher resistance results in increased loading and energy return [41], [42]. Dorsiflexion resistance is used in controlling the speed users advance over the foot when transitioning through mid-stance to pre-swing, while plantarflexion resistance dampens the amount of ankle plantarflexion at heel strike [41], [42]. The Echelon foot, a hydraulic system, was shown to provide decreased rates of loading and increased protection of the distal segment of the residual limb [42].

Microprocessor-controlled ankles allow for individual customization and real-time adaptation to variations in gait and terrain [43]. Microprocessors expand the performance of passive foot-ankle systems through intelligent control of features such as ankle position, plantarflexion-dorsiflexion resistance, and energy storage-release [43]. Microprocessor technology has been successfully

leveraged in commercial foot-ankle systems: Össur PROPRIO FOOT® [44], Endolite élan foot [43], the Hosmer Raize™ Ankle [38], and the Ottobock Triton smart ankle [38]. Microprocessor-based systems may contain sensors providing information pertaining to the movements of the ankle system [45], [46]. However as proprietary devices, most commercial microcontroller-based ankle systems do not allow researchers easy accessibility to sensor data.

#### **2.2.2.2 Passive Knee Systems**

Prosthetic knee design differs from the foot-ankle system as a consequence of different functional requirements. Although fixed knee prostheses (consisting of a locked knee incapable of buckling) exist, free-knee prostheses are more commonly used [47]. The primary design objectives of passive free-knee prosthetic knees are stance-phase stability and swing-phase control as opposed to energy storage and release. Four major classes of passive prosthetic knees exist: mechanical single-axis, polycentric, hydraulic, and microprocessor. Single-axis knees represent the most basic prosthetic knee design consisting of a single revolute joint at the knee center. These components utilize a combination of prosthetic alignment and voluntary muscle control of the user (hip extension) to maintain stability during stance [48]. Limited by friction in the knee joint, single-axis knees provide unrestrained movement in swing [48]. The benefits of single-axis knees include functional simplicity and ease of maintenance.

Rather than a single revolute joint, polycentric knee designs embody a multi-bar linkage. The inclusion of a multi-bar linkage results in a changing instantaneous center of rotation during gait [38]. This design aspect offers features beneficial to both stance-phase and swing-phase performance [38]. When compared to single-axis designs, polycentric knees provide more stability in stance and increased toe clearance in swing [38].

Hydraulic knees are comprised of pistons within cylinders filled with fluid (hydraulic) or air (pneumatic) and used for improved stance [49] or swing phase control [50]. In stance phase, hydraulic knee systems optimize the maximum locking torque for body-weight support. Thus, hydraulic stance control systems allow maintenance of knee extension without the use of hip extensor muscles [49]. Hydraulic knee systems also control the swing function of the knee, adjusting according to the user's walking speed [50]. During swing, gait speed modulation is achieved through control of valves located on the cylinder containing the fluid. As the user speeds

up, valves within the cylinder close; this limits the flow of fluid and ultimately the flexion range; the opposite is true while users slow down [50].

The most sophisticated single-axis passive knee systems rely on microprocessor control for enhanced performance and stability [51]. Microprocessor knees actively control resistance in the knee for improved functionality, allowing for active adaption to alterations in the environment or gait [51]. These systems expand the range of configurations for which the prosthesis provides stable load-bearing by providing weight-bearing support in fully extended and flexed-knee positions [51].

### **2.2.3 Active Components in Lower-Limb Prostheses**

While passive components provide a host of functional capabilities resulting in significant restoration of lower-limb ambulatory function, net-positive power generation at the knee and ankle have been commercially lacking until recently.

#### **2.2.3.1 Active Foot-Ankle Systems**

The BiOM® Ankle System is a powered foot-ankle prosthesis which provides programmable ankle stiffness control and power assist [52]. By utilizing unidirectional parallel springs and series-elastic actuators, the BiOM allows for ankle impedance modulation and the output of human-scale torque and power generation [52]. The metabolic costs and gait patterns enabled by the BiOM® are comparable to that of individuals without amputation [52]. The Odyssey® is another powered foot-ankle system which uses a spring ankle composed of DC motors, leadscrew transmission, and helical springs [53]. The helical spring in conjunction with the motor stores stance-phase kinetic energy that is then released during toe-off, providing powered plantarflexion of the foot-ankle system [53].

#### **2.2.3.2 Active Knee Systems**

Similar to the BiOM®, the Össur POWER KNEE™ is a powered knee capable of producing physiologic torque and power outputs [54]. The knee can provide stance-flexion cushioning during heel contact and propulsion during level walking, ramp traversal and stair climbing [54]. Freedom Innovations offers a combined powered knee-ankle system, also capable of providing physiologic power and torque generation at both the knee and ankle [55]. The powered knee-ankle system allows for a combination of movements such as powered knee extension, powered ankle

plantarflexion, and knee flexion at heel strike, otherwise unattainable by other above-knee systems [55]. A case study involving an individual with a unilateral transfemoral amputation demonstrated the system's ability to provide gait kinematics similar to non-disabled participants [55].

#### 2.2.4 Concluding Remarks on Lower-Limb Prosthesis Technologies

Despite the functionality demonstrated by the emerging bionic limb technology, continued development is still needed in many areas, including motor technology, improved battery systems, issues relating to power and energy density, and cost reduction. The affordability of these lower-limb systems is key for wider acceptance of these technologies. Passive lower-limb components (zero net power generation) still dominate the prosthesis landscape; however, with the exception of microprocessor-based componentry, these systems cannot provide information regarding movement of the device. Microcontroller-based components contain sensing technologies capable of tracking prosthesis movement embedded within the device, yet this information is not readily accessible to researchers.

### 2.3 Gait and Lower-Limb Prostheses

#### 2.3.1 The Gait Cycle

During movement, users of lower-limb prostheses may need to employ compensatory movements in order to achieve stable gait and continue forward progression. Comparing the gait cycle deviations and gait kinematics and kinetics of prosthesis users to non-disabled individuals provides a deeper understanding of how amputation and prosthetic devices affect ambulation. Additionally, the gait speed has been shown to influence gait pattern, kinematic and kinetic characteristics. Assessing the effects of gait speed during movement of prosthesis users might provide further understanding of gait differences relative to the nominal population.

Gait refers to locomotion accomplished by repetitive movement of the lower limbs [56]. The gait cycle is comprised of two periods, weight bearing (stance) and advancement (swing) for each limb [56]. The major requirements of walking include progression, stance stability and energy conservation [56]. Forward falling of the body weight is the dominant progression force, although contributions from the contralateral swinging limb are present [57]. The momentum generated by these progressive actions is the driving force in the initiation of movement [57]. During walking, the body can be partitioned into two segments, passenger (head, upper limbs, torso, pelvis) and

locomotor (pelvis, lower-limbs). The balance of the top-heavy passenger is challenged during gait by continual alteration of the locomotor. With the exception of the pelvis, which exists in both functional units, the passenger unit is carried and does not directly contribute to walking [58]. Weight-bearing stability of the lower limbs is greatest when the thigh, leg, and foot are vertically aligned [59]. During walking, the shifting center of mass of the passenger is stabilized by selective muscular control [59]. Nominal gait is also optimally conservative metabolically [60]. This is accomplished through the use of momentum instead of muscle action as evident in progression [60].

### 2.3.1.1 Phases of the Gait Cycle

The interaction between the major components of walking results in a complex and dynamic cycle, which affects various limb segments during movement; each joint performs a representative pattern of movement. As a consequence, the hip undergoes a single arc of extension and flexion during the gait cycle [16], [61]–[64] whereas, the knee and ankle experience two phases of flexion-extension and plantar flexion-dorsiflexion, respectively [16], [61]–[64]. The eight functional units, which constitute one phase of the gait cycle are a consequence of subdividing limb action during movement to achieve these requirements [16], [61]–[64]. These functional units include: initial contact, loading response, midstance, heel off, pre-swing, early-swing, mid-swing, and late-swing.

Initial floor contact is commonly used as the start of the gait cycle [16], [61]–[64], although, due to the repetitive nature of walking, any functional unit might designate the start of the cycle. **Initial contact** (also known as heel strike) refers to a short period of time beginning when the foot strikes the floor marking a transition to double limb support [56]. Although a momentary posture, heel strike has a significant influence on subsequent knee action during the gait cycle [56], [62]. Successful heel strike is achieved through control of both the knee and ankle joint [56], [62]. Prior to heel contact with the floor, 30 degrees of hip flexion and full knee extension are observed, and the ankle is dorsiflexed.

After heel contact and into the **loading response**, the ankle transverses from a dorsiflexed position into plantar flexion, at which time knee flexion increases [56], [62]. During this loading response phase, the body absorbs the impact at the foot [56], [65]. As weight descends on the limb, a heel rocking action is initiated, which aids body weight acceptance, limb stability, and continual progression.

The functional objective of *midstance* is the progression of the body and contralateral leg over a stationary foot [56]. A period of single limb support initiates when the contralateral limb is elevated in preparation for swing. Maximum stability is achieved by keeping the ipsilateral foot stationary [56]. Progression is continued through a rocking-like action of the ankle derived from the residual momentum generated by the contralateral swinging limb. The knee begins to extend after reaching maximum flexion, and the ankle becomes supinated and dorsiflexed [56], [63], [64], [66], [67]. During this phase, the body transitions from force absorption to force propulsion [56], [63], [64]. As the heel leaves the floor, the metatarsals absorb the body weight [56], [66], [67]. During this process, a transition from hip extension to flexion is observed [56], while the knee becomes flexed and the ankle supinates and plantarflexes [56], [66], [67].

*Pre-swing* (also known as toe-off) prepares the ipsilateral limb for swing; the quick transfer of body weight to the stationary leg as initial contact of the contralateral foot is instigated also supports this preparation. During pre-swing, the hip becomes less extended, the knee is flexed at 35-40 degrees and plantar flexion of the ankle increases to 20 degrees [56], [66], [67].

During *early swing*, the hip is initially extended to 10 degrees followed by flexion as a result of contraction and lateral rotation by the iliopsoas muscle [56], [66], [67]. The knee flexes to 40-60 degrees, and the ankle transitions from plantar flexion to dorsiflexion and finally a neutral position [56], [66], [67]. In *mid-swing*, contraction of the adductor muscles flexes the hip to 30 degrees [56], [66], [67]. Sartorius muscle contraction flexes the knee by 60 degrees, then extends the joint by 30 degrees [56], [66], [67]. The ankle is dorsiflexed due to activity of the tibialis anterior muscle [56], [66], [67]. In *late swing* (also known as declaration), advancement of the swinging limb ends as the limb is prepared for stance. Late swing begins with hip flexion of 25-30 degrees, complete knee extension, and a neutral position of the ankle [56], [63], [64], [66], [67].

### Non-Disabled Gait Kinematics

Five primary domains of spatiotemporal gait performance are generally identified when studying gait [51], [63], [64], [68]. The rhythm domain typically pertains to cadence and temporal parameters (e.g., stride time). Parameters constituting distinct divisions of the gait cycle ordinarily encompass the phase domain. The variability domain includes step variability and gait cycle parameters. Gait speed, step and stride length characterize the pace domain. Finally, the base of support domain is described by step width and step width variability. Several studies have

identified gender differences across domains and age groups [63], [64], [68]. In terms of rhythm, men often walk at lower cadences with greater step, stride, swing, stance, and single limb support times than their female counterparts, with significant gender differences [63], [68]. Age group differences exist in the double-limb support time parameters, while both age and gender differences exist in the double-limb support phase of the gait cycle [63], [64], [68]. In terms of pace, women walk slower with shorter step and stride lengths compared to their male counterparts. However, the gender difference in gait speed was negated when normalized to height [63], [68]. Younger age groups typically have greater gait speed, step lengths and stride lengths [63], [64], [68]. Neither the gender nor age group main effects were found to be statistically significant for the variability measurements [63], [64], [68].

Gait speed has been shown to influence the kinematics of progression. Specifically, the knee and ankle joint kinematics correlate with gait speed [69]–[72]. Kwon et al. conducted a study to determine how the kinematic variables of joints in the lower-limbs alter with various gait speeds [71]. They recruited 40 male participants with no previous musculoskeletal or neurological disorders. Each participant was asked to walk down a hallway (10 m) at a slow, normal and self-selected speed. Kinematics for the lower-limb joints were quantified with force plates and a VICON motion capture (mocap) system. Their results suggest that, at increased gait speeds, a coupling of the knee and ankle joint is observed. Therefore, as gait speeds increase, the joint angles reached by the knee and ankle increase correspondingly. The hip's joint angle trajectory was shown to be largely independent of gait speed.

### 2.3.2 Analysis of Gait for Users of Lower-Limb Prostheses

The gait cycle of prosthesis users is affected by the type and alignment of the prosthesis, the condition and length of the residual limb and the remaining musculature [73]–[75]. To generate similar gait patterns to their non-disabled counterparts, users of lower-limb prostheses rely on different muscle groups for movement [73]–[75]. Limb loss results in greater energy expenditure due to the increased exertion required for compensation of the missing appendage and loss of power generation [73]–[75]. The metabolic requirements for individuals with intact limbs correlate with increased walking distance and speed [73]–[75]. In lower-limb prosthesis users this metabolic cost is much higher than non-disabled ambulation, even at normal walking speeds [73]–[75].

### **2.3.2.1 Gait of individuals with Transfemoral (Above-Knee) Amputation**

An above-knee prosthesis user must compensate for the loss of two joints, resulting in greater compensations during gait compared to below-knee prosthesis users. The overall energy expenditure of above-knee prosthesis users is greater than that of below-knee prosthesis users, due to the loss of power generation across the two joints. As a result, the muscles of the intact hip must exert more energy to ensure stability [48], [51], [73], [76]–[82]. A major focus of the gait cycle is preventing the knee from buckling during stance [77]. Above-knee prosthesis users have the option to use either a fixed knee prosthesis or a free-knee prosthesis utilizing stance or swing phase control. Fixed-knee prostheses, as the name suggests, utilized a locked knee incapable of buckling. Unlike fixed-knee prostheses, free-knee prostheses allow for knee flexion during swing, which supports a more natural swing phase during gait. A drawback of a free-knee prosthesis is that, during stance, greater exertion of the remaining hip muscles is required for stabilization [73], [76], [78], [80], correlating with prolonged heel strike [73], [80] and an extended period of knee extension during stance [82].

Due to decreased stability when compared to non-disabled individuals, and increased period of stance is observed for the intact limb of above-knee prosthesis users, similar to that of below-knee users [73], [74], [80]. Hip extensors and calf muscles of the limb contralateral to the amputation generate propulsive forces during the swing phase of the prosthesis [73], [74], [80], whereas the prosthesis is unable to generate equal propulsive forces during stance to advance the swing phase of the intact limb [73], [74], [80].

Users of a fixed knee prosthesis also experience reduced floor clearance during swing, due to the lack of knee flexion and ankle dorsiflexion [73], [74], [80]. This may force above-knee prosthesis users to elevate their hip using both trunk and hip muscles to prevent dragging their prosthesis [73], [74], [80]. Due to the loss of both the ankle and knee, above-knee prosthesis users can experience a variety of gait deviations. The most common above-knee gait deviations include lateral trunk bending [83]–[85], abducted gait [83], [86], circumduction [87], vaulting [88]–[91], foot slap [92], and exaggerated lordosis [93]–[95].

### **2.3.2.2 Gait of Individuals with Transtibial (Below-Knee) Amputation**

In general, ankle prostheses have reduced range of motion compared to their anatomical counterparts; these differences affect various segments of the gait cycle. During initial contact

and the loading response, knee flexion can be decreased due to various factors: excessive plantar flexion of the foot, posterior displacement of the socket over the foot, anterodistal discomfort, and weakness of the quadriceps muscle [74], [75], [96]–[99]. The reduction of knee flexion and stiffness of the prosthetic ankle and foot affects gait progression by not allowing absorption that typically dissipates the momentum from forward falling [74], [75], [96]–[99]. Energy generated during the stance phase with the prosthesis is also decreased, resulting in greater energy compensation by proximal muscles and in the contralateral limb [74], [75], [96]–[99]. The reduced knee flexion on the ipsilateral side of the prosthesis demands larger energy expenditure from the hip muscles to ensure stability [74], [75], [96]–[99].

In order to gain adequate step length of the intact limb, heel rise on the prosthesis must occur earlier [74], [75], [96]–[99]. This results in an increased elevation of the body and ultimately a larger loading force on the intact limb during the loading response [74], [75], [96]–[99]. The intact limb must generate greater contractions in the quadriceps to absorb this increased loading force [99].

During pre-swing, hip flexors must compensate for the reduction in push-off force produced by the prosthesis [99]. There is also a tendency for either early knee flexion (drop-off) or delayed knee flexion. Early knee flexion is due to the lack of anterior support as the body's center of gravity passes over the toe break [74], [75], [96]–[99]. Delayed knee flexion is predominantly caused by excessive displacement of the socket or keel [74], [75], [96]–[99].

### 2.3.3 Concluding Remarks on Gait and Lower-Limb Prostheses

Through exploring gait differences between persons with lower-limb amputations and non-disabled individuals, significant differences are observed in many aspects. Different levels of amputation introduce varying gait deviations, which decrease the efficiency of ambulation, increasing instability and the risk of falling. In turn, these gait deviations cause changes in the spatiotemporal and kinematic gait parameters of prosthesis users when compared to non-disabled individuals.

## 2.4 Inertial Measurement Units for Tracking Lower-Limb Movement

As described in Section 2.2, information pertaining to the movement of a lower-limb prosthesis is not readily accessible to researchers. Although some lower-limb prostheses contain embedded technologies capable of tracking the device's movement, this information is inaccessible without comprising the normal functions of the system. Generally, these embedded technologies capable of tracking movement rely on IMUs [38]. IMUs (comprised of accelerometers and gyroscopes) are frequently used for tracking human and robotic pose, position, and orientation (Figure 2.2). Accelerometer and gyroscopic signals generally suffer from noise, leading to signal drift and incorrect movement data. To combat drift, researchers have suggested both additional hardware (e.g., magnetometers) and algorithmic solutions which tend to delay or mitigate drift altogether. The major issues in using IMUs for tracking human movement include constraints on limb kinematics, relating sensor readings to anatomical movements through calibration, fusion of signals from multiple sensors, and error correction from external disturbances (e.g., magnetic disturbances). IMUs offer a promising solution for monitoring human and prosthetic movement. This section explores IMUs in relation to their use in tracking lower-limb movement of both non-disabled and prosthesis users.

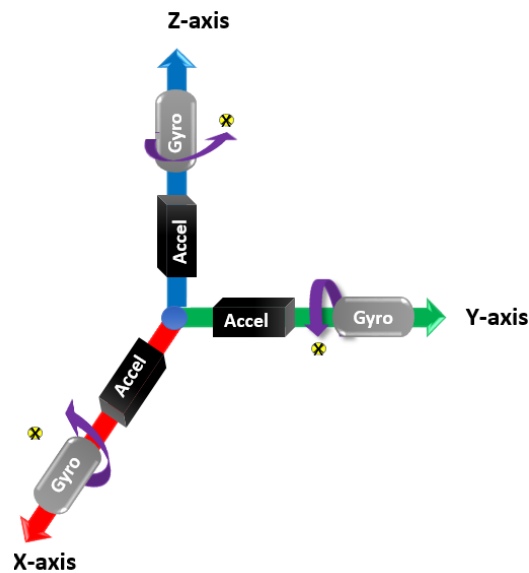


Figure 2.2: Generally, an inertial measurement unit is comprised of accelerometers and gyroscopes capable of monitoring changes in the individual axis of the device. Note: The X's, which are enclosed by a yellow area, indicate a rotation arrow entering the page.

### 2.4.1 Kinematics and Constraints

To simplify calculations, techniques utilizing IMUs for human-based movement tracking (HBMT) typically assume human limbs are rigid bodies [80], [100]–[106]. Representing human limbs as rigid bodies reduces the HBMT problem to that of simply determining position, pose or orientation. With the addition of more limbs, kinematic chains can be modeled. Kinematic chains allow for constraints which, when augmented with IMU sensor fusion algorithms, provide more realistic estimations of human movement [100]–[103]. IMUs represent limb positions through orthonormal coordinate systems (Cartesian frames), and the literature presents several methods to extract orientation measurements from these frames. Due to their potential for intuitive physical meaning, Euler-Cardan angles are the most common choice in transforming coordinate frames to orientation [100], [104]–[111]. A major limitation of Euler-Cardan angles is the possibility of singularities due to gimbal lock [112], [113]. As a result, other methods such as quaternions have been used [114], [115]. Although the use of quaternions does not result in singularities, quaternions do not provide intuitive or anatomical orientation measurements.

### 2.4.2 Sensor Fusion Techniques

To extract signals regarding limb pose and orientation for both robotic tracking and HBMT, signals gathered from IMUs need suitable sensor fusion algorithms. The most common sensor fusion algorithms involve the use of Kalman filters and complementary filters. More complex approaches to sensor fusion such as optimization-based approaches [116] and particle filters [117] exist; however, they are not commonly implemented for HBMT. Most sensor fusion algorithms estimate unknown variables (e.g., quaternions) through discrete settings at successive time steps which rely on current and past sensor measurements.

Kalman filters are the most widespread sensor fusion technique implemented [118]. They can be further subdivided into linear and non-linear filters. In many cases, linear Kalman filters perform adequately for sensor fusion [103], [110], [119], [120]. However, non-linear Kalman filters are typically implemented. Although the extended Kalman filter is frequently implemented to address nonlinearities [121]–[124], the Unscented Kalman filters can also be used to address nonlinearities [125]–[128]. Comparisons between extended and unscented Kalman filters provided conflicting results as performance is heavily influenced by application [129]–[132]. The extended Kalman

filter is typically more computationally efficient, whereas the unscented Kalman filter is typically more robust to initialization issues [130].

Complementary filters provide an alternative solution to sensor fusion by exploiting the unique frequency spectra of the various sensors comprising IMUs [133], [134].

### 2.4.3 Issues in IMU-Based Movement Tracking

Recurring issues with HBMT through IMUs include sensor calibration, sensor drift and magnetic disturbances. IMU-based tracking algorithms for HBMT require parameters which express sensor orientation relative to the body segments being tracked. These parameters are typically assumed to be known [135]–[138]; however, these parameters can also be obtained through an initial calibration [103], [128], [139].

Several calibration procedures have been proposed for obtaining IMU and limb parameters for HBMT. The neutrum-pose (N-pose) is the most common procedure, requiring individuals to stand still with arms resting vertically alongside the trunk [128], [140]–[142]. However, other calibration poses, such as the T-pose [103], [128], [143], [144] or dynamic calibration methods which require individuals to perform movements about different joint axes also exist [104], [138], [145].

Inertial sensor drift is predominantly the result of the integration of gyroscopic measurements. Many techniques have been developed for drift reduction, and some of the most common methods are outlined below. Since drift is a consequence of gyroscope bias, sensor drift might be eliminated by accounting for the bias in the estimation [137], [146]–[148]. Another solution exploits constraints from kinematic chains to mitigate drift when estimating attitude of limbs relative to each other [123], [124], [126]–[128], [137], [142], [147], [149]–[151]. A further solution, zero velocity updates, is typically used in lower-limb tracking and exploits the minimal velocity of the foot during midstance [122], [148], [152], [153]. Many of the methods used to reduce sensor drift rely on the use of magnetometers. However, signals from magnetometers are influenced by external magnetic fields [154].

### 2.4.4 Tracking Lower-Limb Movement

IMU-based lower-limb tracking has been applied in many settings including gait analysis [104], [150], [155], clinical diagnoses [156], [157] and rehabilitation [109], [158]. Dejnabadi et al. developed a method of monitoring lower-limb movement in the sagittal plane [139]. Two IMUs

with biaxial sensors were attached to the leg and lower-leg. The tracking algorithm was implemented by integrating the difference between the acceleration of each segment and that of gravity. Using biomechanical constraints and two IMUs with triaxial sensors attached to the leg and lower-leg, Cooper et al. were able to estimate knee joint movements [120]. Kalman filters were used to approximate the sensors orientation and kinematically model the knee as a hinge joint. However, the use of a simplified single hinge knee joint is a major limitation of this algorithm. Similar to Cooper et al, Liu et al. were able to align IMU poses to the knee joint rotation axis and estimate the joint's movements [159]. Favre et al. developed a comparable method for monitoring knee ligament injury [145], [156]. Seel et al. were able to estimate the knee angle through the use of two techniques which did not rely on magnetometers to eliminate drift [104]. Both techniques were able to transform the axis of rotation of the knee joint to the sensors' axis of rotation. The first method relied on the single hinge approximation and integration of angular speeds to determine the knee angle. Whereas, the second method exploits IMU orientation estimation to acquire the knee angle. Both methods removed drift from an acceleration-based joint angle estimation. Each method was verified by comparing the determined knee joint angles from the IMUs with that of an optical mocap system on both human and prosthetic knees. Both methods were able to track knee movement of the prosthesis with higher success than the human knee. Yuan and Meng et al. utilized lower-limb reconstruction to aid localization during HBMT. Yuan et al. exploited detection of contacts with the ground and a lower-limb kinematic model to correct for the limitations of the sensor [160]. Meng et al. implemented Kalman filters to estimate a limb's orientation from multiple IMUs [161]. The Kalman filters estimate sensor bias and errors in limb orientation to correct orientation estimates. The authors also implemented a zero-velocity update to mitigate effects of external disturbances and drift. Joukov et al. used two kinematic models (modeling the support and swing leg) and five IMUs to track movement [150]. The first kinematic model (stance leg) connected the feet to the ground using a single hinge joint. The second kinematic model (swing leg) connected the hip to the ground using three hinge joints. An extended Kalman filter was used to combined data from the IMU's and kinematic models. Ten gait cycles were used to validate this method, with the authors reporting only knee joint angles. Rather than using magnetometers to combat drift during HBMT, Zihajehzadeh et al. [162] used ultra-wideband tags (low energy short-range radio) [163]. They used 3 ultra-wideband tags positioned at the feet and pelvis and seven IMUs located on the pelvis, thigh, shank, and feet to reconstruct movement.

Two Kalman filters were used to extract joint angles. The first Kalman filter estimated inclination of seven IMUs based on accelerometer and gyroscopic data. The second filter relied on signals from the radio sensors to estimate the orientation of the feet and pelvis. This method was able to achieve less than 5 degrees of orientation error and 5 cm of position error during walking, jumping and ascending validation trials.

#### 2.4.5 Differences in Tracking Prosthetic and Human Single-Axis Joints

Different techniques have been applied to HBMT of single-axis joints as opposed to robotic or prosthetics hinge joints. In relation to single-axis robotic joints, two IMUs attached to each side of a joint can estimate the hinge joint angles through integration of angular rates. This is possible as the coordinate axes of IMUs can be aligned with the hinge joint axis. In contrast, single-axis human joints (e.g., the knee) are not perfect hinge joints [104], [105]. Therefore, IMUs are not easily attached to these joints in such a manner that local coordinate axes coincide with corresponding joint axes [104], [115], [164]. HBMT typically requires the use of body straps [104], [105], [164]. The body straps allow for placement of inertial sensors in various orientations, resulting in further misalignment of axes; hinge joint angles are then calculated from inertial measurement data. To obtain joint angles representative of the anatomical movement, data from both IMUs is transformed into a joint-related coordinate system. This transformation ensures that at least one of each sensor's axes coincides with the joint axis. Transforming sensor data such that the sensor and joint axis align typically requires a calibration procedure [145], [157], [164].

#### 2.4.6 Concluding Remarks on Inertial Measurement Unit-Based Lower-Limb Movement Tracking

IMUs are frequently used for tracking human and robotic orientation and movement. Although these sensors suffer from gyroscopic drift, there have been many hardware and algorithmic solutions presented to mitigate these effects. IMU-based lower-limb monitoring has been applied in various environments, including gait analysis, clinical diagnoses, and rehabilitation. The use of IMUs for HBMT offers many challenges as the single-axis body joints are not ideal hinge joints. As a result, it is not easy to mount inertial sensors to human joints such that local coordinate axes align with the corresponding joints axes. However, as single-axis robotic joints (e.g., prosthetic knees) are hinge joints, IMUs offer a promising solution for tracking joint movement.

## 2.5 Sensory Feedback Mechanisms in Relation to Prostheses

A variety of sensory feedback systems for the use in prosthetic devices have been proposed in the literature. However, commercial feedback systems for prosthesis users do not exist. Sensory feedback mechanisms use sensing technologies to extract information about the prosthesis and environment and relay this information back to the user. Sensory feedback mechanisms integrated into prosthetic devices have the potential to improve mobility for prosthesis users.

### 2.5.1 Sensorimotor Integration

Sensorimotor integration is the process by which the central nervous system utilizes sensory input to update and modulate motor output [165]. Intact limbs require a continuous stream of information from a variety of afferent sensory organs to function properly; these include, but are not limited to skin, joints, muscles, and various other tissues [165]. The central nervous system utilizes this stream of information to make predictions about the environment to help guide movement. Therefore, accurate and fluid motor control, which allows exploration of the world, is immensely dependent on proper sensorimotor integration [166], [167]. This becomes extremely relevant when considering conditions when sensory-motor function is impaired (e.g., amputation). Understanding the basic physiology of sensation is also vital for the development of artificial sensory feedback systems since the interactions of the various components of the somatosensory system result in an accurate depiction of the location, shape, texture, and movement of tactile stimuli [167].

#### **2.5.1.1 Cutaneous Receptors**

Discriminative tactile receptors located in the skin include Meissner, Pacinian and Ruffini corpuscles, hair follicle endings and Merkel complexes [165]. Free nerve endings of the skin are categorized under nociceptors which evoke painful stimuli resulting from tissue-damaging interactions [165]. Pacinian corpuscles located deep under the skin are responsible for detecting rapid vibratory pressure and touch sensations with an optimal sensitivity in the range of 100-300 Hertz (Hz) [168]. Deformations which exceed the receptors' threshold result in a volley of action potentials [165]. The magnitude of a stimulus is encoded in the frequency of the action potentials; the greater the deformation, the higher the frequency of the action potentials [165]. Table 2.1 provides a summary of the key attributes of various cutaneous mechanoreceptors.

Table 2.1: Summary of cutaneous mechanoreceptors and their attributes

Receptors	Sensation	Signals	Type	Location	Adaptation Rate	Responsive to Continuous Stimulation
Meissner's Corpuscles	Touch: Flutter & Movement	Frequency (<50 Hz), Velocity & Direction	Encapsulated and layered	Superficial skin	Rapid	No
Pacinian Corpuscles	Touch, Vibration	Frequency (100-300 Hz)	Encapsulated and layered	Deep skin	Rapid	No
Ruffini Corpuscles	Touch Skin Stretch	Direction & Force	Encapsulated Collagen	Deep skin	Slow	Yes
Hair Follicle	Touch, Movement	Direction & Velocity	Unencapsulated	Wide distribution	Depends on signals	Yes
Merkel Complex	Touch, Pressure, Form	Frequency (15 Hz), Location & Magnitude	Specialized epithelial cell	Superficial skin	Slow	Yes
Free Nerve Endings	Pain, Touch, Temperature	Tissue damage, Contact, or Temperature change	Unencapsulated	Middle layer of skin	Depends on signals	Yes

Meissner's corpuscles are encapsulated by unmyelinated nerve endings responsible for sensitivity to light touch. These receptors are located in the superficial skin layers and possess an optimal sensitivity to stimulations lower than 50 Hz [167]. Due to the rapidly adapting nature of Meissner corpuscles, physical deformations to the corpuscle produce action potentials in nerves which quickly diminish and terminate [165]. Merkel's nerve endings are most sensitive to vibrations at low frequencies (15 Hz) [169]. These nerve endings are sensitive to touch, providing information regarding pressure and texture. Merkel complexes are slowly adapting receptors with no encapsulation, allowing for a sustained nerve response to continued mechanical deformations [165], [169], [170]. Ruffini corpuscles are slowly adapting mechanoreceptors, sensitive to skin stretch, located in the deep layers of the skin [165]. Free nerve endings are the most common type of nerve endings often located in the skin [165], [171]. The free nerve endings inhabit the middle layers of the skin and are capable of detecting temperature, mechanical stimuli (touch, pressure, stretch) and pain [165].

Cutaneous receptors transduce an external stimulus into action potentials which are ultimately perceived by the somatosensory cortex [165], [167], [172]. The time in which nerves decrease their firing due to constant stimulation (sensory adaptation) varies with the receptor. Slowly adapting receptors (Ruffini corpuscles and Merkel complex) show little adaptation to sustained stimulus, unlike receptors which demonstrate rapid adaptation (Meissner and Pacinian corpuscles). The specific sensory pathway, which transmits information regarding a stimulus, differs based on the specific modality of the pathway [165]. Pathways encoding distinct signals end in different areas of the somatosensory cortex [165], [173]–[175]. While the stimulus type is coded by the particular pathways activated, the intensity is coded through action potential frequency and the quantity of activated receptors [165].

Stimulus perception is the result of simultaneous activation of many pathways and integration of various sensory systems within the brain [165], [173]–[175]. In terms of cutaneous receptors, all pathways bypass the thalamus prior to entering the somatosensory cortex [165]. The two major somatosensory pathways traversed include the dorsal column pathway (Ruffini, Meissner, Pacinian corpuscles and Merkel complex's) and the spinothalamic tract (free nerve endings). In the dorsal column pathway, the dorsal root connects first-order peripheral nerves to the spinal cord. Axons from first-order neurons will climb the spinal cord through the ipsilateral dorsal column culminating at the medulla oblongata [165]. At the medulla oblongata, first-order neurons synapse with second-order neurons, which cross over to the contralateral side of the medulla [165]. Second-order neurons in turn synapse with third-order neurons at the thalamus, prior to terminating at the appropriate region of the somatosensory cortex [165], [166]. The spinothalamic tract transmits information pertaining to nociceptors and free nerve endings. In this tract, first-order peripheral nerves will enter the spinal cord synapsing with second-order neurons at the dorsal horn [165]. Similar to the dorsal column pathway, second-order neurons ultimately synapse to third-order neurons at the thalamus prior to terminating at the appropriate region of the somatosensory cortex [165].

### 2.5.2 Sensory Feedback

Sensory feedback mechanisms developed to aid prosthesis users in improving the control and functionality of their device must try to circumvent disruptions to sensorimotor integration caused by amputation. These sensory feedback mechanisms rely on sensors, positioned on prosthetic

devices, to provide either continuous or discontinuous streams of information. Data pertaining to the configuration of the prosthesis is then provided back to the user. There are a variety of mechanisms in which sensory feedback is communicated to prosthesis users (Figure 2.3). These various feedback methods can be organized into three categories: substitution, modality-matched and somatotopic-matched.

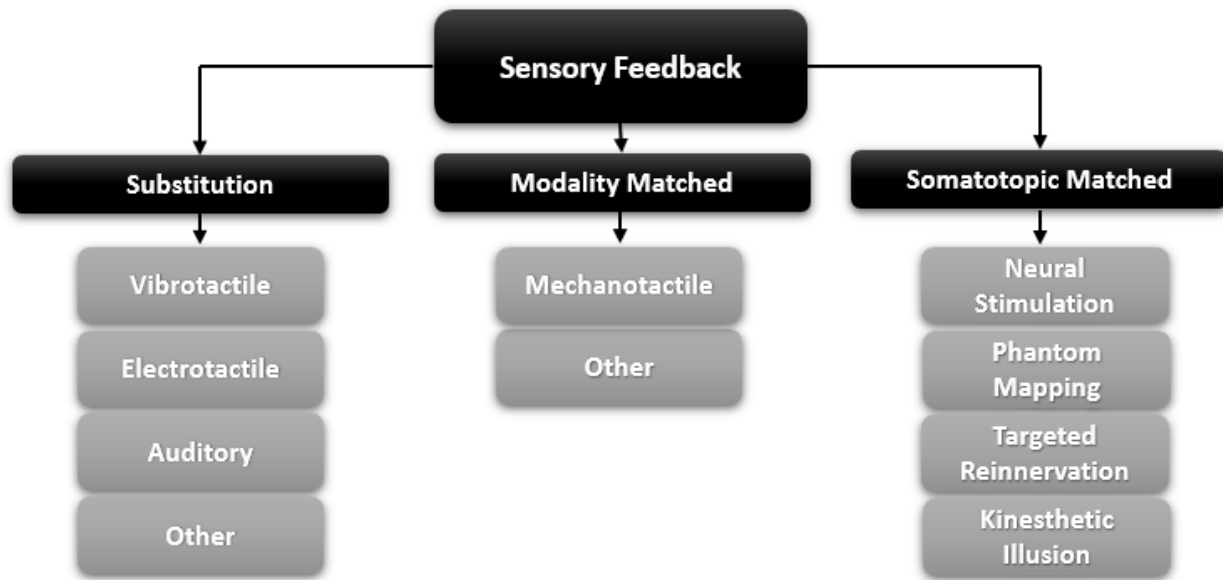


Figure 2.3: The mechanisms in which sensory feedback is communicated to prosthesis users can be partitioned into three subgroupings: substitution, modality matched and somatotopic matching.

### 2.5.2.1 Sensory Substitution

Sensory substitution techniques communicate prosthesis state information through sensory channels not physiologically representative of what a healthy limb would experience. Substitution is a technically straightforward approach as it does not consider modality or somatotopic matching [20], [176], [177]. The success of the approach depends on the capacity of prosthesis users to interpret the provided stimulus and associate it with their prosthetic device, increasing the cognitive load of the user [34]. For example, body-powered systems utilizing a hook and cable system requiring a user to learn and associate tension of the system with the movement of the prosthesis. Substitution methods can be vibrotactile (utilize mechanical vibration) [176], [178]–

[180], electrotactile (utilize electrical current) [20], [176], [181], or other methods less frequently utilized (e.g., auditory cues) [35], [36].

### Vibrotactile Feedback

Vibrotactile feedback communicates sensory information from a prosthesis to the user through the application of mechanical vibration to a strategic area of the user's skin; this is the most common type of feedback in the prosthetic literature [20], [23], [36], [176], [178], [179], [182]. Mechanical vibration activates numerous cutaneous mechanoreceptors when introduced to the skin [167]; the response of individual receptor types is a function of vibration frequency, amplitude, and duration [167]. Vibration is often a baseline standard to which other feedback methods are compared [176]. The advantage of vibrotactile systems is that they can be small and inexpensive [20], [36]. In the upper limb, vibrotactile sensory substitution is most often applied to communicate tactile information during grasping tasks. A tactor produces continuous or intermittent vibration stimuli when the prosthetic prehensor comes into contact with an object [23], [183]. For this population, the introduction of vibrotactile feedback can reduce excessive prehensor force applied by inexperienced users, but negatively influences those with previous myoelectric prosthetic experience [180]. Vibratory feedback has also been shown to increase confidence and success rates in performing grasping tasks, and to compliment visual feedback for users of upper-limb prosthesis [176], [182], [184].

In the lower limbs, vibrotactile feedback has been used to relay information on the gait cycle to prosthesis users [23], [180]. Marayong et al. developed a system comprised of two vibrating motors, a solenoid, a goniometer, and a control interface [179]. The system could produce feedback through short vibrations (motors) or a single knock (solenoid). The device was positioned between the ankle and the socket adapter, such that feedback is transmitted to the enclosed limb. This system was tested by introducing the vibrotactile feedback at swing phase during a random gait cycle as participants walked at their preferred pace on a level surface. Participants were able to perceive and differentiate between both forms of tactile feedback generated by the device during the experiment. However, a delay between the device activation and actuator output was observed. Inconsistencies in knee angle measurement also affected the device activation accuracy during the swing phase [179].

Another system consisted of six vibrators [180]. Half the actuators were positioned in front of the thigh, the remaining on the back. Using a myoelectric controller, prosthesis users were tasked to control and position a virtual ankle with different feedback conditions. The results showed, participants could detect greater changes in stimulation position than amplitude changes [180].

### Electrotactile Feedback

Electrotactile feedback uses electrodes placed on the skin to relay sensory information. Modulation of the electrical current (amplitude, frequency, pulse rate) and electrode placement have been used to transmit sensory information [20], [36], [176], [181], [184]. These parameters were mapped such that a touch or force stimulus introduced to the prosthesis corresponded to a specific electrical signal presented to the user's skin. Despite the mismatched modality, upper limb testing has shown that non-disabled participants using electrotactile feedback improve in their ability to reach and maintain specific grasp force values [185]. With electrotactile feedback, users of upper-limb prostheses demonstrated improvements in user confidence, control, and grasp force discrimination [20], [176], [181]. Despite these improvements over vibrotactile feedback, there was a lower acceptance rate of electrotactile systems [20]. Evoked sensations correlate with multiple stimulation parameters such as contact force, current, voltage and electrode size, as well as physiological factors such as skin location, thickness, and electrochemistry [20], [36], [181]. These varying factors reduce repeatability of a specific sensation, hindering learning of the substitution system. Participants have also demonstrated adaptation to electrotactile stimulation over time [181].

### Auditory Feedback

Auditory feedback has been demonstrated as a technique to convey contact of a robotic hand to an object, the position of the hand's digits and an intended grasping pattern [35], [36], [186]. Methods of auditory feedback have provided information on the state of a robotic or prosthetic hand through varying frequencies of tones or sounds. Audio-based sensory substitution systems inherently require training for effective use. The user must learn to interpret auditory stimulation as tactile stimulation and associate these audio cues with specific prosthetic limb states. Although with training a prosthesis user may be able to utilize this feedback system, the substitutive challenge may create an excessive cognitive burden and a significant barrier to effective use.

### Other Substitution Methods

Other methods have been investigated to achieve sensory substitution. For example, one mechanism used a motorized elbow to apply extension torques to the elbow proportional to grasp force [184]. Many of these other substitution methods have yet to be studied extensively with prosthesis users.

#### **2.5.2.2 Modality Matched**

Modality matched feedback mechanisms are those in which communicated stimuli are matched in type of sensation. These systems have the potential to decrease the cognitive load required of users as the modality of the feedback signal does not require interpretation. Common modality matched feedback methods such as mechanotactile [17], [20], [36] and thermal stimulation [25], [36], [187] have been utilized on a number of upper-limb prosthesis types; they have, however, not been implemented on lower-limb prosthetic devices.

#### Mechanotactile

Mechanotactile feedback has been used to relay touch or grasp sensations from the terminal device to upper-limb prosthesis users [17], [20], [36], [188]. Touch and grasp are communicated as a perpendicular force or pressure applied to a specific location on the user's body [17]. Tactors used to provide mechanotactile feedback allow users to differentiate between various levels of graded forces or pressures [17], [188]; there have been many tactors designed for this purpose [17], [20], [23], [25], [36], [182], [183], [188]. When compared to other feedback mechanisms, greater time delay, increased power consumption, and increased size is major drawbacks of modality matched feedback mechanisms [17], [20], [36], [188].

#### **2.5.2.3 Somatotopic Matching**

Somatotopic matched methods deliver feedback such that prosthesis users sense the stimulus as though it were applied to the same corresponding location of their missing limb. Compared to substitution or modality matching methods, somatotopic matched feedback may further reduce the cognitive burden for prosthesis users [34], implying reduced training and attention to interpret feedback signals. Somatotopic matching techniques are generally also matched in modality, through direct neural stimulation [189], the rerouting of sensory nerves using TR to the skin [24] or through use of the KI [29].

### Peripheral Nerve Stimulation

Following amputation, original afferent pathways are preserved proximally and might be used to restore physiological feedback through strategic electrical stimulation [24]. Peripheral nerve stimulation has been investigated in prosthesis users using a number of electrode designs: nerve-cuff electrodes [21], [31], longitudinal intrafascicular electrodes [189], and Utah slant array electrodes [190]. Through peripheral nerve stimulation, individuals with amputations have reported referred sensations to the missing limb including touch and pressure, as well as proprioceptive sensations such as position sense or movement [191]. Through manipulation of the electrical frequency and current, investigators were able to influence the location, magnitude, and modality of the solicited sensations [21], [31], [192]–[194]. Successful excitation of a particular sensation in a specific location is dependent on the system's ability to selectively stimulate specific sensory afferents in a particular fascicle [189], [192], [195]–[197].

### Phantom Mapping

Phantom mapping depends on the ability to consistently elicit sensations of the missing extremity through stimulation of skin overlaying the residual limb of a person with amputation [34], [188]. This feedback mechanism requires identification of areas on the residual limb that elicit a specific and consistent sensation to guide tactor placement. Tactors (mechanotactile [17] or vibrotactile [23]) are positioned at locations on the amputated limb which elicit sensations pertaining to the missing limb, and are linked to relevant inputs from the prosthesis. When activated, the tactors provide somatotopic and potentially modality matched sensations to the user. Phantom mapping has been shown to improve feedback discrimination for upper-limb prosthesis users [34], [188], but has not been applied to those utilizing lower-limb prostheses. Phantom mapping has the potential to provide both somatotopic and modality matched feedback to prosthesis users; however, it is limited by the reliability and level of sensations experienced by the individual.

### Targeted Reinnervation

Targeted reinnervation (TR) a surgical technique where the sensory and motor nerves formerly innervating amputated limbs are reinnervated to new muscle and skin sites [22], [198]–[201]. After targeted muscle reinnervation, there exists a greater number of muscle signals available for prosthetic control [22], [28]. Users of upper-limb prostheses have been able to exploit this increase in control sites to use myoelectric prostheses (electrically controlled prosthetic devices) in a more

intuitive manner [22], [199]. Although the surgery was initially designed to increase the number of motor control sites for myoelectric prostheses, it was found that the redirected sensory afferents also reinnervated overlying skin [22], [24], [27], [198]. In targeted sensory reinnervation, skin surrounding the targeted muscle is denervated, then reinnervated with afferent fibers from residual nerves [198], [200]. As a result, when reinnervated areas of the skin are stimulated, prosthesis users experience sensations from their missing limbs [22], [24], [27], [198]. Similar to phantom mapping, the reinnervation creates an expression of the hand map, once stimulated causes individuals to experience sensations about the amputated limb [24], [198]. Unlike phantom mapping, targeted sensory reinnervation allows the reinnervated sites to be selectively placed and provide repeatable sensations [24], [198]. Ongoing research is required to develop effective means of utilizing these reinnervated sensory sites to provide sensation within wearable sockets for long term use, unlike the robust progress made in motor control.

#### **2.5.2.4 The Kinesthetic Illusion**

The kinesthetic illusion (KI) is a physiological phenomenon by which the introduction of vibration to musculotendinous regions of a limb induce movement sensations, even though the limb remains stationary [18], [202], [203].

##### Proprioceptors and Kinesthesia

Kinesthesia and proprioception are often studied in parallel due to the collective involvement of peripheral afferent systems. Proprioception is the collection of systems which facilitates an individual's spatial awareness of limb and body positioning [203]. This overarching framework includes kinesthesia. Kinesthesia can be defined as the summation of afferent signals resulting in a sense of movement [203]. Although kinesthesia in particular and proprioception in general play important roles in facilitating a spatial awareness of one's limbs and body, kinesthesia (the sense of movement) has important implications in both non-disabled and prosthetic movement control. Various afferents contribute to kinesthesia. Movement causes a deformation of the muscles, tendons, skin, and other tissues surrounding joints. These deformed tissues contain mechanically sensitive receptors which contribute to the kinesthetic sensation [203]. Although a wide range of receptors exist within tissues, past efforts have shown that muscle spindles are the dominant contributor to kinesthesia [18], [203]–[206].

## Muscle Spindles

Muscle spindles are located deep within muscle – within the intrafusal layer – parallel to the extrafusal (outer) fibers. They are sensory receptors, with the primary role of detecting changes in muscle length. There are four types of muscle spindles: nuclear chain fibers, dynamic and static nuclear bag fibers (bag1 and bag2 fibers respectively) and general afferent nerve fibers. Nuclear bag and chain fibers are responsible for detecting dynamic and sustained muscle contractions, respectively [207]. Muscle spindles convey muscle deformation to the central nervous system using sensory fibers which traverse the dorsal column pathway [165], [206], [208].

Muscle spindles possess both sensory and motor components. Sensory signals are communicated through the annulospiral endings (type Ia sensory fibers) and the flower-spray endings (type II sensory fibers) [165], [208]; these sensory fibers transmit information through stretch-induced action potentials [165], [208]. The motor activities of muscle spindles are governed by the alpha motor neurons and the fusimotor neurons (gamma and beta motor neurons). Alpha and gamma motor neurons supply extrafusal fibers and intrafusal fibers, respectively, while beta motor neurons supply both extrafusal and intrafusal spindles [165], [208]. Though alpha motor activation results in large force generation through contraction of the extrafusal muscle spindles [165], [208], the activation of fusimotor neurons results in a stiffening of the terminal segments of the muscle fibers [165], [208]. Fusimotor neurons can be either static or dynamic depending on their effect on the annulospiral and flower-spray neurons and the type of muscle fiber innervated [165], [208]. Static neurons innervate the bag2 fibers and increase activation of both sensory afferents [165], [208]. Dynamic neurons increase activation of annulospiral afferents through stiffening of the bag1 intrafusal fibers [165], [208].

The role of muscle spindles in proprioception and kinesthesia is thought to be significant, and has often been investigated using the KI [203], [206]. Vibration to musculotendinous regions of a limb induces movement sensations in a similar manner to that of natural muscle stretch or contraction. When a muscle is stretched, changes to the muscle are conveyed to the spinal cord through the annulospiral sensory fibers. Flower-spray sensory neurons respond in a similar manner to muscle strain, but with lower velocity sensitivity [165], [208]. While this occurs, signals from the annulospiral neurons also transmit to alpha motor neurons of the stimulated muscle [165], [208]. As a result, alpha motor neurons stimulate extrafusal fibers which resist the stretch [165], [208].

The annulospiral sensory signals also inhibit the alpha motor neurons of the antagonist muscles through inhibitory interneurons [165], [208]. The combined efforts of both afferent and efferent nerves ultimately result in the interpretation of limb movement.

### Eliciting the Kinesthetic Illusion

Consistency in elicitation and manipulation of the KI is essential for its effective use as a sensory feedback mechanism for prosthesis users. Consequently, understanding how vibration is introduced is critical in achieving this. With a few exceptions, the vibratory stimulus is usually introduced as a sinusoidal waveform with two key parameters: frequency and amplitude [18], [206]. However, it is difficult to state the importance of one variable without fully defining the other. Goodwin et al. were successful in eliciting the kinesthetic percept using a hand-held vibrator oscillating at 100 Hz with a 2 mm amplitude (peak-to-peak) [209]. Roll et al. determined that perceived velocity increased when the vibratory frequency was increased from 10 to 70 Hz, by systematically manipulating frequency and monitoring perceived percept velocity [204]. Higher frequencies (80 to 120 Hz) reduced the percept velocity [204]. However, this study allowed amplitude to vary between 0.2 to 0.5 mm, potentially functioning as a confounding variable. Subsequent literature has reported eliciting the movement percept with a bandwidth of 10 [210] to 160 Hz [211]. Clark et al. argued that amplitude contributes significantly to the movement percept [212]; they found that decreasing amplitude results in a decreased velocity of the movement illusion. In previous literature, amplitude has also varied broadly, from 0.4 [205], [213] to 12 mm [214] (peak-to-peak). Schofield et al. undertook a comprehensive study of the effects of vibratory parameters, performing a systematic manipulation of both frequency and amplitude [18]. Incorporation of both parameters allowed them to assess individual effects while also identifying that frequency and amplitude held a co-dependent relationship. They reported that a bandwidth of 70 to 110 Hz and amplitude range of 0.2 to 1 mm (peak-to-peak) was capable of producing the movement illusion. Their work also indicated that higher amplitudes result in a greater movement sensation [18]. The optimal parameters used to elicit the illusion are therefore proposed to be at the center frequency of the abovementioned bandwidth (90 Hz) and amplitude of 1 mm (peak-to-peak).

### The Kinesthetic Illusion in the Upper Limbs

Eklund et al. were the first to demonstrate that administering vibration over a tendon or muscle could cause a sense of limb movement [211], [215]. Goodwin et al. further developed this finding by outlining specific contributions of spindle afferents [209]. They reported that alterations in kinesthetic perceptions were not present when vibration was applied to joints or skin-overlying joints [209]. In fact, vibration introduced to a muscle at specific frequencies and amplitudes can activate muscle spindles and yield illusionary sensations of limb movement [209]. If appropriately administered, these sensations can lead to misjudgments in limb position, sensations of limbs moving to non-anatomical positions, or experienced illusionary distortion of objects or body parts in contact with the stimulated limb [209].

Additional studies suggest that volitional control (efferent outflow) may supplement afferent inflow from sensory organs, predominantly those of muscle spindles, to build a coherent movement percept [216]. Beyond amplitude and frequency, the experimental setup used in administering the illusion may impact the movement percept. Craske et al. have shown that limb positioning that increases the muscle stretch also increases the sensitivity to the movement percept [217], whereas contraction and fatigue of a muscle decrease the perceived movement velocity [217]. If participants are able to view their stimulated limb [218], [219], experience movement in the contralateral arm [220], [221], or are provided with tactile feedback [210], [222], a significant reduction of the illusionary sensations is experienced. The “kinesthetic aftereffect”, an additional aspect of the KI, is often experienced as the vibrated limb returns to its original position. This aftereffect is assumed to be a result of motor-cortical processing of the unbalanced sensory information from the stimulated and unstimulated muscle spindles [214].

Contractions of the muscle to which a vibratory stimulus is applied may also result in a tonic vibration reflex (TVR). Similar to the KI, TVR manifests from spindle afferent activation [209], [223], [224]. As a result, TVR diminishes sensations felt from the KI since the direction of the vibrated muscle contraction is inverse to the KI [202]. Depending on the state of joints and activities of muscles during vibratory stimulation, individuals can experience either the isotonic or isometric TVR. Isotonic TVR occurs while joints are free to move during vibratory stimulation; it is characterized by an onset latency of roughly 30 seconds and a long slow rise to the movement plateau lasting roughly 20-60 seconds [223]–[231]. Compared to isotonic TVRs, the isometric

TVR persists for a few milliseconds, with a negligible onset latency, and derives from muscle contractions, during vibratory stimulation, of fixed immobile joints [223]–[231]. The effects of TVR can be mitigated by asking study participants to relax during experimentation and by eliminating visual feedback [220]; however, TVR cannot always be suppressed.

Several studies have also investigated the cortical involvement during illusory movement sensations. One of the first studies examining cortical activity through functional magnetic resonance imaging was conducted by Romaguiera et al. [232]. They found that the perception of movement illusions relates to activation in the sensorimotor, premotor, supplementary motor and cingulate motor areas. Other studies have also identified the involvement of the somatosensory cortex area in stimulus perception [233]. Casini et al. highlighted the contributions from the motor and posterior parietal areas in illusory hand movement by means of magnetoencephalography – a functional neuroimaging technique for mapping brain activity [234].

#### Functional Use of the Kinesthetic Illusion for Upper-Limb Prosthesis Users

Currently, a single study has examined the functional use of the movement illusion for individuals with upper-limb loss who have undergone TR [29]. Marasco et al. demonstrated that providing this physiologically relevant movement sensation to upper-limb prosthesis users could produce perceptions of complex hand grip movements, improve the efficiency of reach and grasp movements and establish a sense of agency (ownership) over movements [29].

#### The Kinesthetic Illusion in the Lower Limbs

Vibration introduced to the lower limbs of non-disabled individuals has been shown to result in the KI, vibration-induced falling, and to produce other effects on gait during ambulation [215], [235], [236]. Vibration to the musculotendinous regions of the hamstring has been shown to evoke a knee extension movement percept. With three non-disabled participants, Honda et al. quantified the KI that was elicited with vibration of two different hamstring muscles (the bicep femoris and semitendinosus muscle) [237]. They attached goniometers to both knee joints of a participant lying prone. Both the left (stimulated) and right (reference) knee angles were initially set to 45 degrees. The participant was instructed to demonstrate experienced movement percepts of the stimulated limb using the reference limb. The vibration of the left leg was initiated and stopped when the reference leg reached a predetermined angle. For all trials, each participant reported feeling as if their vibrated limb was extending. Two out of the three participants demonstrated a quicker

movement percept with the stimulation of the semitendinosus muscle when compared to the biceps femoris muscle. The authors explained this quicker rate movement percept by noting that the semitendinosus muscle contributes greater to knee flexion/extension than the biceps femoris, which contributes more to hip joint movement.

Vibration-induced falling refers to the perception of body movement while remaining stationary (with the eyes closed) as a result of vibratory stimulation of the leg muscles [215], [235], [236]. For example, vibration of the Achilles tendon produces high levels of activation of spindle endings in the ankle plantarflexors [215]. These high levels of afferent activity are thought to be interpreted by the brain as an increase in muscle length [215], [235], [236]. Since a change in muscle length is normally associated with body movement, individuals try and correct for this deviation (e.g., step backward) [215].

Vibration has also been used to influence ambulation. During stationary marching, simultaneous vibratory stimulation of the hamstring, in both limbs, has been shown to result in the perception of forward progression [238]. The speed of progression can be modulated through simultaneous stimulation of different muscle groups in both limbs [238]. Stimulation of muscle groups in only one of the lower limbs during stationary marching is perceived as walking along an arc [238]. All these works demonstrate that it is possible to generate the KI in the lower limbs of non-disabled individuals. However, kinesthetic feedback has yet to be investigated in those with lower limb amputation or incorporated in a sensorimotor prosthesis design. There currently exists a gap in the literature concerning the functional use of the KI for users of lower-limb prostheses.

### 2.5.3 Concluding Remarks on Prosthetic Sensory Feedback Mechanisms

Ideal sensory feedback systems should communicate the state of the prosthesis to users in an intuitive, non-invasive, and relatively inexpensive manner. In this context, somatotopic and modality matched mechanisms show the greatest promise in communicating sensory input. While systems providing touch and force sensations have been studied extensively, those focusing on providing the user with a sense of joint position and movement should be investigated further. Allowing an individual to sense the position of their prosthesis in space without requiring visual attention has the potential to greatly improve dynamic prosthetic control. The KI, a physiological phenomenon by which the introduction of vibration to musculotendinous regions of a limb induces movement sensations, demonstrates potential as both a somatotopic and modality matched

feedback mechanism capable of resorting movement sensations. The KI has been explored for individuals using upper-limb prostheses, particularly those who have undergone TR. However, the response of individuals with lower-limb amputation and prosthesis users who have not undergone TR remains unknown.

### 3. Kinesthetic Illusion in Individuals with Lower-Limb Amputation

#### 3.1 Introduction

As outlined in Chapter 2, it has been shown that, with appropriate stimulation, the muscle spindles in the residual limb of individuals with an upper-limb amputation having undergone targeted reinnervation (TR) can still evoke a kinesthetic response [29], even with the anatomical and physiological changes resulting from amputation. This is achieved through the kinesthetic illusion (KI), a phenomenon whereby mechanical vibration at the musculotendinous regions of limbs elicits a perception of limb movement [18]. However, it is not known whether individuals with non-TR lower-limb amputations can still experience this kinesthetic sensation. As both a somatotopic and modality matched approach to sensory feedback, the KI offers an intuitive way of restoring movement sensations to prosthesis users. Restoring kinesthesia could allow individuals using lower-limb prostheses to distinguish when their prosthesis is moving, potentially improving balance [9], gait [16] and overall quality of life [6]. However, techniques used to administer the KI need to be effectively incorporated into prosthetic devices, as existing prosthetic devices are incapable of providing sensory feedback. Currently, prosthesis users rely on an open-loop movement control system where they initiate movement of their prosthesis; however, information pertaining to movement of the prosthetic limb is not relayed back to users (Figure 3.1). This chapter describes an exploratory study to establish whether individuals with non-TR lower-limb amputations can still experience the KI.

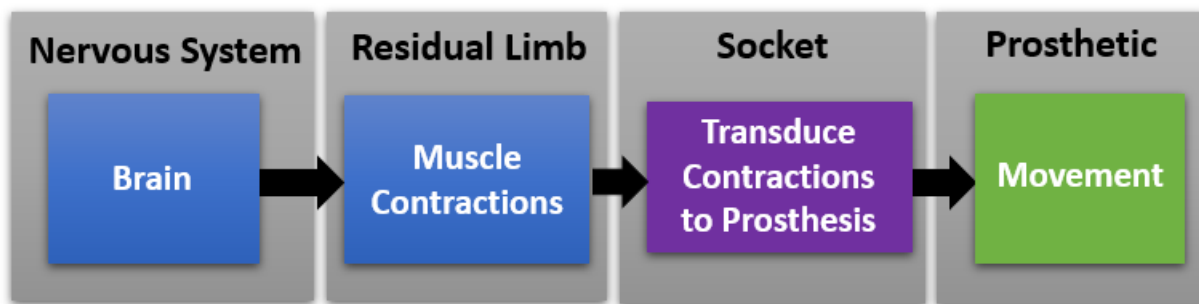


Figure 3.1: Users of prosthetic devices initiate muscle contractions and resulting movements of the residual limb are transferred to the socket interface to biomechanically control the movement of the prosthesis. This is an open-loop control system that does not communicate the state of a prosthesis to user's in a functional or intuitive fashion.

## 3.2 Methods

### 3.2.1 Participants

Nine participants with lower-limb amputations (3 transfemoral, 4 transtibial, 1 knee disarticulation, 1 bilateral – knee disarticulation and transtibial) were recruited (7 males, 2 females; age:  $43.2 \pm 19.6$  years; mean  $\pm$  standard deviation). Participant information is summarized in Table 3.1. All participants had not undergone TR and reported no current or previous neurological or muscular health conditions, other than the amputation. All participants provided verbal and written informed consent prior to participating in the study (Appendix A). This study design was approved by the research ethics board at the University of Alberta (Pro00063695) and conducted according to the criteria set by the declaration of Helsinki.

Table 3.1: Summary of participant information.

<b>Participant</b>	<b>Amputation</b>	<b>Cause</b>
P1	Left Transfemoral	Vascular
P2	Right Transfemoral	Trauma
P3	Right Transfemoral	Vascular
P4	Right Transtibial	Trauma
P5	Left Transtibial	Vascular
P6	Left Transtibial	Vascular
P7	Left Transtibial	Trauma
P8	Right knee disarticulation	Trauma
P9	Left knee disarticulation; Right leg transtibial	Trauma

### 3.2.2 Experimental Setup

The vibration was introduced to the participants using a hand-held vibratory system (VB200, Vibrasense, Besancon, France) attached to a flat-faced probe tip (2.7 cm diameter) (Figure 3.2).

Participants were seated in a chair or laid on a bed, depending on the muscle group being stimulated. Consideration was given to limb positioning such that relaxation of the tested muscle group was promoted, as muscle contraction has been shown to influence the KI [204], [239]. Video and audio footage of participant trials was digitally recorded. This experimental procedure was adapted from work performed in the upper-limb transhumeral population [29].

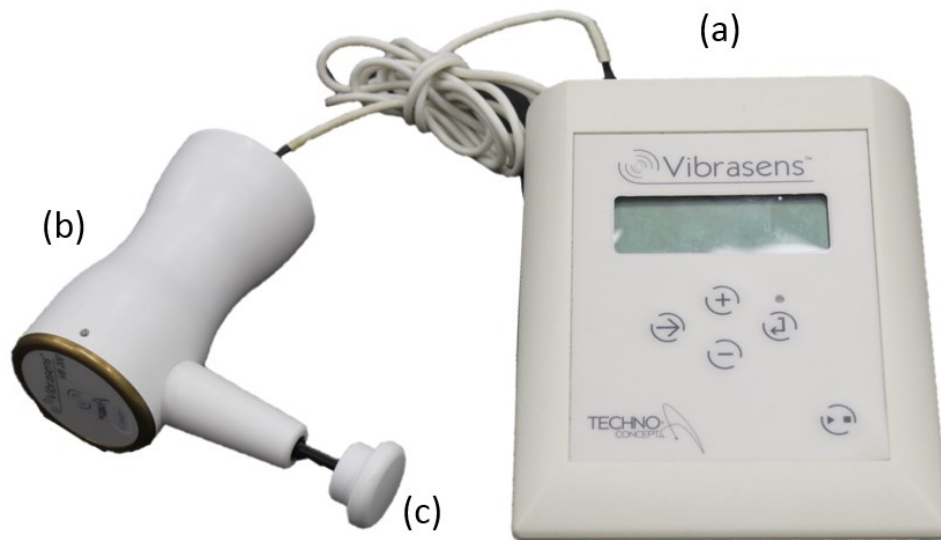


Figure 3.2: Vibrasense VB200 vibratory system. (a) the controller of the vibratory actuator, which allows for change of vibration parameters (frequency, amplitude); (b) the hand-held segment or vibrator actuator that produces the vibration; and (c) the tactor head contacting the participant's limb.

### 3.2.3 Experimental Protocol

The experimental protocol was divided into two parts: percept mapping and illusion quantification. Percept mapping is the process of identifying sites on the residual limb which elicit strong and consistent movement percepts. KI quantification includes the use of motion capture (mocap) to quantify the kinematics of the experienced movement illusion and its strength. Participants were not informed that the intent of the study was to investigate movement sensations nor provided with specific information describing the KI. During the experiment, participants were fitted with noise-canceling headphones and an eye mask to occlude vision. These precautions were taken as vision

or environmental distractions might affect the participant's ability to experience the movement percept [218]. Participants were also asked to remove their prosthesis for the duration of the experimental procedure.

### **3.2.3.1 Percept Mapping**

For each participant, vibration testing was conducted to explore possible movement percepts and identify locations within the residual muscle that, when vibrated, consistently elicited strong kinesthetic sensations. Participants were positioned with their residual limb supported for comfort and such that the target muscle group could be easily subjected to vibration. Using the hand-held vibrator, vibration at a frequency of 90 Hertz (Hz) and an amplitude of 1 mm (peak-to-peak) was introduced to the participant's residual limb. These vibration parameters were previously determined to be optimal for elicitation of the KI [18]. Participants were instructed to report "any sensations beyond simple vibration". The hand-held vibrator was systematically pressed into various locations on the residual limb with 2 to 5 Newtons of pressure as measured by an in-line load cell (iLoad Pro, Loadstar Sensors, Fremont, USA). Each location was tested for approximately 20 seconds prior to moving to the next. If a participant reported a kinesthetic sensation, probing of the surrounding tissue was conducted to identify the location most consistently producing the strongest kinesthetic sensation. The participant would be asked to compare adjacent stimulus locations with the investigator prompting: "Which location gives the strongest sensation of movement, number one or number two?" This was continued until a location consistently producing an illusion stronger than the surrounding tissue was identified. If participants failed to experience movement precepts after 10 minutes of testing, they were seeded with information that "some participants report feeling movement in their knee/ankle". If the participant continued not to experience any movement percepts after an additional 5 minutes of testing, they were informed that "some participants report that their knee/ankle is flexing/dorsiflexing" in the expected direction.

### **3.2.3.2 Illusion Quantification**

#### Psychophysical Quantification

Following each trial, the psychophysical strength of the illusion was quantified using a 5-point Likert scale [18]. The participant was prompted: "On a scale of one to five, we want you to describe how strong the sensation of leg movement is; with one being no movement sensation, and five

being an extremely strong movement sensation.” In addition to reporting on the strength of movement illusion, the participant was asked to mimic the experienced movement using their intact limb, with respect to the perceived direction, range, and speed of movement.

### Illusion Kinematics

At each stimulus location at which a sensation of movement was elicited, participants were instructed to use their contralateral leg to match what they felt in configuration, velocity, and duration, similar to techniques employed in the upper-limb literature [18], [29]. The final stimulus location most consistently eliciting the strongest movement percept was marked on the participant’s skin with a felt-tipped marker. Once a site producing a strong and consistent illusion was determined, demonstrations by the contralateral leg were captured using an optoelectronic mocap system (OptiTrack, OR, USA). Stimulation was repeated 30 times, with the corresponding movement demonstration captured, to quantify each movement percept experienced by the individual. Two mocap plates, each containing four reflective markers, were placed proximal and distal of the contralateral knee joint or ankle joint for individuals with transfemoral or transtibial amputations, respectively. The mocap plates were used to quantifying the demonstrated 3-dimensional (3D) movement; limb segments were assumed to behave as rigid bodies.

Once the plates were attached to the limb segments, a calibration procedure was performed. The calibration procedure aimed to align the rotation axis of the joint of interest to that of the global coordinate frame of the mocap system. The positioning of the participant’s limb for calibration was dependent on which muscle group was being stimulated. The muscle of the anterior thigh and entire lower leg (calf and shin) were accessible while the participant sat on a chair, whereas, proper stimulation of the hamstrings required a participant to lay prone on a bed. In both settings, mocap plates were attached proximal and distal to the knee or ankle of the participant such that they were visible to the mocap cameras. When seated on the chair, the calibration position was taken with the participant in a relaxed seated position, and the chair was positioned such that the flexion/extension axis of the participant’s knee rotation was aligned to the Z-axis of the mocap coordinate system. On the bed, the participant’s intact limb was positioned on a 45 degree incline while lying face down, similar to Honda et al [237]. The bed was positioned such that the flexion/extension axis of the participant’s knee rotation was aligned to the Z-axis of the mocap coordinate system. After placement of the mocap plates and proper positioning, the positions of

the mocap markers on the plates were sampled by the mocap system, used to generate local coordinate frames and ultimately rotation matrices describing the plates position. This rotation matrix was then applied to subsequent coordinate frames of the mocap plates. Finally, Cardan angles representing the joint movement of interest were extracted from the relative change in orientation of the corresponding limb segments [240]. Calibration was performed at the start of testing, after transitions to testing of a different muscle group (e.g., quadriceps to hamstrings) or if the participant deviated from their initial start position (e.g., repositioning due to comfort).

The joint coordinate frame outlined by the International Society of Biomechanics was used: X-axis – abduction/adduction; Y-axis – axial rotation; and Z-axis: flexion/extension [241]. The International Society of Biomechanics also recommends a ZXY moving axes Cardan angle rotation sequence, as the flexion/extension axis has been shown to be the most important in human movement, followed by abduction/adduction and axial rotation [241]. The ZXY sequence was used to calculate the 3D joint angles of the participant's intact knee or ankle. For both the knee and ankle joint, there is no risk of gimbal lock as both joints are unable to abduct/adduct to 90 degrees [241], [242]. A digital video recorder (Pro9000, Logitech, Morges, Switzerland) was also used to capture the demonstrations and provide a reference for mocap analysis.

### Calibration

Cardan angles describing the movement of each joint were calculated using the following method: Each mocap plate's coordinate frame, at the time of calibration, was defined by Equation 3.1:

$$T_{Calibration\ Position} = \begin{bmatrix} X_i & Y_i & Z_i \\ X_j & Y_j & Z_j \\ X_k & Y_k & Z_k \end{bmatrix} \quad (3.1)$$

where the columns represent the 3D coordinates of the X, Y, and Z unit vectors of the mocap plate's coordinate frame of a given segment, after the proper positioning of the participant's intact limb on the chair or bed. The matrix represents a single, constant matrix, which was not time-varying. The set of time-varying coordinate frames of the mocap plates defined during demonstrations of movement percepts was designated as the provisional coordinate frame ( $T_{provisional}$ ). Each mocap plate's coordinate frame was calibrated relative to the global coordinate frame of the mocap system. Since the global coordinate frame of the mocap system can be set up

as any orthonormal basis, it was set to match the frame recommended by the International Society of Biomechanics. As a result, the calibration matrix can be calculated by solving Equation 3.2:

$${}^{[T_{Calibration\ Position}]}[R_{Calibration}] = \begin{bmatrix} 1 & 0 & 0 \\ 0 & 1 & 0 \\ 0 & 0 & 1 \end{bmatrix} \quad (3.2)$$

Solving for  $R_{Calibration}$  and using a property of the special orthogonal rotation group ( $T^{-1} = T^T$ ) results in Equation 3.3:

$$R_{Calibration} = [{}^{T_{Calibration}}]^T \begin{bmatrix} 1 & 0 & 0 \\ 0 & 1 & 0 \\ 0 & 0 & 1 \end{bmatrix} \quad (3.3)$$

This calibration matrix is only generated once for each mocap plate and applied to all subsequent frames of the mocap plates.

### Joint Angle Calculation

After calibration, rotation matrices encoding the time-varying orientation of both the proximal and distal mocap plates (Equation 3.1) can be multiplied by their respective calibration matrix to yield a rotation matrix representing the orientations of the appropriate limb segment (Equation 3.4):

$${}^{T_{Limb\ Segment}} = [{}^{T_{Provisional}}][R_{Calibration}] \quad (3.4)$$

Then, a rotation matrix encoding the joint angles of interest is determined through Equation 3.5:

$${}^{proximal}_{distal} R_{Joint\ Angle} = [{}^{T^T_{Limb\ Segment - proximal}}][{}^{T_{Limb\ Segment - distal}}] \quad (3.5)$$

$${}^{proximal}_{distal} R_{Joint\ Angle} = R_{ZXY}(\alpha, \beta, \gamma) = \begin{bmatrix} c\gamma c\alpha & -s\beta s\gamma c\alpha & c\alpha s\gamma + c\gamma s\beta s\alpha \\ c\alpha s\beta s\gamma + c\gamma s\alpha & c\beta c\alpha & -c\gamma c\alpha s\beta + s\gamma s\alpha \\ -c\beta s\gamma & s\beta & c\beta c\gamma \end{bmatrix} = \begin{bmatrix} r_{11} & r_{12} & r_{13} \\ r_{21} & r_{22} & r_{23} \\ r_{31} & r_{32} & r_{33} \end{bmatrix} \quad (3.6)$$

The associated rotation matrix of the recommended ZXY moving axes Cardan angle rotation sequence (International Society of Biomechanics) is used to extract the joint angles (Equations 3.7-3.9):

$$\alpha = \text{flexion angle} = A \tan 2(-r_{12}, r_{22}) \quad (3.7)$$

$$\beta = \text{abduction angle} = A \sin(r_{32}) \quad (3.8)$$

$$\gamma = \text{axial rotation angle} = A \tan 2(-r_{31}, r_{33}) \quad (3.9)$$

where  $cx$  and  $sx$  represent  $\cos(x)$  and  $\sin(x)$ , respectively,  $A\sin(x)$  represents  $\arcsin(x)$ , and  $A\tan 2(x)$  computes  $\arctan(x)$  using the sign of each quadrants. The joint detection algorithm was adapted from Hamill et al. [240]. The software which implements the joint angle calculations can be found in Appendix B.

### 3.2.4 Experimental Data Processing and Analysis

Mocap data were processed using MATLAB 2016b (MathWorks, Natick, MA, USA). An orthonormal coordinate frame was derived for each mocap plate. These local coordinate frames were used to obtain a rotation matrix defining the time-varying orientation of each mocap plate. Each mocap plate contains four markers: top left (tLeft), top right (tRight), bottom left (bLeft) and bottom right (bRight). An orthonormal coordinate frame was generated by first creating a position vector along the X-axis (Equation 3.10). The Y-axis was determined by crossing the X position vector by another vector along the plane of the marker plate (Equation 3.11). Finally, the Z-axis was generated through the cross product of the X-axis and Y-axis (Equation 3.12). These axes were then used to generate a rotation matrix, encoding the orientation of each mocap plate (Equation 3.13).

$$\vec{t}_x = tLeft - bLeft \quad (3.10)$$

$$\vec{t}_y = \vec{t}_x \times (bLeft - bRight) \quad (3.11)$$

$$\vec{t}_z = \vec{t}_x \times \vec{t}_y \quad (3.12)$$

$$T = \{\vec{t}_x, \vec{t}_y, \vec{t}_z\} \quad (3.13)$$

Cardan angles representing the respective joint movement were then extracted using the joint angle calculations outlined above. Since gait cadence of non-disabled and prosthesis users does not exceed 2 Hz [73], [80], [97], [243], [244], a second order, low-pass Butterworth filter with a cut-off frequency of 4 Hz was used to eliminate potential high-frequency noise.

### 3.3 Results

While blind to the researcher’s intent, two participants (P1 and P4) spontaneously reported movement percepts about their phantom knee (P1) or ankle (P4) in the direction characteristic of the KI. With continued stimulation of illusion sites, participants P1 and P4 would intermittently report a stationary phantom limb materializing in the same orientation as their intact limb. Participants P2 and P3 experienced a movement sensation more representative of the patellar reflex, i.e., a singular outward jerk of the knee. Participants P2 and P3 did not experience the patellar reflex consistently as this sensation ceased after 1-2 instances. The remaining participants did not experience any movement sensations even with additional seeding information (Table 3.2). However, excluding participants P5 and P7, vibratory stimulation materialized a phantom limb for participants unable to experience any movement percepts (P6, 8-9). This phantom limb was positioned similarly as the participant's intact limb; it was absent prior to stimulation and retreated following the termination of stimulation. The phantom limb was reported to be most prominent when the actuator was applied with enough force to deform the skin and be well-seated in the muscle belly of the participant’s residual limb. Vibration also induced tingling, pressure sensation, temperature variations, and pain on the phantom limb.

Table 3.2: Time intervals and information provided to participants to experience movement sensations.

<b>Testing Time (Minutes)</b>	<b>Information Provided</b>	<b>Participants Experiencing Movement Sensations</b>
0-10	None (participants uninformed)	P1-P4
10-15	“Some participants report feeling movement in their knee/ankle”	None
15-30	“Some participants report that their knee/ankle is flexing/dorsiflexing”	None

### 3.3.1 Percept Mapping

#### 3.3.1.1 Participants that Experienced the Kinesthetic Illusion

##### Participant P1: Transfemoral

Shortly after the administration of vibration, participant P1 described “a sinking feeling”, stating that the vibration was “trying to push [their] leg back” (i.e., bend the knee) and that they had “to oppose it”. The participant also articulated the sensation felt as if “the top of [their] thigh [was] not working” and that this forced “the shin [to move] in order [to] compensate”. The participant explained that the “pull sensation... [felt] so strong” and that they had “to compensate by pushing” (i.e., kicking out). When they did this, the pushing sensation transformed into a “kicking sensation”. This sensation was experienced in multiple sites on the anterior segment of the residual limb (Figure 3.3). After informing the participant to relax and embrace the sensations felt, they continually reported movement perceptions of knee flexion in multiple sites on their residual limb. The participant reported a 4 or 5 on the Likert scale for each location producing the illusion on both the anterior and posterior portions of their leg. Vibrations located on Site 1 ultimately produced the most consistent perception of knee flexion; this was the site used for determining the illusion kinematics. In the posterior portion of the residual limb, the participant experienced similar sensations such as their “[phantom] leg [appearing]” similar to their intact leg, including “everything from knee to toes”, a “pull slightly inwards”, and their leg “pushing down”. The movement percept pertaining to knee extension was experienced through the stimulation of a location mirroring Site 1 on the posterior segment of the participant’s residual limb. Although the strength of the illusion was reported as a 4 on the Likert scale, it occurred with a lower frequency than that of Site 1.



Figure 3.3: The anterior lateral view of the residual limb of P1 (left thigh): the numbers (written in red ink) represent the center of areas that, when stimulated, resulted in perception of knee flexion. Site 1 represents the location with the most consistent movement percept; this was the site used for determining the illusion kinematics.

Site 1 (Figure 3.3) was used for quantifying P1's illusion kinematics. Even though this was the site with the most consistent movement percept, the participant would periodically report their phantom limb appearing in a stationary manner. Only 15 of the 30 trials evoked the movement percept. In the remaining trials, the participant experienced other sensations; either their leg appeared partly ("to shin" or "just the knee"); or their entire leg appeared and remained stationary; or their limb would vanish before vibration ceased. The 15 trials are plotted in Figure 3.4, with

similar trajectories color-coded to aid in visualization. The participant's movement percepts can be generally described as an inverted sigmoidal curve with an initial, center, and terminal phase. Movement percepts described by the red trajectories occurred across all trials but were most present for earlier trials. The blue trajectories occurred mostly for some middle trials, demonstrating a quicker movement percept with greater flexion range. Finally, the black trajectories occurred for two of the later trials and presented longer, slower movement percepts with a smaller range of knee flexion. The participant indicated that in the final eight trials the perceived movement of the knee would have continued if the vibration had been continued, whereas the first seven trials reached a terminal flexion angle.

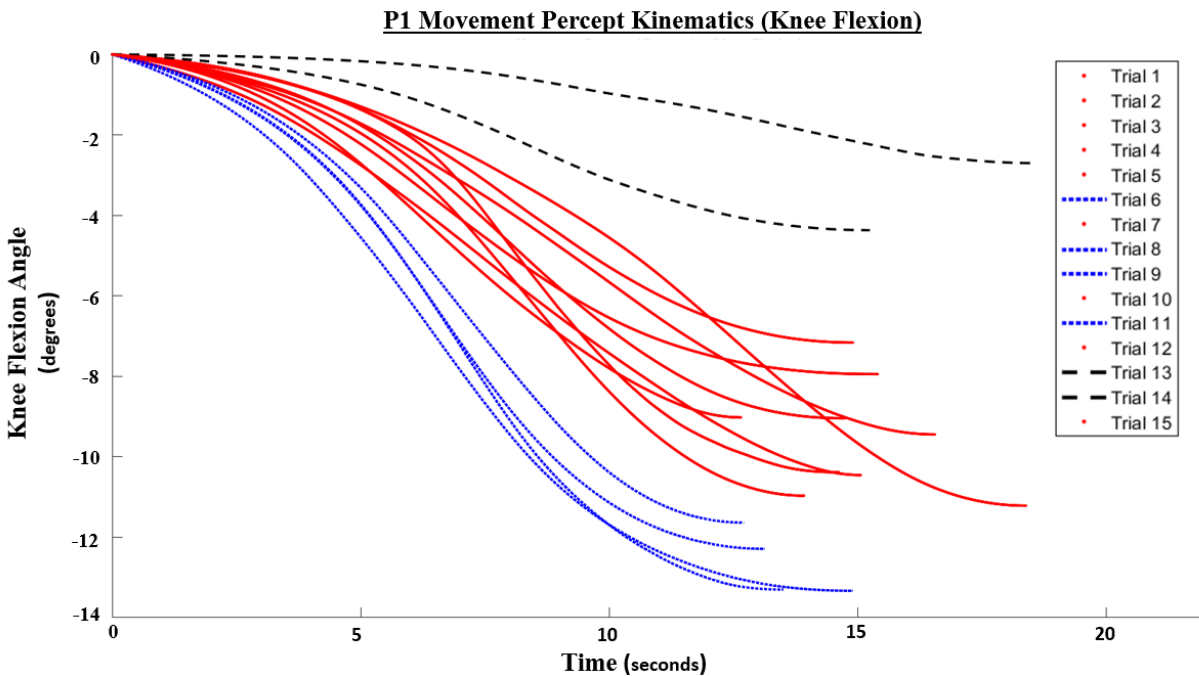


Figure 3.4: The movement percepts (knee flexion) of participant P1, as demonstrated by the participant's intact limb (captured by mocap plates), are plotted, with similar trajectories color-coded. The movement percepts of participant P1 can be generally described as an inverted sigmoidal curve. Red trajectories occurred across trials, but mostly for earlier trials. Blue trajectories mostly occurred for middle trials, demonstrating a quicker movement percept with greater flexion range. Finally, black trajectories occurred for two later trials and presented longer, slower movement percepts with smaller range of knee flexion. The participant indicated the first eight trials reached a terminal flexion angle, unlike the remainder of trials which would have continued to indicate movement if the vibration had not been terminated.

### Participant P4: Transtibial

Participant P4 experienced movement perceptions of ankle dorsiflexion shortly after the administration of vibration. At Site 7 (Figure 3.5), the participant reported that vibratory stimulation caused “the ankle joint [to become] really tight”, which eventually caused the “foot [to start] torquing inward” (inversion) until “it got so tight the ankle couldn’t move it anymore”. Stimulation of Site 8 (Figure 3.5) caused “intense vibration all along [the] top of [the] foot” such that “it [wanted] to lift outward, pointing up” (dorsiflexion). Vibrations at Site 9 (Figure 3.5) “torqued [the foot] up”, and the participant “really felt it in [their] ankle” as the percept was “torquing tight”.



Figure 3.5: The lateral view of the residual limb of participant P4 (right leg): the numbers represent the center of areas which, when stimulated, resulted in movement percepts. Sites 6/7 and Site 8 are located anterior and posterior of the participant’s fibula, respectively; Site 9 is located on the participant’s gastrocnemius. Sites 7 and 8/9 represent locations where the participant experienced movement percepts of ankle dorsiflexion coupled with inversion and eversion, respectively. Site 8 represents the location with the strongest movement percept and used for determining the illusion kinematics. Site 6 corresponded to sensation on the heel. Note: image is blurred to mask identifying information.

Participant P4 also reported that vibrations invoked a feeling on the foot as if “someone cupped [their] ankle and started squeezing”. The participant elaborated that they “could feel it on the outside of the heel on the back of the foot, not towards the toes” and that “it cupped the heel and around the inside of the heel and up in the arch”. This sensation was experienced by stimulation of Site 4 and Site 5 (Figure 3.6) as well as Site 6 (Figure 3.5).

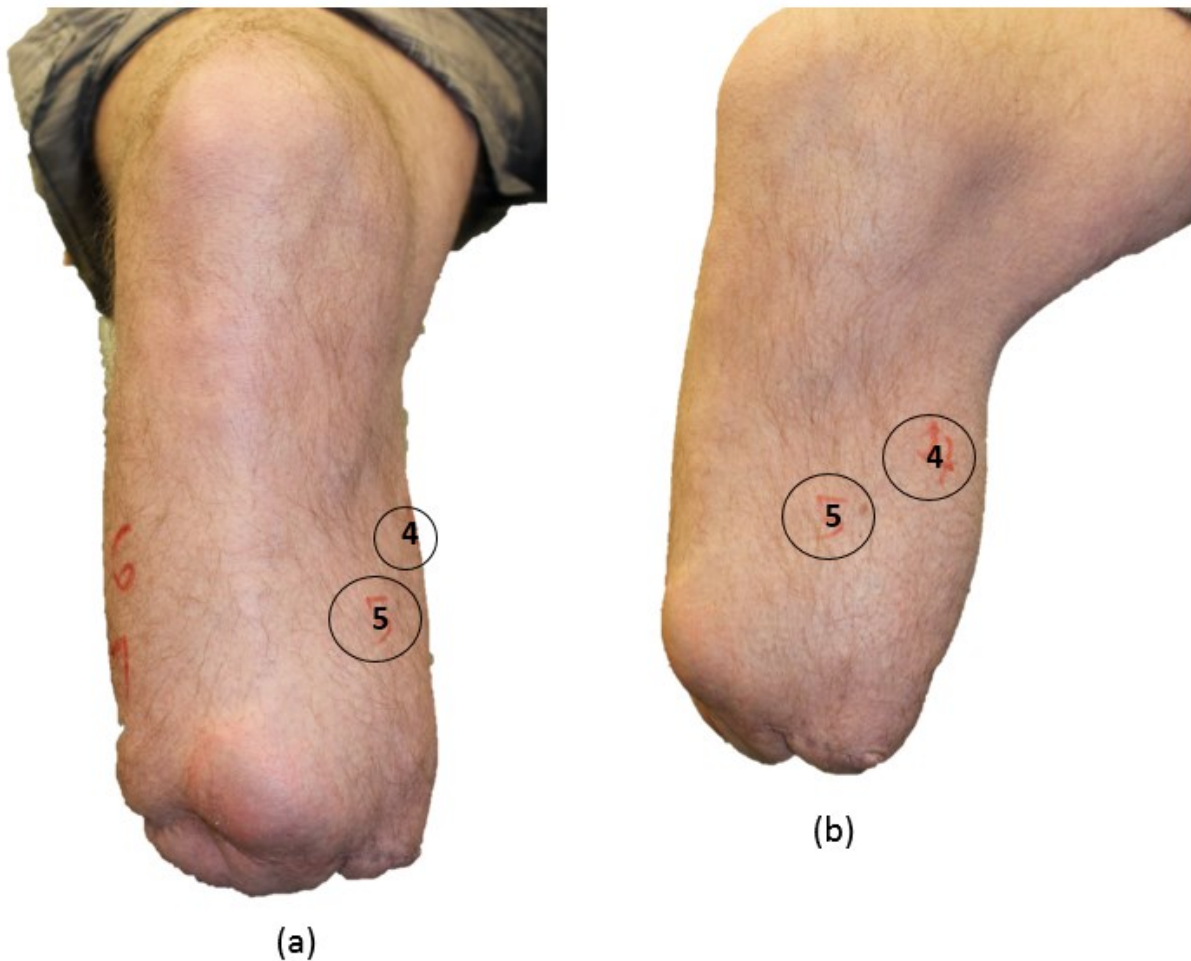


Figure 3.6: The anterior (a) and medial (b) views of the residual limb of participant P4: Stimulation of Site 4 and Site 5 generated a sensation as if “someone cupped [the] ankle and started squeezing”.

The participant reported a 3 or 4 on the Likert scale for each location producing the illusion on their residual limb. For participant P4, Site 8 (Figure 3.5) produced the strongest and most consistent movement percepts; this was the site used for determining the illusion kinematics. 12

out of the 30 trials evoked the movement percept of dorsiflexion. Similar to participant P1, participant P4 would periodically report their phantom limb appearing in a stationary manner. The 12 trials with movement illusions are plotted in Figure 3.7, with similar trajectories color-coded to aid in visualization. Red and blue movement percept trajectories occurred for earlier trials, whereas other blue trajectories and black trajectories occurred for later trials in an alternating manner. Red trajectories can be generally described as a sigmoidal curve with an initial, center and terminal phase. Blue and black trajectories are better described by either a square root or logarithmic curve. The participant indicated the phantom movement would have continued in two of the blue trials (7 and 9) if vibration was sustained, whereas the remaining trials had reached a terminal flexion angle.

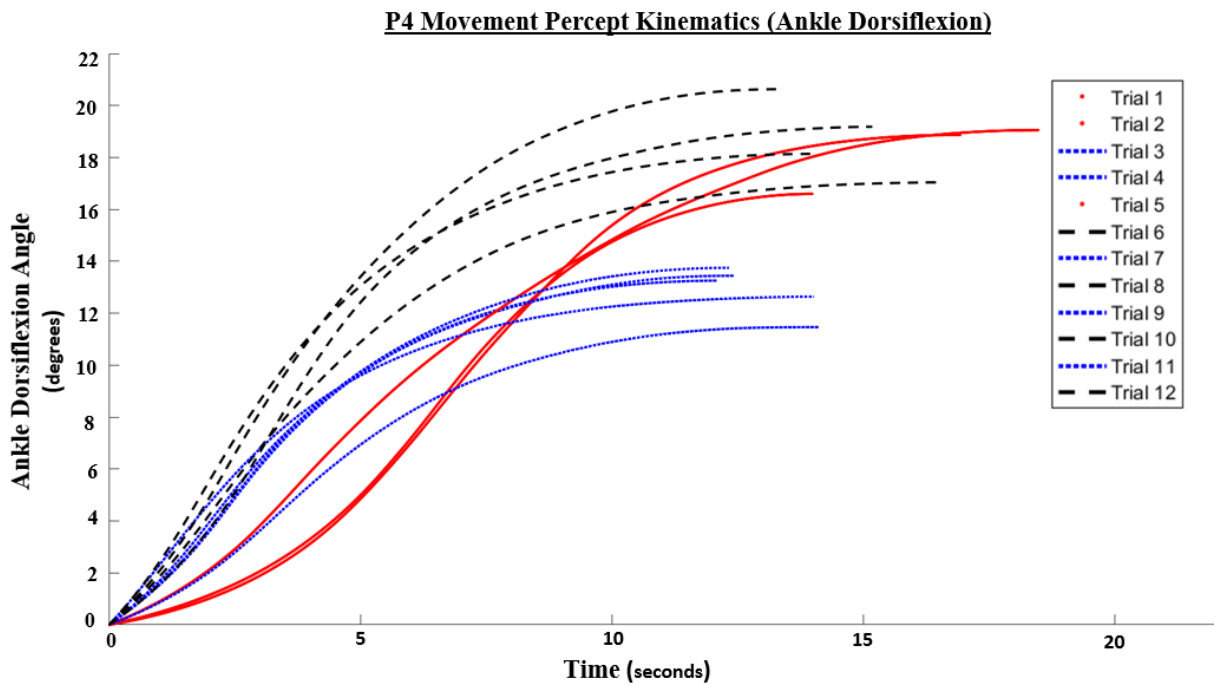


Figure 3.7: The successful movement percepts (ankle dorsiflexion) of participant P4 are plotted, with similar trajectories color-coded. Both red and blue trajectories occurred for earlier trials, whereas other blue trajectories and black trajectories occurred for later trials in an alternating manner. Sigmoidal curves can be used to describe some of the movement percepts for earlier trials (red). Movement percept for later trials (blue and black) are better described by either a square root or logarithmic curve. The participant indicated the perceived movement would have continued in two of the blue trials (7 and 9), whereas the remaining trials had reached a terminal flexion angle.

### 3.3.1.2 Remaining Participants and Other Sensations

#### Participant P2: Transfemoral

Vibration induced a multitude of sensations on participant P2's phantom limb, including tingling sensations, pressure points, vibration, tension, and the patellar (knee) reflex. The tingling sensations can be grouped into a static or dynamic sensation experienced in the participant's phantom limb. The static tingling was experienced by stimulating Sites 2, 4 and 7 (Figure 3.8). This static tingling was felt "across [the] toes" and more specifically at the "underside of three middle toes". The static tingling sensation was also experienced at the "end of knee and a little bit on the top of the calf". Tingling sensations, which traversed various segments of the phantom limb, were identified by stimulating Sites 3 and 6 (Figure 3.8). This dynamic tingling was often described as a "waving back and forth" that was "more pronounced" than the static sensation and concentrated on the phantom foot. Vibration on these sites also induced various pressure points on the phantom limb, such as: "a barely discernable ... touch feeling on [the] tips of [the] toes", "a touch sensation on [the] shin", or "deep pressure on the foot" and "calf". Vibrations on Site 3 ultimately produced a sensation similar to "a really strong shock from static electricity" applied to the phantom knee; this site was avoided in further testing to minimize discomfort to the participant. Vibrations on Site 5 (Figure 3.8) produced a similar vibration "through [the] inner side of calf bone". Vibration at Site 1 (Figure 3.8) produced a sensation in the phantom knee like that experienced in "the doctor's office [when] they check your knee reflex". This sensation was not consistent and eventually evolved to a "tingly pressure under the knee and up under kneecap".

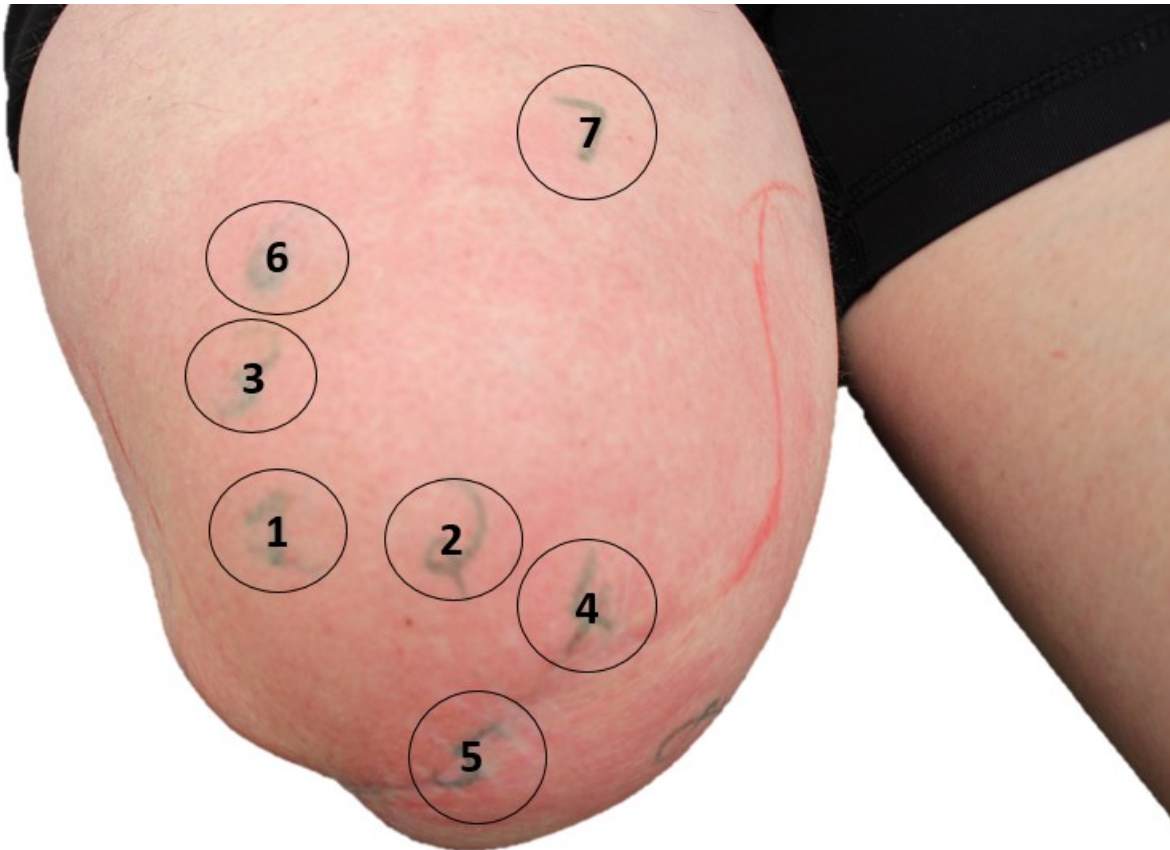


Figure 3.8: The anterior view of participant P2's residual limb (right leg): the numbers represent the center of areas which, when stimulated, produced unique sensations. Vibration at Site 1 produced a sensation in the phantom knee similar to the patellar reflex. Through continual stimulation, the sensation ceased and was replaced by a tingling sensation. Stimulation of Sites 3 and 6 resulted in a tingling sensation on that phantom foot which was described as a “waving back and forth”. Vibrations on Site 3 were ultimately stopped as they resulted in painful sensations for the participant. Stimulating Sites 2, 4, and 7 produced a static tingling sensation concentrated on the phantom foot. Vibration on Site 5 produced a similar vibration on the phantom calf bone.

#### Participant P3: Transfemoral

Stimulating Site 3 (Figure 3.9) resulted in participant P3 also experiencing the patellar reflex sensation about their phantom knee. Similar to participant P2, the reflexive sensation eventually transformed into a tingling sensation. The participant articulated that, “if I had a knee it would

want to kick out a little”. This sensation was only experienced once. Through continued stimulation, the reflexive sensation ceased, and the participant began to “[feel] a tingling along [their] phantom limb”. This sensation was “strongest after [vibration]” ceased. The remaining sites produced tingling sensations on various segments on the phantom limb.



Figure 3.9: The lateral view of participant P3’s residual limb (right leg): the numbers represent the center of areas which, when stimulated, produced unique sensations. Vibration at Site 3 produced a sensation in the phantom knee similar to the patellar reflex. Through continual stimulation, the sensation ceased and was replaced by a tingling sensation. The remaining sites produced tingling sensations on various segments of the phantom limb.

#### Participant P5: Transtibial

Participants P5 and P7 reported no phantom sensations. However, P5 reported that stimulation of the medial portion of their residual limb, on their distal thigh, produced a temperature change in

the anterior lateral portion of the limb. Referring to the affected site, the participant described that “it felt like it was [cooler]... when you were vibrating”.

Participant P6: Transtibial

Stimulation of various segments of participant P6’s residual limb resulted in a consistent “tingling” sensation “at the stump”. The exception being stimulation of the lateral segment of the residual limb, proximal to the knee, which evoked “a slight electrical shock”. To mitigate discomfort, this site was avoided in further testing.

Participant P9: Bilateral

Vibrating various segments in the transtibial residual limb of participant P9 produced a variety of sensations in their phantom limb, especially the foot. The participant felt tingling sensation in very specific locations of the phantom limb. This included the “shin”, “front of calf”, “ball of foot”, “left side of ball of foot”, “ring toe”, and “arch of foot”. The tingling sensations experienced at the ball of the foot eventually developed into an “intense feeling, almost pain”, much like the electrical shock experienced by other participants; this site was avoided in further testing.

Table 3.3: Summary of other sensations not related to the kinesthetic illusion.

<b>Participant</b>	<b>Sensations Experienced</b>	<b>Vibration Induced Phantom Limb</b>
P2	Patellar reflex, Tingling, Pressure, Vibration, Shock	Yes
P3	Patellar reflex, Tingling	Yes
P5	Change in temperature	No
P6	Tingling, Shock	Yes
P7	None	No
P8	None	Yes
P9	Tingling, Shock	Yes

### 3.4 Discussion

When vibration of a certain amplitude and frequency is introduced to musculotendinous regions of a limb, an illusory sensation that the limb is moving may occur. Studies on eliciting the KI suggest a similar range of vibratory stimuli parameters (amplitude and frequencies) for both the upper [18] and lower limbs [215], [235], [236] is capable of evoking these movement responses. Recent work in the upper-limb population suggests that, within this range, vibrations of 1 mm in amplitude (peak-to-peak) and 90 Hz in frequency are optimal for producing the movement percept [18]. It has also been shown that vibrating the muscles in the residual limb of individuals with upper-limb amputation who have undergone TR can evoke this kinesthetic response [29]. This is the case even with the anatomical and physiological changes resulting from amputation (i.e., the physical absence of the limb). The work presented in this chapter has expanded the literature by showing that individuals with non-TR lower-limb amputation are capable of experiencing the KI. The remainder of this section further examines the kinesthetic feedback mechanism and highlights potential challenges associated with applying the feedback approach in an applied setting (e.g., ambulation).

Our data suggest that movement illusions are not necessarily experienced immediately or by all participants. Two participants (P1 and P4) out of the nine participants experienced movement percepts during the first 10 minutes of testing (Table 3.2), in the direction consistent with the KI. In the same time frame, participants P2 and P3 experienced sensations similar to the patellar knee reflex, i.e., a singular outward jerk of the knee. The remaining participants did not experience any movement percepts. There are a few possible explanations for these results.

The first explanation as to why movement percepts were not experienced by all users may relate to the tonic vibration reflex (TVR), specifically the isometric TVR. The isometric TVR is a natural reflex that derives from muscle contractions, during vibratory stimulation, of fixed immobile joints [223]–[231], [245], [246]. The isometric TVR is suspected as opposed to the isotonic TVR as individuals with transfemoral or transtibial amputations do not possess moveable knee or ankle joints, respectively; and isotonic TVRs only occur while joints are free to move during vibratory stimulation [223]–[231], [245], [246]. Additionally, participants described the sensations as rapid movements with no onset latency. The isometric TVR fits this narrative as it only persists for a few milliseconds and contains a negligible onset latency [204], [225], [227], as opposed to the

isotonic TVR which is characterized by an onset latency in the order of seconds [247] with a long slow rise to the movement plateau, lasting roughly 20-60 seconds [223]–[231]. As the contraction of the vibrated muscle has been shown to weaken or abolish the KI [204], it is possible that the isometric TVR and the KI may have competed. To experience the KI, participant P1 had to be repeatedly asked to relax the residual limb and resist the impulse to contract during vibration. Initially, the participant felt as if they “[had] to oppose” the movement percept. After relaxing, P1 stopped experiencing the “kicking sensation” (isometric TVR) and started to experience the “pull sensation” of knee flexion (the KI). Some participants (P2 and P3) only experienced sensations of the patellar reflex (i.e., a singular outward jerk of the knee), most likely due to the isometric TVR; they were unable to sufficiently relax to experience the KI.

The isometric TVR has practical implications for the possible use of the KI as a feedback mechanism. Since tissue is generally compressed within a socket, a prosthesis user may have greater difficulty relaxing when the feedback mechanism is integrated within a socket, making them more susceptible to the isometric TVR; potential discomfort from improper socket fit will also increase a user’s vulnerability to the isometric TVR. Moreover, participants will be more susceptible to priming muscles for the isometric TVR while performing activities of daily living, e.g., during the cyclic nature of voluntary contractions resulting from ambulation. Conversely, the isometric TVR might also be leveraged as a form of movement feedback. The KI as a feedback mechanism benefits from periods of movement lasting longer than a couple of seconds, however, some activities (e.g., single steps, rotary movements – pivots, etc.) occupy a short duration of time. Therefore, the isometric TVR might be used as a means to relay these rapid singular movements to prosthesis users. However, since the TVR competes with the KI, transitions between the two physiological phenomena might not be practical and the TVR may need to be avoided completely.

A second explanation as to why movement percepts were not experienced by all users may relate to how each participant interpreted the sensations experienced. It was common for participants to have difficulty articulating the sensations. For example, participant P1 initially described the sensation as if “the top of [their] thigh [was] not working” and that this forced “the shin [to move] in order [to] compensate”. Although providing the remaining participants with small amounts of information did not cause them to experience the illusion, follow up studies might produce different results. Since the KI is a psychophysical phenomenon, having a clearer mental image of

how to interpret the sensations experienced might provide benefit in articulating the sensation. These findings suggest that eliciting the KI may require more than the simple introduction of vibration to muscles or tendons. In research applications, investigators must be aware that achieving illusory movements may require time and a strategy for revealing enough information without biasing results. Conversely, practical implementation of the KI, as a restorative sensory mechanism, may require biasing for quicker results. The use of the KI for rehabilitative applications, such as sensory feedback for prosthesis users, may also require a degree of participant training to acclimate users to the movement sensations. The introduction of visual feedback congruent with the experienced movement percepts might aid in participant training. Since vision was occluded during experimentation, participants had to rely solely on their internal representation of the illusory movement percepts. The addition of vision would augment the participant's internal representation of the movement percept, allowing quicker familiarization with the experienced movement sensations [29].

The limb matching experiments largely served as a means of quantifying the kinematics of the illusion. When compared to similar experiments in individuals with intact limbs and those with upper limb amputations, limb matching for individuals with lower limb amputations resulted in movement sensations in the expected direction when appropriate locations on the residual limb were stimulated [18], [29], [215], [237], [238]. Sites 1 (Figure 3.3) and 8 (Figure 3.5) most likely correspond to stimulation of the residual rectus femoris and peroneus longus muscles for participants P1 and P4, respectively. As expected, the experienced movement percepts, knee flexion and ankle dorsiflexion/inversion, were in the opposite direction of the stimulated muscles' action. The rectus femoris and peroneus longus muscles are major contributors to knee extension and ankle plantarflexion/eversion, respectively.

Unlike other limb matching studies, the movement percept trajectories of the experienced sensations were quantified using motion capture, which allowed determination of different types of movement percept trajectories. The difference in trajectory found in the anterior portion of the leg of participant P1 (sigmoidal) and the anterior lateral portion of the lower leg of P4 (sigmoidal initially, then logarithmic) is most likely a result of the length and amount of muscle fibers stimulated in each location [248]. Both muscles are composed of roughly an equal amount of fast and slow twitch fibers [249]; however, the major difference between the two muscle groups is the

length and number of muscle fibers present [248], [250], [251]. Since the parallel fibers of the peroneus longus extend further than the pennate fibers of the rectus femoris, they are capable of a larger range of motion [248], [252]. Figures 3.4 and 3.7 support this claim as participant P4 experienced a greater dorsiflexion movement percept (reaching 20 degrees) when compared to the knee flexion movement percepts of participant P1 (below 14 degrees). Since the rectus femoris contains a larger muscle belly than the peroneus longus muscles, it can be inferred that vibration stimulates less of the total bulk in the rectus femoris. Thus, sigmoidal movement percepts might be linked to greater muscle spindle activation compared to logarithmic trajectories. It is also possible that spindles located deep within larger muscle bellies (e.g., rectus femoris) may be stimulated at a frequency and amplitude that is lower than the optimal values (90 Hz, 1 mm peak to peak). Therefore, spindles activated with slightly different stimulation parameters due to the size of their corresponding muscles might also contribute to the movement trajectory differences observed between the two muscles groups.

The trajectories changed over successive vibrations. Early trials for participant P1 (Figure 3.4) demonstrated sigmoidal movement percept trajectories (red curves). Although the majority of red curves concentrate in the early trials, they intermittently occurred throughout the experimental session. During the middle of the experimental session, the average speed of the sigmoidal movement percepts (blue curves) increased by 0.5 degrees/second, compared to the 1 degree/second average speed of the red curves. Likewise, at the end of the trials, the average movement percepts (black curves) demonstrated a decrease of slightly over 0.5 degrees/second when compared to the average of the red curves; the average of all three curves maintained a similar flexion range; similar patterns were observed for participant P4 (Figure 3.7)

The initial increase in illusion speed and flexion angle is most likely due to thixotropy – a property of passive muscles and their underlying spindles. Thixotropy can produce significant changes in perceived limb position [203]. This is due to the fact that simply contracting and relaxing muscles, without changing their length, can result in changes in the spindles discharge rate. Thixotropy is the result of long-lasting stable linkages which form between myofilaments at their resting length during muscle relaxation. The presence of these stable linkages prevents muscles from acquiring shorter configurations during contraction, resulting in muscle slack. Muscles at shorter lengths are more vulnerable to slack than the same muscles at longer lengths. The challenge with studying

muscles in the amputated limb is that the length of the muscle cannot be controlled due to loss of the distal attachment. Therefore, each participant may have a different muscle length or tension which would change their susceptibility to the KI. As well, small contractions may occur in the residual limb that are unnoticed (due to no distal limb or joint movement), and contractions as low as 5-10% of the maximum voluntary contractions can result in thixotropy [203]. This is likely the case for at least the participants that had muscle tension in their limb and had to be continually prompted to relax the muscle. The eventual decay in speed and flexion might be a result of neural or central fatigue resulting from repeated stimulation.

In addition to the behaviour of the residual limb during stimulation, the use of the intact limb to mirror the experienced movement percepts may also contribute to the movement percept trajectories observed. With successive demonstrations of the illusionary movement, the indicator limb might have started to not adequately reflect the perceived movement sensations – as the position sense of the indicator limb might have been altered over time by the repetitive movement and muscle contractions.

Results from the limb matching experiments present potential challenges for clinical translation of the KI as a possible feedback mechanism. For example, changes in the KI response over time could be problematic for real-time applications, as the experienced movement percepts may not align with the actual movements of the performed activity. The aforementioned challenges might be overcome with user training, as the KI is malleable and adaptable [29]. For example, Marasco et al. developed a game to condition upper-limb prosthesis users to visually couple their perceived illusion to faster operation of a virtual hand, actively controlled by electromyography [29]. As the speed of the virtual hand was altered, they observed a similar change in percept speed with their participants. These results suggest that illusionary movement percepts could adapt to match the speed of a user's prosthetic device [29].

Other sensations experienced by the remainder of the participants include tingling, pressure gradations, “electrical shock”, and change in temperature on the residual and phantom limb. Sensations on the residual limb are a result of cutaneous receptor activation, whereas sensations felt on the phantom limb could be due to the reinnervation of skin cutaneous receptors from the amputated nerve ending or stimulation of free nerve endings, resulting in referred sensation. When stimulated, the Merkel complex is responsible for touch and pressure sensations [170], [253]. Free

nerve endings encode and transmit sensations of pain, touch, and temperature [254]. In the context of the residual limb, the combination of the Merkel complex and free nerve endings could account for the range of other sensations experienced during mapping. Extreme care would need to be taken to protect prosthesis users from the “electrical shock” sensations (effects of free nerve endings) which were experienced by three participants (P2, P6, and P9) and described as “a really strong shock from static electricity” (P2). Clinical implementation of the KI would require a thorough mapping procedure to prevent placement of socket-integrated tactors in areas evoking painful sensations.

### 3.4.1 Limitations

This study was conducted in only nine individuals with lower-limb amputations to understand the KI, with the goal of exploring its use in a sensory feedback paradigm for prosthesis users. Although nine individuals are an adequate sample size for a preliminary study, further investigation into the KI would benefit from a larger sample size. Future study of the KI may include refinement of the experimental design to include training, visual reinforcement, and introduction of voluntary muscle activation (as required for prosthesis use); and secondly to proceed with integrating this feedback mechanism into a prosthetic system in participants that experienced strong KI sensations. Moreover, this study was conducted with a specific choice of vibration parameters (1 mm amplitude, 90 Hz frequency). Although the vibration parameters are within the reported range of KI-inducing stimuli, they are optimized for the upper limbs [18]. Due to variations between muscles (e.g., muscle fiber type, length and volume) existing in the lower limbs when compared to those in the upper limbs, a different range of vibratory stimulation might be required to be more effective in eliciting the KI for muscles of the lower limbs.

Evaluation of the translatability of the techniques developed in this chapter requires implementation of these methods into a functional prosthesis. However, a variety of technical barriers exist that impede the development of such a system, many of which relate to the integration of the feedback device without compromising prosthetic fit or function. Intuitive use of the KI will require movement of the prosthesis to trigger activation of the feedback system, as the mechanism to administer the movement percepts should be linked to the movement of the prosthesis.

### 3.4.2 Conclusions

In the context of prosthetic sensory feedback, this work has built upon initial testing completed in individuals with TR upper-limb amputations, by expanding exploration into individuals with non-TR lower-limb amputation. The results show the potential to elicit the KI in this more prevalent population while highlighting the challenges and variability that must be overcome before it can be implemented into practical systems. Through this work, early strides have been taken towards understanding how to elicit the sense of kinesthesia in those with lower limb amputation. Further investigation into how movement percepts might be realized as a practical method for providing movement feedback to prosthesis users is warranted. However, the realization of lower-limb prostheses capable of providing intuitive, relevant feedback that is readily interpreted by the users as occurring in their missing limb requires overcoming technical barriers, such as socket integration, and linking activation of the feedback mechanism to actual movement of the prosthesis. Chapter 4 addresses the latter challenge through the development and validation of a low-cost wireless sensor capable of tracking the single-axis movement of lower-limb prostheses.

## **4. Development and Validation of a Wireless Sensor for Tracking Single-Axis Prostheses Movement**

### **4.1 Introduction**

The previous chapter explored the kinesthetic illusion (KI) in individuals with lower-limb amputation. This chapter outlines the design and development of a wireless system, based on an inexpensive inertial measurement unit (IMU), for the purpose of tracking the single-axis movement of a prosthetic knee. A technical validation is performed to compare the efficacy of the developed system in tracking the single-axis movement against a commercial IMU (cIMU) and a motion capture (mocap) system. Although the KI is currently administered at a fixed amplitude and frequency (Chapter 3), future work may allow for modulation of the sensory feedback mechanism. Therefore, a system capable of reliably tracking the single-axis movement of lower-limb prostheses will be instrumental in linking the movement of a prosthetic device to the kinesthetic feedback mechanism.

### **4.2 Methods**

#### **4.2.1 Development of a Wireless Sensor for Tracking Single-Axis Movement**

##### **4.2.1.1 Hardware Design**

The componentry and wiring diagram of the wireless IMU-based system (WIBS) is outlined in Figure 4.1. The system includes the RN42 Bluetooth module (Microchip Technology, Chandler, AZ, USA), BNO05 IMU module (BOSCH, Gerlingen, Germany), and a lithium-ion battery with a boost converter (SparkFun, Niwot, CO, USA), which are used along with an Arduino Pro Mini microcontroller (Arduino, Somerville, MA, USA). The cost of the described hardware is approximately US \$100.

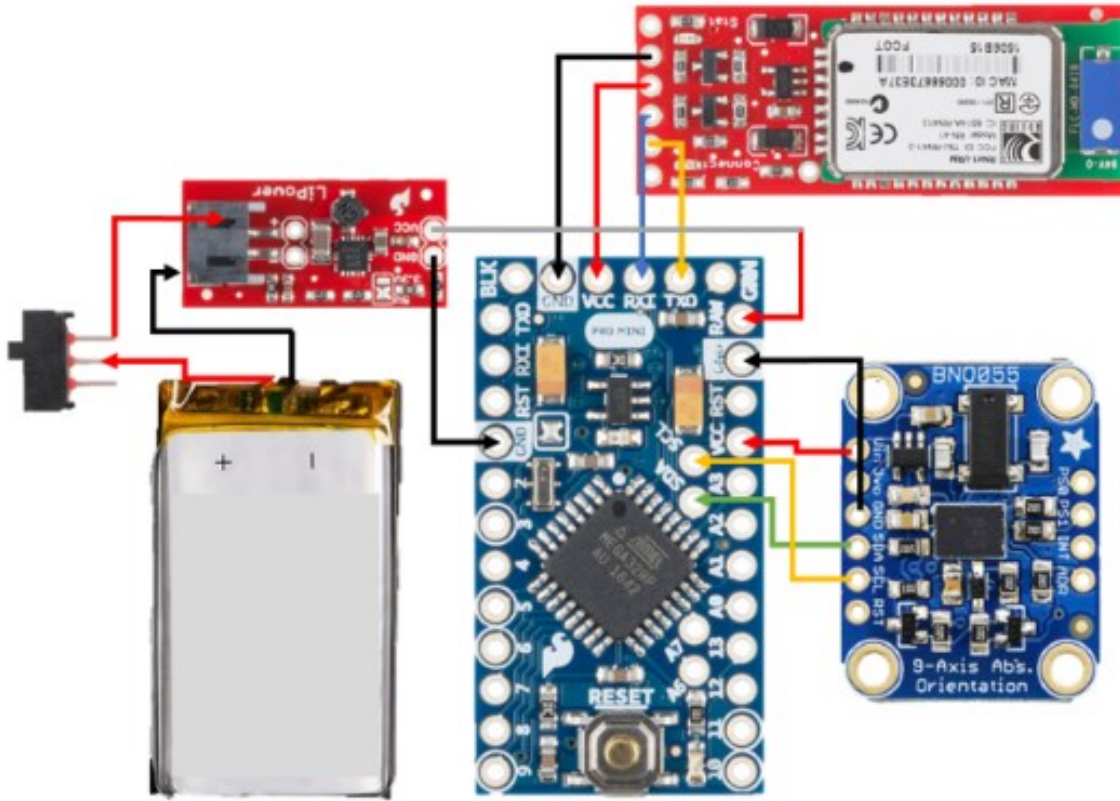


Figure 4.1: The system is comprised of an Arduino Pro Mini microcontroller (center), a Bosch BNO05 inertial measurement unit (bottom right), an RN42 Bluetooth module (top right), a lithium-battery, and a boost converter (left of the microcontroller).

An Arduino Pro Mini was chosen due to its small size and capacity for rapid prototyping [255]. The Arduino communicates with the Bluetooth and IMU module through serial and I2C communication protocols, respectively. The RN42 is a wireless Bluetooth radio capable of delivering up to 3 megabits per second of data at distances of up to 20 meters. Bosch's BNO05 IMU module is a 9 degree of freedom (DoF) inertial sensor comprised of an accelerometer, gyroscope, and magnetometer. The BNO05 provides: a magnetic field strength vector at 20 Hertz (Hz), a linear acceleration vector at 100 Hz, a gravity vector at 100 Hz, an acceleration vector at 100 Hz, an angular velocity vector at 100 Hz, ambient temperature at 1 Hz, Euler angles at 100 Hz, and quaternions at 100 Hz. This IMU module was chosen due to its low cost, high sampling rate, and a simple calibration procedure. Calibration of the accelerometer,

gyroscope, and magnetometer is required for accurate readings from the IMU. Keeping the device stationary in any position is sufficient to calibrate the gyroscope. The magnetometer requires either a figure eight or sufficient vertical displacement of the device to calibrate. Finally, the BNO05's accelerometer must be placed in six standing positions along the positive and negative axes of the sensor to be calibrated; the calibration data is preserved until the device is powered off. The calibration status of the accelerometer, gyroscope, magnetometer, and overall system is represented by four numbers ranging from 0 to 3, where zero indicates poor calibration. A lithium-ion battery offering 400 milliampere-hours (mAh) and a corresponding boost converter are used to provide power to the system. The current draw of the system is approximately 100 mA, yielding a battery life of approximately 4 hours (h). Another IMU module with similar specifications or a battery with a greater capacity could be easily substituted into the system.

### Data Flow

The microcontroller extracts four-unit quaternions from the IMU board and transmits these quantities through the Bluetooth radio at a baud rate of 9,600 bits per second; each unit quaternion is represented by two bytes. Unit quaternions are then packaged into a series of bytes. A package is transmitted at 85 Hz, at a lower frequency than the initial sampling rate of 100 Hz and is composed of 14 bytes in total: two leading flags, followed by eight bytes representing the four unit quaternions, and finally the calibration status of the IMUs gyroscope, accelerator, magnetometer, and overall system, each one byte long (note that a parity bit was not utilized). The initial sampling rate of 100 Hz is decreased to 85 Hz as a result of Arduino processing and limitations of wireless transmission. Since serial streams contain a continuous flow of data, flags are essential in identifying when the receiver should start reading the contents of a transmitted message. It is essential that the flags are not present within the content of the transmitted message. Since the content of each transmitted package only contains bytes encoding numerical values (integers and floats), any hexadecimal value outside of this group can be chosen as a flag (e.g., 0x2E, ASCII hexadecimal code for a period – full stop). The probability of a single flag byte corrupting is approximately 0.78% (1:128 ASCII values), which may disrupt data retrieval. To combat this, two consecutive flags are used, reducing the probability of a false flag to 0.0061%.

### Enclosure Design

An enclosure (70 mm x 35 mm x 35 mm) for the electronics was designed using SolidWorks 2016 (SOLIDWORKS, Waltham, MA, USA). The enclosure was manufactured using fused deposition rapid prototyping via 3-dimensional (3D) printing with polylactic acid filaments (MakerBot, NY, USA) and the MakerBot Replicator (MakerBot, Brooklyn, NY, USA). The enclosure was designed to protect sensor components, manage wires, improve ergonomics and aesthetics, and most importantly fixate the IMU module, for the accuracy of measurements (Figure 4.2). See Appendix C for more details on the hardware development of the WbS.

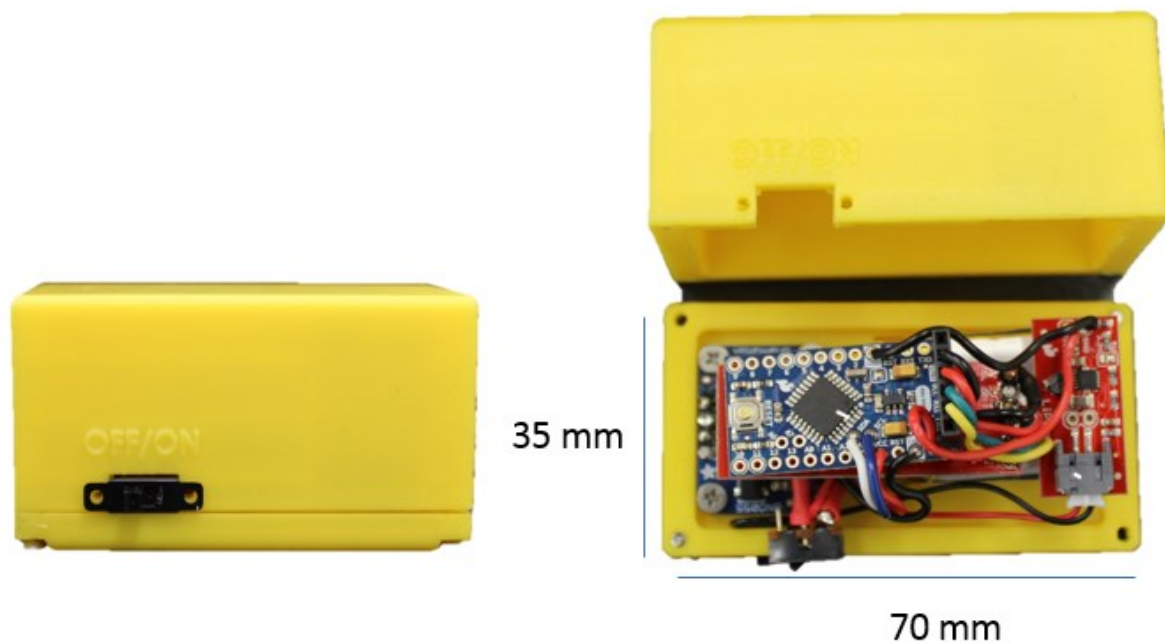


Figure 4.2: Enclosure for the wireless inertial measurement unit-based system. The dimensions and placement of the electronics within the enclosure are shown above.

#### **4.2.1.2 Software Design**

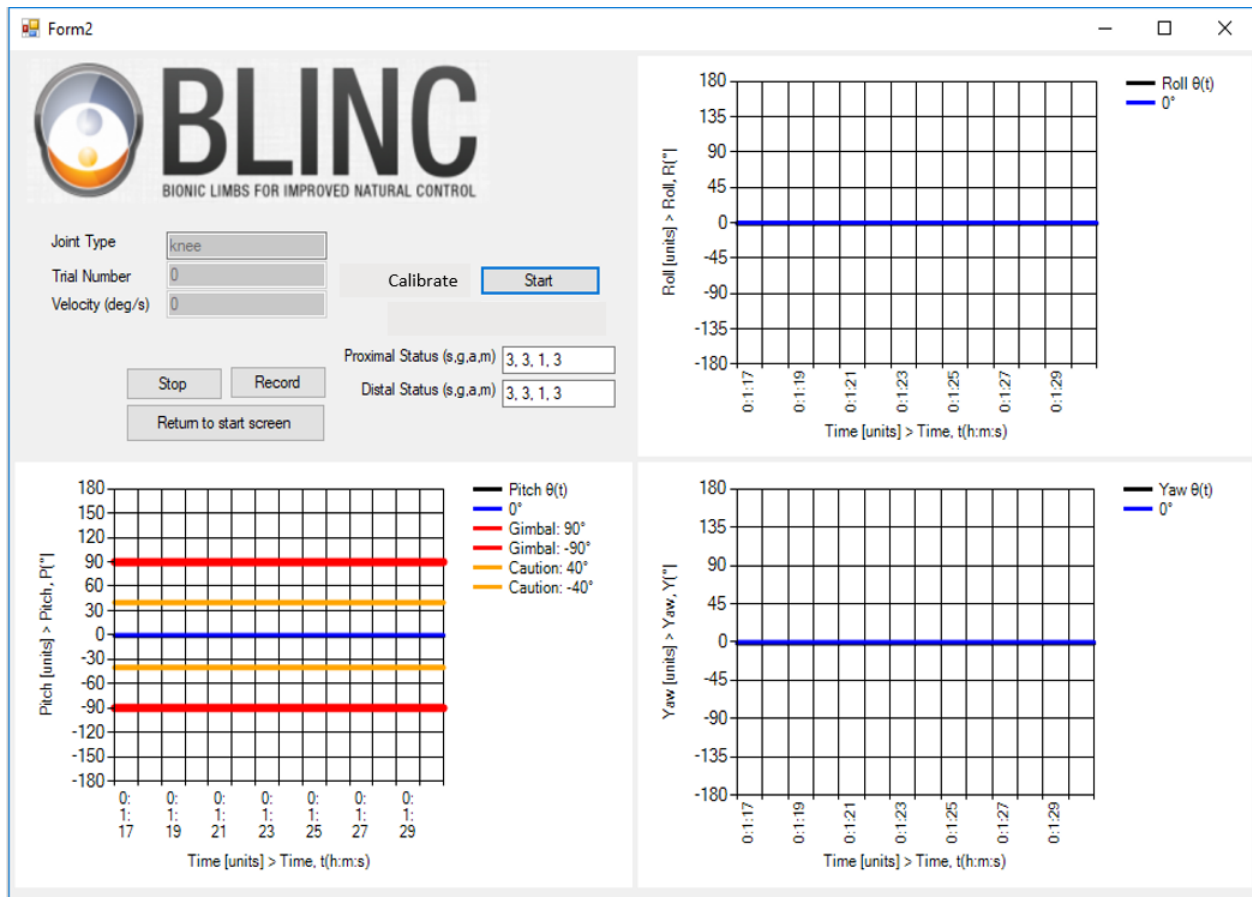
A graphical user interface (GUI) was developed in the C# programming language to log and visualize the data received from two WbS (Figure 4.3). The entrance GUI (Figure 4.3 (a)) is predominately used to establish a connection between the software and the two WbS. The second GUI (Figure 4.3 (b)) allows real-time data visualization and data logging. Cardan angles representing the angular displacement between the two WbS are displayed in the three plots of

the GUI. The second GUI (Figure 4.3 (b)) displays the calibration status of each WiBS. Using this software, data from each WiBS is logged at a rate of 33 Hz, which is lower than the transmitted rate of 85 Hz. The sampling rate for the transmitted data is decreased from 85 to 33 Hz due to the greater computation demand of the GUI as the logged data includes quaternions, the calibration status, the recording time of each WiBS, and the 3D angles between the two WiBS. However, 33 Hz exceeds the 2 Hz maximum gait cadence of non-disabled and prosthesis users [73], [80], [97], [243], [244]. Appendix C provides additional information on the GUI of the WiBS.

The screenshot shows a software window titled "Form1" with the BLINC logo and the text "BIONIC LIMBS FOR IMPROVED NATURAL CONTROL". The interface includes several input fields and buttons:

- IMU Type:** A text box containing "BNO05".
- Trial Number:** A text box containing "0".
- Com Port:** Two dropdown menus. The first is set to "COM7" with a label "WiBS: proximal". The second is set to "COM9" with a label "WiBS: distal".
- Buttons:** A "Reset" button and a "Submit" button.

(a)



(b)

Figure 4.3: Graphical user interface (GUI) for data collection. (a) outlines the entrance GUI, which is used to enter information about the device and trial, as well as establish a connection with the movement sensors; (b) is the second layer of the GUI and is released after a secure connection to the movement sensors is established. This interface allows for the monitoring and logging of data. The angles between two connected, wireless modules are shown in the three plots. The calibration status of each inertial measurement unit is also shown on this page.

#### 4.2.1.3 Prosthetic Knee Joint Angle Detection Algorithm

Determining the angle of a prosthetic knee using the WIbS is very similar to determining joint angles with rigid mocap plates described in Chapter 3, Section 3.2.3. An overview of the joint angle detection algorithm is depicted in Figure 4.4 [240]. To determine the angle of a prosthetic knee, two WIbS must be placed on rigid segments of the prosthesis, proximally and distally of the

knee. On the rigid segments, the WbS can be placed in any position and orientation, eliminating the need for trained personnel to accurately determine the knee joint center or other relevant anatomical landmarks [164], [256].

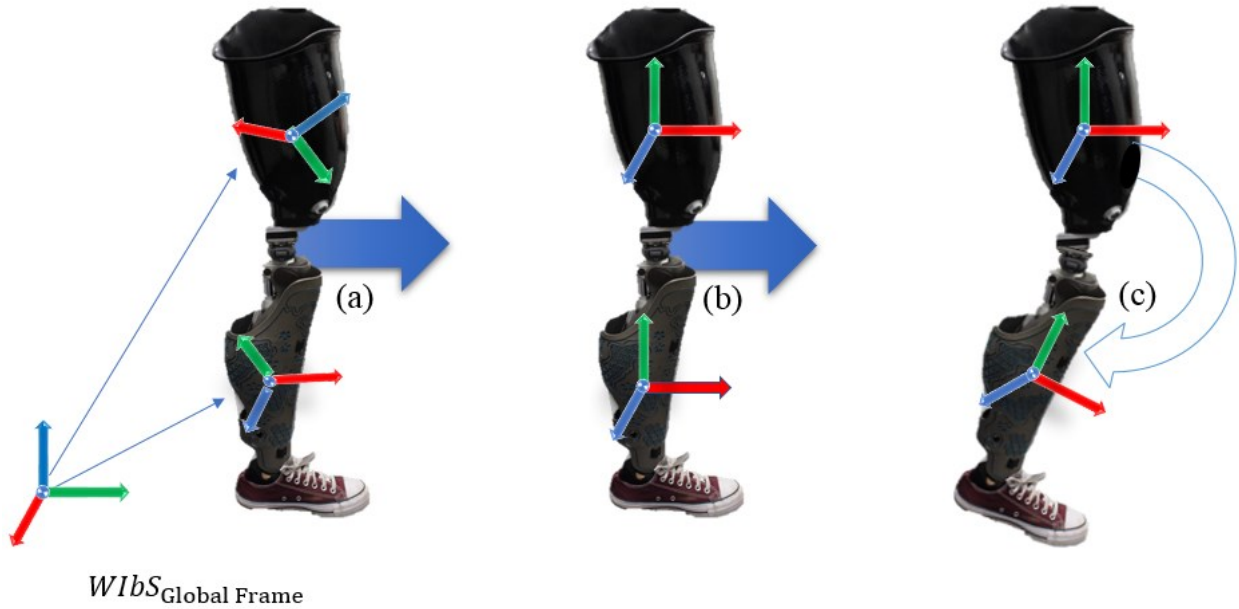


Figure 4.4: The global coordinate frame for the two movement sensors is shown on the left. Two movement sensors are placed proximally and distally of the knee joint on a prosthetic leg (a). A calibration procedure is performed once the prosthesis is in full extension, to align the coordinate frames of both movement sensors with the relevant axis of rotation of the prosthesis according to the recommendations by the International Society of Biomechanics (b). The movement of the prosthetic knee is determined by extracting Cardan angles from the relative orientation between the two movement sensors (c).

A stable connection to the prosthetic componentry is essential, as any shifting of the WbS will result in inaccurate output angles. The unit quaternions from each WbS are used to generate rotation matrices that encode the orientation of each device through Equation 4.1. Note, in Equation 4.1,  $q_r$ ,  $q_i$ ,  $q_j$  and  $q_k$  represent the single real and three complex components of a unit quaternion; each component contains values between zero and one.

$$R_{WIbS} = \begin{bmatrix} 1-2(q_j^2 + q_k^2) & 2(q_i q_j - q_k q_r) & 2(q_i q_k + q_j q_r) \\ 2(q_i q_j + q_k q_r) & 1-2(q_i^2 + q_k^2) & 2(q_j q_k - q_i q_r) \\ 2(q_i q_k - q_j q_r) & 2(q_j q_k - q_i q_r) & 1-2(q_i^2 + q_j^2) \end{bmatrix} = \begin{bmatrix} X_i & Y_i & Z_i \\ X_j & Y_j & Z_j \\ X_k & Y_k & Z_k \end{bmatrix} \quad (4.1)$$

Once the WIbS are positioned, a calibration procedure is performed to align the coordinate frames of both WIbS with the relevant axis of rotation of the prosthesis. In order to do this, the prosthesis (in full extension) is positioned such that the prosthetic knee's rotation axis is aligned with the Z-axis (flexion axis), as recommended by the International Society of Biomechanics: X-axis – abduction/adduction; Y-axis – axial rotation; and Z-axis – flexion/extension [241]. Once the prosthetic device is in position, data is collected to determine a static rotation matrix that will accomplish this calibration. The calibration matrix is only generated once for each WIbS and applied to all subsequent frames of the WIbS. Once both the WIbS are placed on the prosthetic leg and the prosthetic leg is positioned in the proper calibration position, Equation 4.1 is used to generate a rotation matrix from unit quaternions for each WIbS as shown in Equation 4.2:

$$R_{WIbS \text{ initial position}} = \begin{bmatrix} X_i & Y_i & Z_i \\ X_j & Y_j & Z_j \\ X_k & Y_k & Z_k \end{bmatrix}_{\text{initial position}} \quad (4.2)$$

The IMU used in the WIbS contains a fixed global coordinate system, the standard orthonormal basis, that is defined when the device is powered. Consequently, the WIbS' global coordinate system does not meet the axes definitions recommended by the International Society of Biomechanics [241]. Therefore, to align the axis of rotation of the WIbS with the axis of rotation of the prosthetic knee using the joint coordinate system proposed by the International Society of Biomechanics, a rotation matrix  $R_{Calibration}$  is identified to satisfy Equation 4.3:

$$[R_{WIbS \text{ initial position}}][R_{Calibration}] = \begin{bmatrix} 0 & 1 & 0 \\ 0 & 0 & 1 \\ 1 & 0 & 0 \end{bmatrix} \quad (4.3)$$

Solving for  $R_{Calibration}$ , and using a property of the special orthogonal rotation group ( $R^{-1} = R^T$ ) results in Equation 4.4:

$$R_{Calibration} = [R^T_{WibS\ initial\ position}] \begin{bmatrix} 0 & 1 & 0 \\ 0 & 0 & 1 \\ 1 & 0 & 0 \end{bmatrix} \quad (4.4)$$

The matrix encoding the initial position of the WibS is then transformed to the coordinate frame recommended by the International Society of Biomechanics through the multiplication in Equation 4.5:

$$R_{WibS\ calibrated} = [R_{WibS}] [R_{Calibration}] \quad (4.5)$$

The calibration procedure is accomplished by clicking “calibrate” on the second page of the GUI (Figure 4.3(b)) once the WibS are placed appropriately on a fully extended prosthesis that is aligned to the global coordinate system of the WibS. After calibration, rotation matrices representing the time-varying orientation of both WibS (Equation (4.1)) can be multiplied by their respective calibration matrix. The resulting matrices are then used to generate a new matrix (Equation 4.6), which encodes the time-varying orientation of the prosthetic knee.

$${}_{distal}^{proximal} R_{Knee\ angle} = [R^T_{WibS\ calibrated - proximal}] [R_{WibS\ calibrated - distal}] \quad (4.6)$$

Cardan angles, representing the joint movements of the prosthetic knee, are then extracted via the ZXY moving axis rotation sequence, in a similar fashion to that of the rigid mocap plates in Chapter 2, Section 3.2.3. Since the prosthetic knee is a single-axis joint, there is no risk of encountering gimbal lock [113]. The second page of the GUI (Figure 4.3(b)) displays these Cardan angles in real-time.

#### 4.2.1.4 Technical Validation of the Wireless IMU-Based System

##### Experimental Design

The accuracy of the WibS and of the knee joint angle computations was determined through a comparison to a gold-standard optoelectronic mocap system (OptiTrack, Corvallis, OR, USA) and a cIMU system (Delsys, Natick, MA, USA). A five DoF robot arm [257] was used as a testing platform, as it allowed repeatable, isolated single-axis movement of the WibS. Three of the five

DoF were used to rotate a WibS about its X, Y, and Z-axis (Figure 4.5 (b)). Each WibS was attached to rigid motion capture plates containing four markers each, and a commercial IMU system. One WibS was placed on a stationary segment of the robotic arm (Figure 4.5 (a)), another on a location capable of moving about the three axes of the WibS (Figure 4.5 (b)).

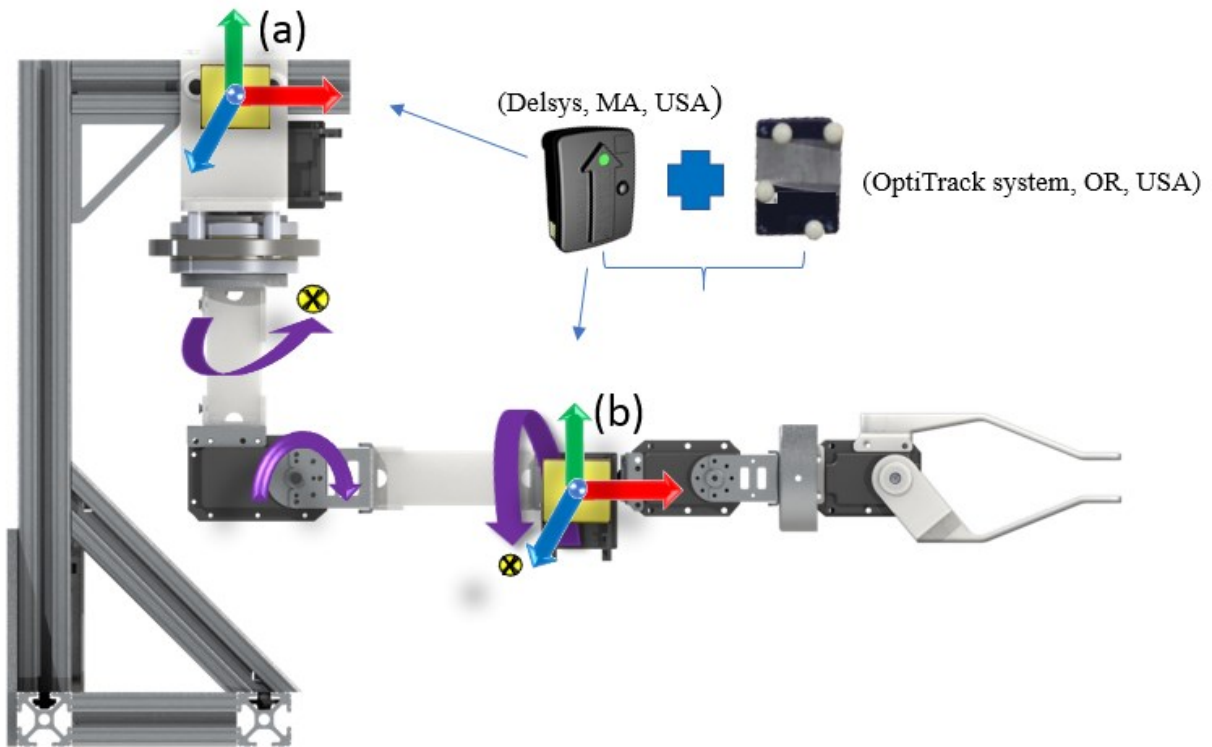


Figure 4.5: A five degree of freedom robotic arm was used as a platform to test the ability of the movement sensors to monitor single-axis movements. The three degrees of freedom used by the robot arm are marked in the figure by the three purple arrows between (a) and (b). The X's, which are enclosed by a yellow area, indicate a rotation arrow entering the page. Two movement sensors were used for the validation, each sensor was attached to a commercial inertial measurement unit system and a motion capture plate, containing four markers each. The movement sensors were then placed on a stationary section of the robotic arm (a) and a location capable of moving about the three axes of the movement sensors (b).

Accuracy and repeatability tests were performed for displacement and velocity using sinusoidal and Gaussian movement profiles. Sinusoidal and Gaussian movement profiles were chosen as they

are presentative of the cyclic nature of walking and have been shown to model single steps, respectively [62]. The sinusoid's frequency of oscillation, the standard deviation of the Gaussian, and the amplitudes of both waveforms were selected based on time-distance and kinematic parameters during gait of non-disabled adults and prosthesis users. The WlBS was tested with maximum velocities of 60, 120 and 180 degrees/second, which encompass the gait speed and cadence for prosthesis users during walking [64], [73], [80], [243]. For individuals with intact limbs, the knee provides a maximum range of motion of approximately 60 degrees during level walking [71], [80], [243] and traversal of stairs [80]. Prosthesis users experience lower knee ranges of motion during walking [73], [80], [243]. The selected range of motion for the two movement profiles spanned 180 and 90 degrees for the sinusoidal and Gaussian respectively, well above the anticipated 60 degrees of knee movement. Individuals with intact limbs take 0.8 s to complete a step [63], which is much quicker than for prosthesis users [73], [80], [243]. As a result, the standard deviation of the Gaussian profile was set such that 99.7% of the movement was achieved in 0.5 s. This experimental protocol was adapted from El-Gohary et al. [148] and Vette et al. [59], with modifications specific to gait as outlined in Table 4.1. Appendix D provides additional details on the cIMU and software used to implement the technical validation.

Table 4.1: Movement profiles and applied parameters.

<b>Movement Profile</b>	<b>Type</b>	<b>Sets</b>	<b>Amplitude</b>	<b>Frequency</b>	<b>Deviation (<math>\sigma</math>)</b>
Gaussian	Position	3	+90 degrees	N/A	0.083 (s)
	Velocity		60/120/180 (degrees/s)		$3(\sigma) = 0.25$ (s)
Sinusoid	Position	3	$\pm 90$ degrees	0.67/1.33/2 (Hz)	N/A
	Velocity		60/120/180 (degrees/s)		

## Data processing and Analysis

Data were processed using MATLAB 2016b (MathWorks, Natick, MA, USA). Mocap data were processed in a similar manner to that described in Chapter 3, Section 3.2.4. An orthonormal coordinate frame was derived for each rigid mocap plate. These local coordinate frames were used to obtain a rotation matrix defining the time-varying orientation of each mocap plate. A calibration process was utilized to align the mocap plates to their respective segments of the robotic limb. Ultimately, Cardan angles representing the appropriate single-axis movement of the robot were extracted from the orientation of the robotic limb segments. A similar GUI to that of the WlbS was developed to extract quaternions from the cIMU system and log the corresponding angles. Similar to other IMU validation studies, the accuracy of the WlbS was quantified by the root-mean-squared-error (RMSE) [67], [102], [109], [136], [139], [145], [147], [148], [159]. First, data from the WlbS (33 Hz) and the cIMU (33 Hz) were resampled to match the sampling rate of the OptiTrack mocap system (120 Hz). Then, any high-frequency noise was eliminated by a second order, low-pass Butterworth filter with a cut-off frequency of 4 Hz (Chapter 3, Section 3.2.4). Next, cross-correlation was used to align the signals temporally. Finally, the RMSE for each profile was calculated. RMSE values from individual trials were averaged across all trials.

## 4.3 Results

Performance of the WlbS is summarized in Figures 4.6 and 4.7 and Tables 4.2 and 4.3. In each plot, the dotted lines represent angles from the WlbS, solid lines angles from the cIMU system, and dashed lines angles from the mocap system. Rows represent results of a specific axis of rotation (X, Y, Z), columns represent results of different speeds (60, 120, 180 degrees/second).

### 4.3.1 Gaussian Movement

Figure 4.6 and Table 4.2 outline the results for the Gaussian profile. Isolated movements about each axis were within one degree and half a degree of agreement (RMSE) with the cIMU and mocap systems, respectively. The angles of both stationary axes for each movement were within one 3<sup>rd</sup> and one 10<sup>th</sup> of a degree of agreement with the cIMU and mocap systems, respectively.

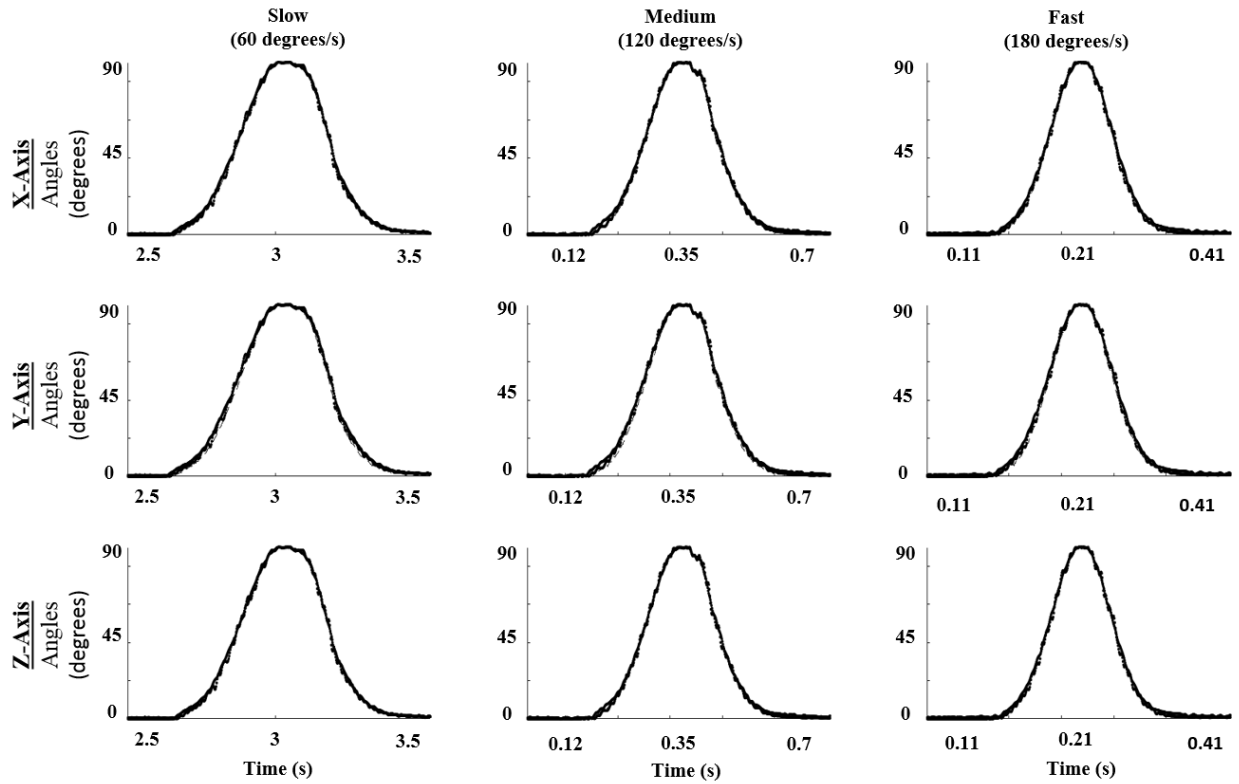


Figure 4.6: The results for the individual axis of the wireless inertial measurement unit-based (WibS) versus the commercial inertial measurement unit (cIMU) and motion capture (mocap) systems for the Gaussian profile. In each plot, the dotted lines represent angles from the WibS, the solid lines angles from the cIMU system, and the dashed lines angles from the mocap system. These lines are difficult to identify in the figure due to their good agreement. Results for individual axes (X, Y, Z) are structured in rows. The columns represent the tested speed. Isolated WibS movements about each axis were within a degree of agreement with both the cIMU and mocap systems. The movement of both stationary axes of the WibS were within a quarter of a degree relative to the cIMU and mocap systems.

Table 4.2: Accuracy and repeatability results for the Gaussian movement profile.

Speed	Moving Axis	RMSE (degrees)		Stationary Axis	RMSE (degrees)	
		Commercial IMU	Motion Capture		Commercial IMU	Motion Capture
Slow (60 degrees/s)	X-axis	0.660	0.257	Y-axis	0.034	0.028
				Z-axis	0.234	0.007
	Y-axis	0.642	0.257	X-axis	0.226	0.007
				Z-axis	0.033	0.028
	Z-axis	0.668	0.257	X-axis	0.240	0.007
				Y-axis	0.034	0.028
Medium (120 degrees/s)	X-axis	0.633	0.147	Y-axis	0.030	0.027
				Z-axis	0.052	0.005
	Y-axis	0.610	0.147	X-axis	0.051	0.005
				Z-axis	0.030	0.027
	Z-axis	0.662	0.147	X-axis	0.053	0.005
				Y-axis	0.030	0.027
Fast (180 degrees/s)	X-axis	0.867	0.279	Y-axis	0.021	0.02
				Z-axis	0.253	0.030
	Y-axis	0.878	0.279	X-axis	0.263	0.029
				Z-axis	0.020	0.02
	Z-axis	0.875	0.279	X-axis	0.251	0.029
				Y-axis	0.021	0.02

### 4.3.2 Sinusoidal Movement

Figure 4.7 and Table 4.3 outline the results for the sinusoidal profile. Isolated movements about each axis were within two and eight degrees of agreement at speeds less than 180 degrees/second for the cIMU and mocap systems, respectively. At 180 degrees/second, the error increased to six

and fourteen degrees of disagreement for the cIMU and mocap systems, respectively. The angles of both stationary axes for each movement and both systems were below one degree of disagreement.

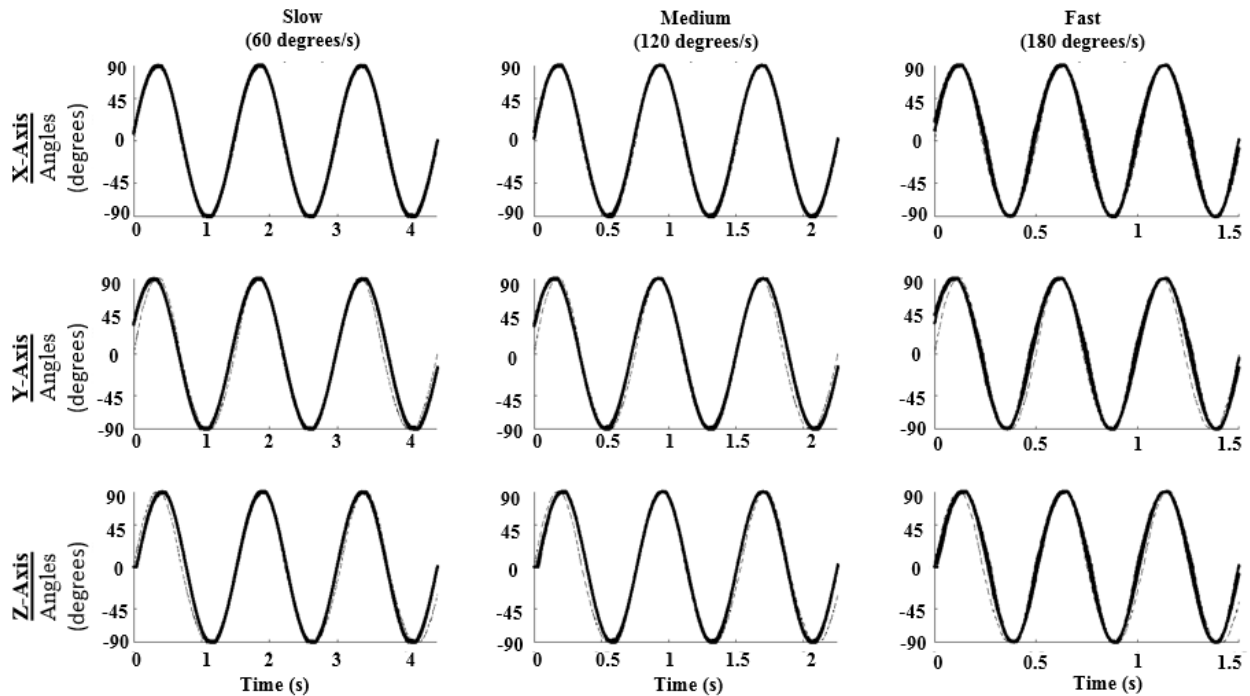


Figure 4.7: The results for the individual axis of the wireless inertial measurement unit-based system (WibS) versus the commercial inertial measurement unit (cIMU) and motion capture (mocap) systems for the sinusoidal profile. In each plot, the dotted lines represent angles from the WibS, the solid lines angles from the cIMU system, and the dashed lines angles from the mocap system. Results for individual axes (X, Y, Z) are structured in rows. The columns represent the tested speed. At the two lower speeds, isolated WibS movements about each axis were within two and eight degrees of agreement with the cIMU and mocap systems, respectively. At the fastest speed, the root mean square error increased to six and fourteen degrees of disagreement relative to the cIMU and mocap systems, respectively. WibS movement for both stationary axes was within one degree relative to the cIMU and mocap systems.

Table 4.3: Accuracy and repeatability results for the sinusoidal movement profile.

Speed	Moving Axis	RMSE (degrees)		Stationary Axis	RMSE (degrees)	
		Commercial IMU	Motion Capture		Commercial IMU	Motion Capture
Slow (60 degrees/s)	X-axis	1.538	5.705	Y-axis	0.028	0.431
				Z-axis	0.678	0.281
	Y-axis	1.494	7.981	X-axis	0.689	0.285
				Z-axis	0.029	0.431
	Z-axis	1.582	4.236	X-axis	0.680	0.278
				Y-axis	0.028	0.433
Medium (120 degrees/s)	X-axis	1.292	5.238	Y-axis	0.202	0.654
				Z-axis	0.463	0.172
	Y-axis	1.258	7.618	X-axis	0.461	0.174
				Z-axis	0.213	0.665
	Z-axis	1.289	3.584	X-axis	0.491	0.171
				Y-axis	0.194	0.643
Fast (180 degrees/s)	X-axis	5.317	11.478	Y-axis	0.138	0.536
				Z-axis	0.397	0.192
	Y-axis	5.357	13.484	X-axis	0.381	0.194
				Z-axis	0.139	0.535
	Z-axis	5.578	9.32	X-axis	0.418	0.192
				Y-axis	0.137	0.539

### 4.3.3 Results Summary

The results for the two movements demonstrate that the WiBS is capable of tracking single steps with less than a degree of error when compared to both the cIMU and mocap systems. Tracking cyclic movements resulted in a greater error, up to eight and fourteen degrees of disagreement with

the cIMU and mocap systems, respectively. The results also show that the WbS is better at tracking slower speeds, with optimal performance at around 120 degrees/second. Faster speeds resulted in greater errors. With two periods of flexion-extension (both approximately 60 degrees) in roughly 1 second, the knee joint reaches speeds around 120 degrees/second during normal walking for non-disabled individuals [80]. Following a similar trajectory, the prosthetic knee joint of above-knee prosthesis users experiences a decreased flexion-extension range (both approximately 20 degrees) in roughly 1.29 seconds, implying a knee joint rate around 62 degrees/second [80]. Below-knee prosthesis users experience a knee-joint range between that of non-disabled and above-knee prosthesis users [243]. Therefore, the developed movement sensor maybe able to provide reliable movement detection during walking for lower-limb prosthesis users but may not be reliable at higher speeds such as running or sprinting. However, since most lower-limb prosthesis users prominently use their prosthesis for ambulating, the limitations of the developed sensor is acceptable [258].

## 4.4 Discussion

In this chapter, we developed a wireless system capable of tracking the single-axis movement of a prosthetic knee. The WbS will ultimately be used to drive vibratory actuators capable of eliciting movement percepts in lower-limb prosthesis users, through the exploitation of the kinesthetic illusion.

### 4.4.1 System Performance

The results for the two movement profiles demonstrate that the WbS is capable of tracking single steps with a maximum error less than a degree when compared to both the cIMU and mocap systems. Conversely, results for cyclic movements showed greater disagreement relative to both the cIMU and mocap systems. The WbS was within two and eight degrees of agreement at speeds less than 180 degrees/second for the cIMU and mocap systems, respectively. At 180 degrees/second, the error increased to six and fourteen degrees of disagreement for the cIMU and mocap systems, respectively. Therefore, the WbS is more reliable in tracking cyclic movements at medium speeds (around 120 degrees/s) or lower.

The tracking capabilities of the movement sensors can be interpreted as a consequence of the underlying sensory fusion algorithm used by the IMU within the WbS. Sensory fusion algorithms

generally gather and combine signals from accelerometers, gyroscopes, magnetometers and other sensors to generate data regarding limb orientation or of the device itself [104], [115], [164]. The majority of sensor fusion techniques estimate unknown variables (e.g., quaternions) through discrete settings at successive times steps, which are dependent on past estimations and current measures [104], [115]. Complementary [133], [134], [146] and Kalman filters [134], [259] are the two main approaches utilized in these fusion algorithms. The BNO05 IMU module within the WbS most likely relies on either the Complementary or Kalman filter approach in estimating quaternions used for the angle approximation. However, as a proprietary device, it is difficult to determine which method was utilized. Consequently, results outlined in this chapter cannot confidently extend to other IMUs.

Ultimately, the WbS was shown to reliably track the single-axis movement of a lower-limb prosthetic device for both movement profiles, for the range of activities commonly performed by lower-limb prosthesis users. Thus, the aim of developing the WbS was achieved.

#### 4.4.2 Practical Use of the Movement Sensor

Even though, in most robotic applications, IMUs are mounted such that local coordinate axes coincide with hinge joint axes, the approach used in placing these devices on the human body offers greater benefit for prosthesis users. For robotic applications, hinge joint angle calculations are achieved through integration of angular rates about respective axes. This approach generally requires careful and precise placement of sensors [105]. Although IMUs are often utilized to determine human joint angles, the human leg is not a perfect hinge joint. Therefore, it is difficult to place inertial sensors on the human body such that a coordinate axis is aligned with the knee joint is difficult. As a result, IMUs are most commonly placed arbitrarily in relation to the joint of interest through the use of body straps [110], [148]. Similar to techniques applied for sensor placement on human limbs, the movement detection algorithm developed for the WbS allows the use of arbitrary placements of the sensors. This arbitrary placement of sensors is beneficial for prosthesis users as sensors might frequently be removed for replacement, recharging, or transferred to a new prosthesis. Therefore, an aesthetically appealing and adjustable strap with permanent attachments to the WbS can be designed to attach sensors proximally and distally of the prosthetic knee joint. The designed strap must be fixable to a prosthesis such that it is robust to disturbances during its use.

Similar to other methods used to calibrate IMU's, the proposed method for calibrating the WbS is simple and quick. When tracking human movement through inertial sensors, several calibration methods exist. The most common procedures such as the neutrum-pose (N-pose) and T-pose require individuals to perform poses or movements vital in obtaining anatomical interpretable joint angles [260], [261]. Tracking single-axis robotic joints (e.g., lower-limb prosthesis) with inertial sensors such as the WbS also require the use of poses. Specifically, calibration (as outlined in Section 4.2.1.3) ultimately requires prosthesis users to stand still (zero knee flexion) for a few seconds. The obtained calibration information is then retained until the removal of the prosthesis.

As the WbS is comprised of an IMU, sensor drift of both the proximal and distal movement sensor may lead to inaccurate detection of movement, resulting in false triggers. However, in practical applications, false movement detection due to drift can be easily combated by exploiting contact of the prosthetic foot with the ground. The velocity of the prosthetic foot is nearly zero when in contact with the ground; this information can be used to recalibrate the movement sensors while moving, greatly reducing drift [106], [152].

Ultimately, the WbS is more ergonomic and easier to set up than a mocap system. Moreover, the wireless sensor is cheaper than both mocap and commercial IMU systems.

#### **4.4.2.1 Limitations**

A limitation of using the developed sensor is that it may only be able to accurately track one angular position at a time, e.g., the knee flexion/extension angle. The results also indicate that the developed sensor may be able to provide reliable movement detection during walking for lower-limb prosthesis users, but not at higher speeds such as running or sprinting.

## **4.5 Conclusions**

This chapter outlined the design and development of an inexpensive inertial measurement unit-based wireless system capable of tracking the single-axis movement of a prosthetic knee. The device was designed to be light-weight and compact to be fitted within a prosthetic system for detecting knee movement. Our results showed that the developed sensor can reliably track single-axis movement of a prosthetic knee with optimal performance at speeds around 120 degrees/second. The tracking capabilities of the sensor imply the developed sensor is capable of reliably tracking walking speeds for lower-limb prosthesis users. In Chapter 5, a benchtop system

will be developed in which the wireless sensor is used to drive vibratory actuators capable of eliciting movement percepts in a prosthesis user, through the exploitation of the kinesthetic illusion.

## 5. Integration of a Kinesthetic Feedback Mechanism: A Case Study

### 5.1 Introduction

Chapter 3 detailed a method in which kinesthetic feedback might be delivered to prosthesis users through the kinesthetic illusion (KI). However, the KI was administered by manual activation of a vibratory actuator (the Vibrasense). For functional use, the mechanism driving the KI must be activated by movement of the prosthetic device (Figure 5.1).

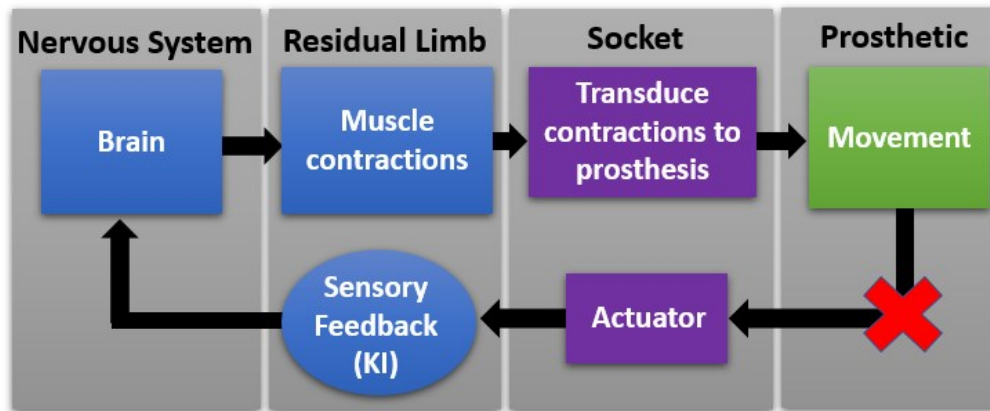


Figure 5.1: The kinesthetic illusion is currently administered manually. Activation of the actuator responsible for delivering the illusion is not connected to the movement of the prosthetic device.

Healthy limbs relay movement sensation in an intuitive manner through the use of biological sensors (e.g., muscle spindles) [206], [262]; lower-limb prosthetic devices must utilize sensing technologies to do the same. The sensed movement of the prosthetic joint can be used to trigger the actuator responsible for eliciting the illusion, in order to provide intuitive and functional movement feedback. Chapter 4 detailed the development of the wireless inertial measurement unit-based system (WibS). The WibS was shown to be capable of tracking single-axis movement of a prosthetic device for the range of walking speeds commonly performed by lower-limb prosthesis users. As detailed in Chapter 3, the KI is administered at a fixed frequency and amplitude; as such, only a binary signal is required to drive the actuator required for eliciting the illusion. Therefore, the WibS can be used to close the sensory feedback loop by relaying movement of the prosthetic joint to the actuator providing movement sensations in an intuitive and functional manner (Figure

5.2). This chapter focuses on developing a method to administer the KI by driving the vibratory instrument in response to movement detected by the WibS. A wired and wireless solution is developed with a corresponding threshold-based controller. Finally, the capacity of the system in administering the KI is determined through a case study with a prosthesis user.

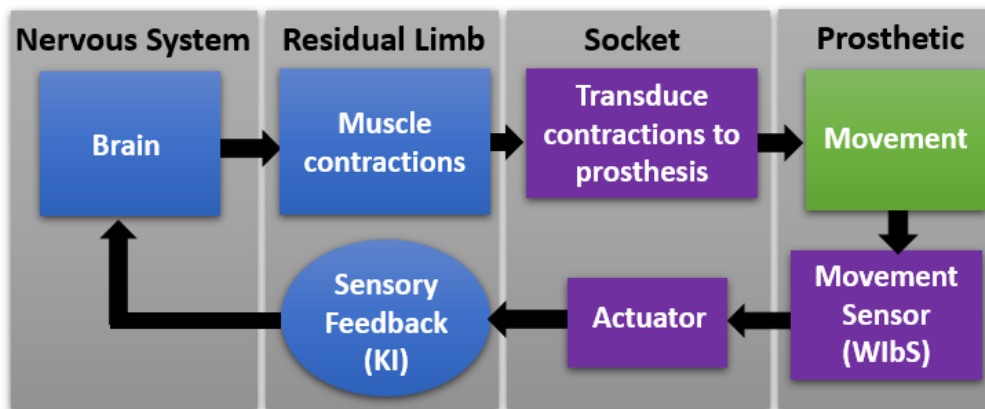


Figure 5.2: The WibS can be used to track the movement of the prosthetic device. This tool can be used to close the sensory feedback loop by activating the KI through a more intuitive and functional manner.

## 5.2 Methods

### 5.2.1 Triggering Systems for the Vibratory Actuator

#### 5.2.1.1 Wired System

The wired triggering system links the WibS to the vibratory actuator through serial communication and the FTDI Chip (Future Technology Devices International, Glasgow, Scotland). Two WibS, placed distally and proximally of the knee joint, transmit signals to a PC running the custom graphical user interface (GUI) of the WibS (Chapter 4, Section 4.2.1). The GUI discerns the movement of the joint through the joint angle computation algorithm outlined in Chapter 4. A threshold-based controller detects movement of the knee joint and sends a signal to activate or deactivate the vibratory actuator. The actuator is triggered through activation of the FTDI Chip (Figure 5.3).

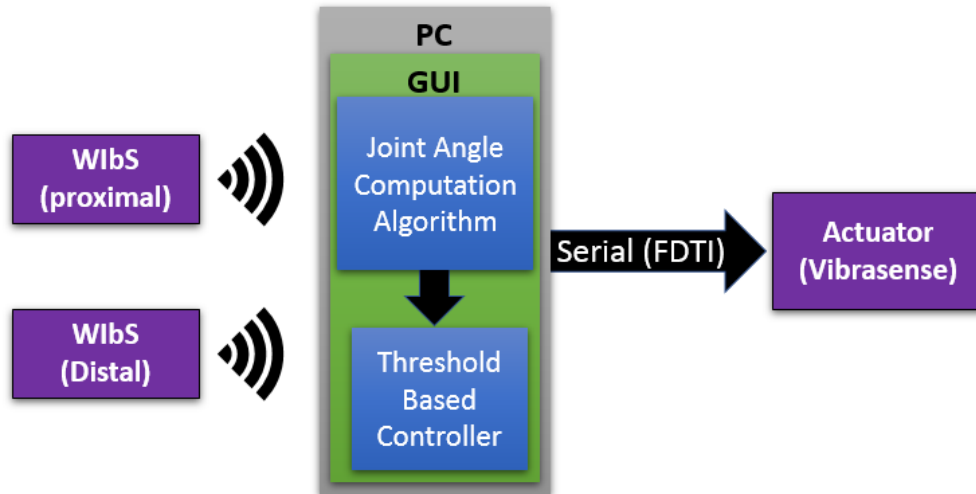


Figure 5.3: In the wired system, signals are received over the air (Bluetooth) from the WibS. These signals are then run through the joint angle computation algorithm and the threshold-based controller before activating the vibratory actuator through serial communication.

### 5.2.1.2 Wireless System

Similar to the wired system, the wireless triggering system uses the same threshold-based controller to determine when the knee joint is moving. The difference is the absence of the FTDI Chip. Using the same technique as that used to transmit unit quaternions from the WibS to the GUI (Chapter 4, Section 4.2.1), the wireless system uses the RN42 wireless Bluetooth module (Microchip Technology, Chandler, AZ, USA) to receive WibS data and trigger the vibratory actuator. The GUI establishes a virtual serial connection with the Bluetooth radio connected to an Arduino Pro Mini microcontroller (Arduino, Somerville, MA, USA). Triggers which encode movement information of the knee are then transmitted in a series of bytes. A package is composed of three bytes in total: two leading flags (0x2E) followed by a single byte representing whether the knee is moving or not. As previously discussed in Chapter 4, Section 4.2.1, the flags are used to identify when the receiver should start reading the message and decrease the probability of signal corruption (Figure 5.4).

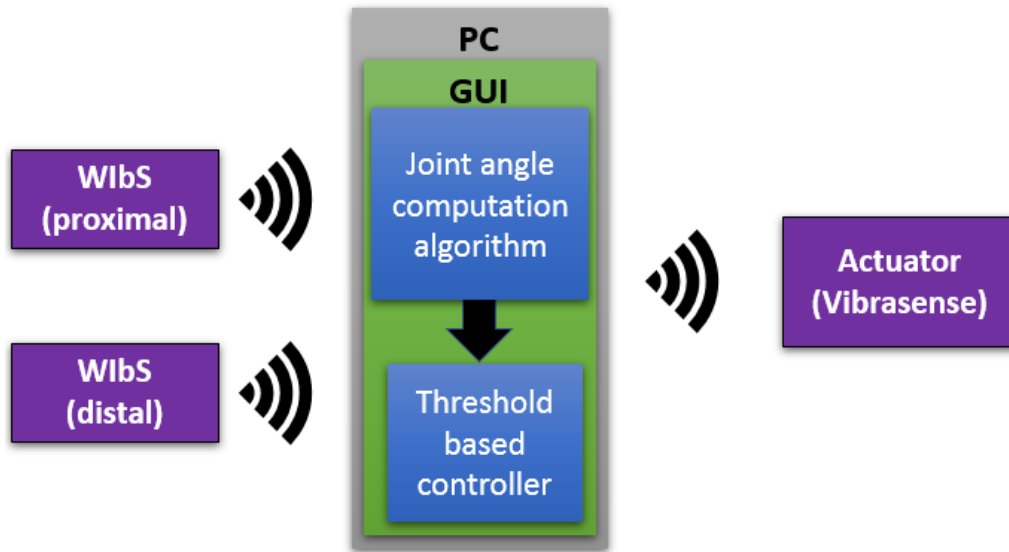


Figure 5.4: Similar to the wired system, the wireless system receives signals over the air (Bluetooth) from the WIBS. These signals are then run through the joint angle computation algorithm and the threshold-based controller before activating the vibratory actuator through a wireless signal.

Appendix E provides details on the development of both the wired and wireless systems.

### 5.2.2 Controller Design

The threshold-based controller infers movement by comparing the difference of successive single-axis joint angles (determined using two WIBS) to a predetermined sampling frequency dependent threshold (0.05 degrees). The threshold value was chosen to test the WIBS' sensitivity in a controlled environment, as discussed below in Section 5.2.4. Practical use of the movement sensor might permit a larger threshold (roughly 1 degree), based on the just noticeable difference for knee joint movement [44], [80], [86], [92], [243], [244], to prevent false movement detection. Moreover, the selected threshold (0.05 degrees) will differ based on the sampling frequency of the system. However, the corresponding velocity of 1.65 degrees/second ( $0.05 \text{ degrees} \times 33 \text{ Hz}$ ) can be as a frequency independent threshold, across systems with varying sampling frequencies. The threshold-based controller functions as follows, if the magnitude of the difference between successive joint angles exceeds the threshold, the knee is assumed to be in motion. In this situation,

the controller checks whether the actuator is already active. If that is the case, no action will be taken; otherwise, a signal is transmitted to activate the vibratory actuator. Conversely, if the difference between successive joint angles falls below the threshold, the system aims to deactivate the actuator if it is currently activated. The software flow diagram of the threshold-based controller is outlined in Figure 5.5.

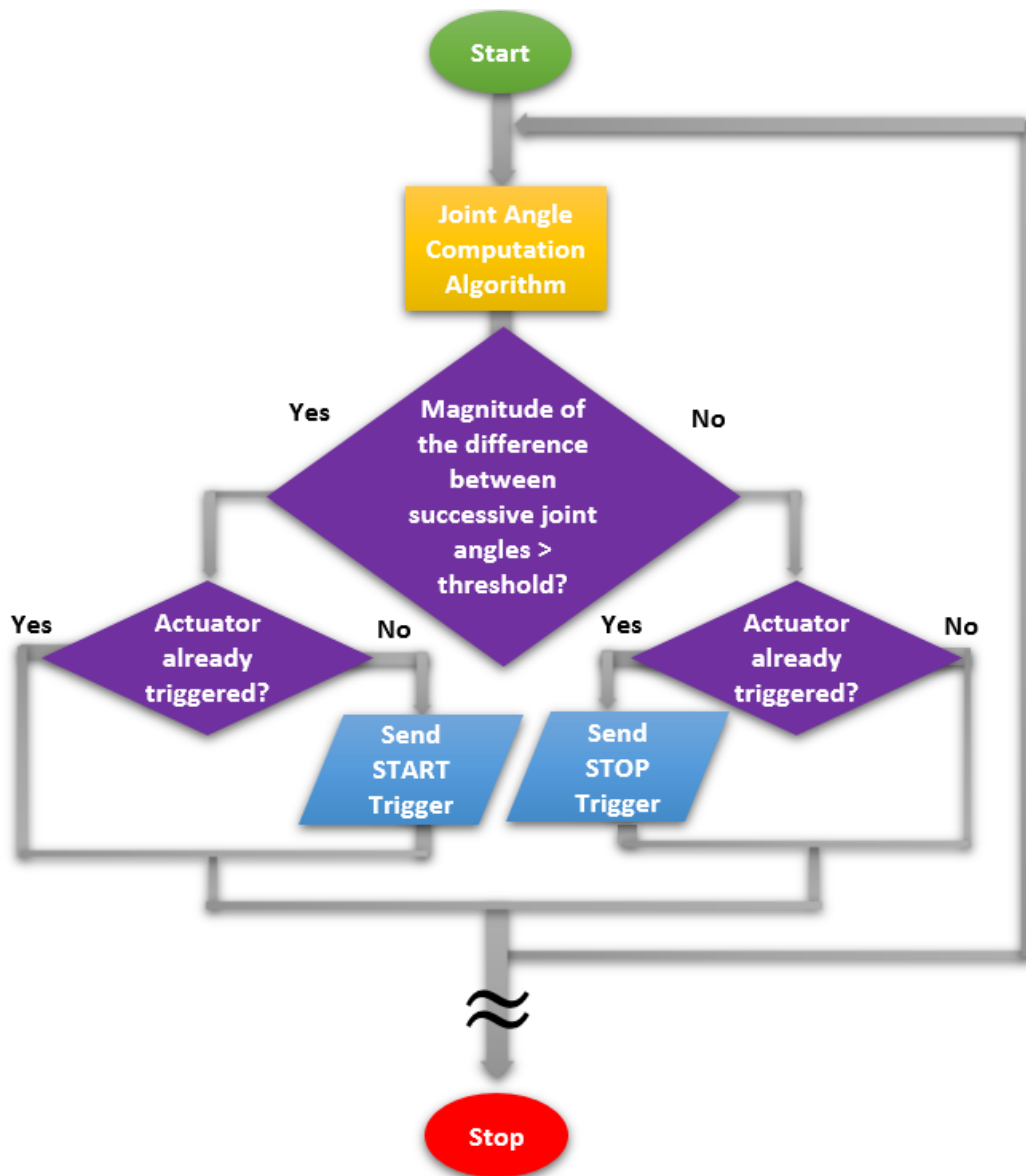


Figure 5.5: To infer movement, the controller determines whether the magnitude of the difference between successive joint angles is greater than a predefined sampling frequency dependent threshold. This controller is used to activate or deactivate the actuator responsible for administering the kinesthetic illusion.

### 5.2.3 Real-Time Filter Design

To eliminate high-frequency noise that may affect the integrity of the controller, while preserving the key features of joint movement, Cardan angles from the WbS were filtered at a cut-off frequency of 4 Hertz (Hz) (Chapter 3, Section 3.2.4), using a 5<sup>th</sup> order low-pass moving average filter.

#### 5.2.3.1 Filter Selection

Two main classes of linear filters exist: finite impulse response (FIR) or infinite impulse response (IIR) filters. On the one hand, FIR filters guarantee stability as all poles of the filter are at zero. However, they generally require many coefficients to achieve a similar performance as IIR filters. The difference equation of a general FIR filter is shown in Equation 5.1, where  $x[n]$  is the input signal,  $y[n]$  the output signal,  $N$  the filter order, and  $b_x$  the coefficients of the filter.

$$y[n] = b_0x[n] + b_1x[n-1] + \dots + b_Nx[n-N] = \sum_{i=0}^N b_i x[n-i] \quad (5.1)$$

On the other hand, IIR filters are recursive (depend on past/present inputs and past outputs) and do not guarantee stability. They are derived from similar analog filters. The difference equation of a general IIR filter is shown in Equation 5.2, where  $x[n]$  is the input signal,  $y[n]$  the output signal,  $p$  the required number of past inputs,  $Q$  the required number of past outputs,  $a_j$  the coefficients of inputs, and  $b_i$  the coefficient of outputs.

$$\sum_{j=0}^Q a_j y[n-j] = \sum_{i=0}^P b_i x[n-i] \quad (5.2)$$

An FIR moving average filter (with guaranteed stability) was chosen for this application as the combination of the rate at which the GUI acquires data and the cut-off frequency results in an acceptable (low) number of coefficients.

#### 5.2.3.2 Filter Design

Recall that the GUI samples data at 33 Hz (Chapter 4, Section 4.2.1). The digital cut-off frequency in Equation 5.4 is obtained by dividing the corresponding angular frequency in Equation 5.3 by the sampling rate.

$$\omega = 2\pi f_c = 2\pi (4\text{Hz}) \approx 25.13 \frac{\text{rads}}{\text{s}} \quad (5.3)$$

$$\Omega = \frac{\omega}{f_s} = \frac{25.13 \frac{\text{rad}}{\text{s}}}{33\text{Hz}} \approx 0.76 \text{ rads} \quad (5.4)$$

The number of terms required for the filter is then determined through the division of the constant  $\pi$  by the digital frequency, resulting in approximately 5 terms (Equation 5.5).

$$\text{Filter Order} = \frac{\pi}{\Omega} \approx 4.13 \Rightarrow 5 \quad (5.5)$$

The corresponding moving average filter is shown in Equation 5.6, where  $y[n]$  is the filter output, and  $\delta$  the impulse function.

$$y[n] = \frac{1}{5} \sum_{k=0}^4 \delta[n-k] \quad (5.6)$$

#### 5.2.4 Experimental Setup

An experimental trial was conducted to test the developed system's ability to elicit movement percepts in a participant with a lower-limb amputation that was capable of experiencing the KI. Participant P1 (Chapter 3, Section 3.3.1) was selected as he experienced strong and consistent movement percepts. The benchtop test was run one week after the initial testing of participant P1 as reported in Chapter 3. The benchtop system consisted of two WlbS attached proximally and distally to a single joint of the robotic arm as described in Chapter 4, Section 4.2.1. The automated robotic system was used for consistently triggering the vibration motor for a similar duration across trials, as opposed to relying on the experimenters manually moving the prosthetic limb, since moving the prosthesis for the same duration and rate across trials would be difficult to achieve manually. However, the participant was informed that movement of their prosthesis, as detected by the WlbS, was responsible for driving the vibratory actuator. To convince the participant, an initial demonstration of the WlbS attached proximally and distally of the knee joint of their dislocated prosthesis was shown to activate the vibration motor. However, after the participant's vision was occluded, the WlbS were transferred onto the robotic arm. A set of empty enclosures, identical to that of the WlbS were then attached to the same locations on the dislocated prosthesis. This was done such that the participant would continue to believe the movement sensors were still

attached to their prosthesis and responsible for activating the vibration motor whenever vision was not concealed. As a result, the participant was unaware that the robotic arm was used for capturing movement instead. Since the illusion is a psychophysical phenomenon, guiding the participant to link movement of their prosthesis to movement percepts has the potential to enhance the KI [263] (Figure 5.6).

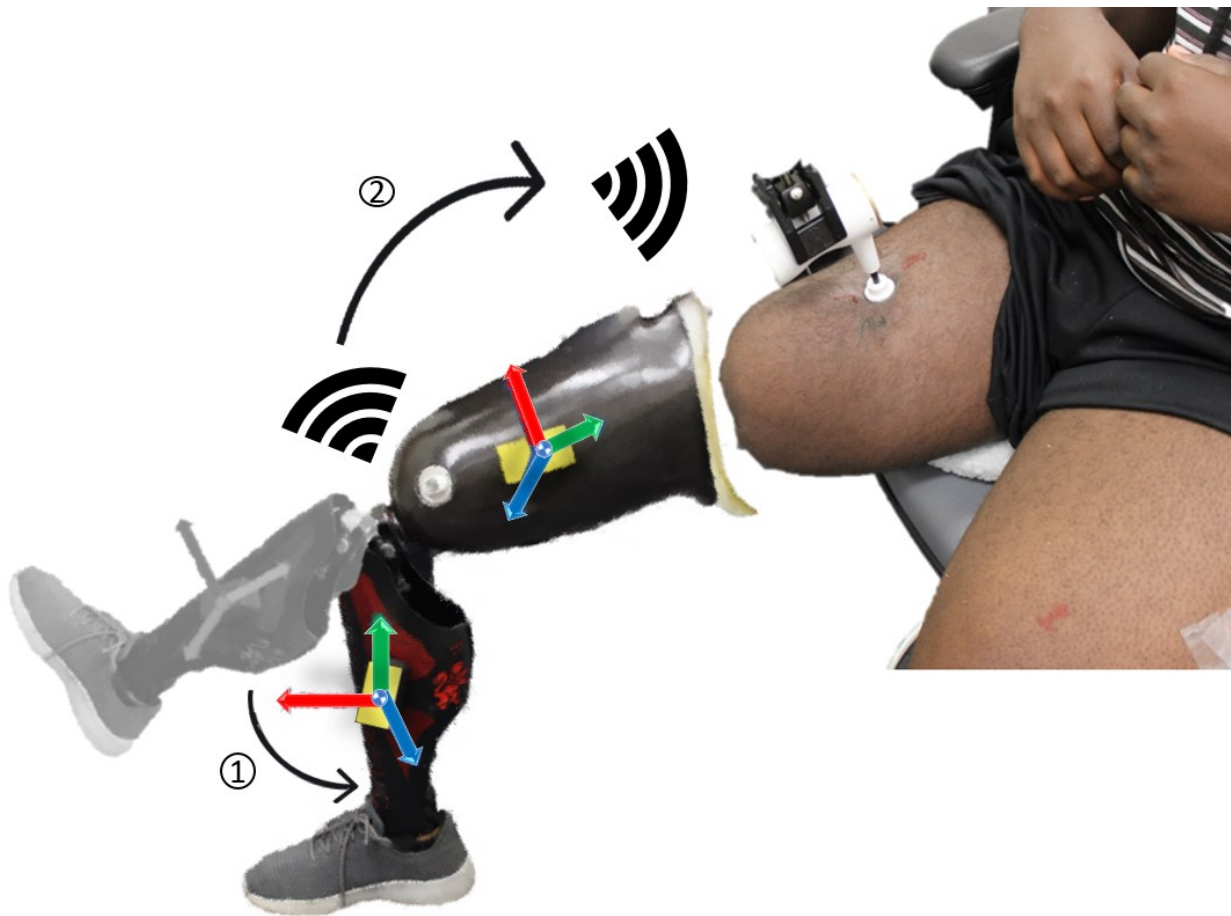


Figure 5.6: The participant was shown his unattached prosthesis with the WIbS attached proximally and distally of the knee joint. He was informed that movement of the prosthesis, as detected by the wireless modules, was responsible for triggering the vibratory actuator. The participant was unaware, however, that the robotic arm was used instead.

As the automated robotic system moved, the WIbS detected its movements and triggered the vibration of the actuator (Figure 5.7 (b)). The vibratory actuator was fixed to a location on the

participant which consistently elicited strong movement percepts (Figure 5.7 (a)), determined through an identical mapping procedure to Chapter 3, Section 3.2.3. Although both the wired and wireless systems were able to trigger the vibratory actuator, only the wireless system was used for the duration of the trial as it is more ergonomic. Even though the wireless system operates with a shorter battery life, it allows for greater flexibility in system placement when compared to the wired approach.

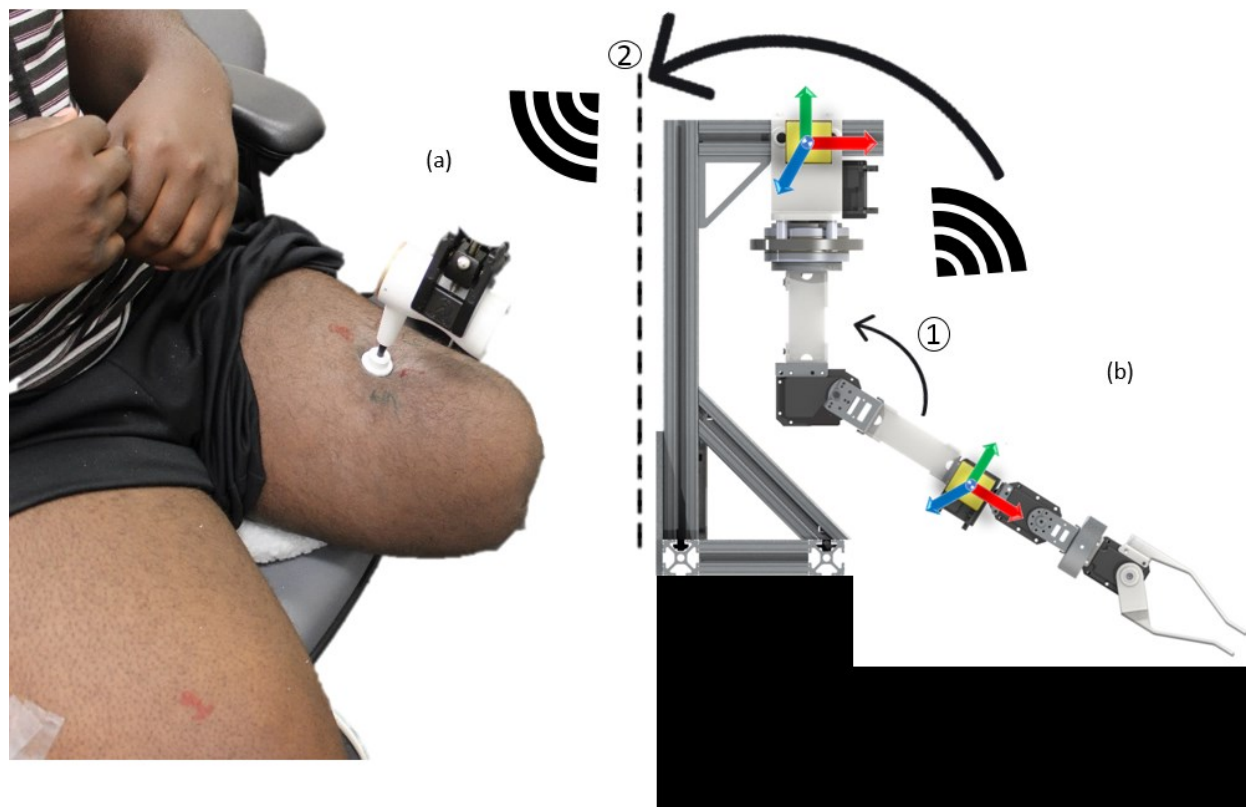


Figure 5.7: The participant was seated with a vibratory actuator pressed into his residual limb (a). A clamp was used to fix the vibratory actuator to a site eliciting strong and consistent movement percepts as determined through a mapping procedure identical to that described in Chapter 3, Section 3.2.3. The vibratory actuator was driven by the single-axis movement of a robotic limb detected by the WiBS (b). This robotic limb was used for repeatability and consistency across the trials.

### 5.2.5 Experimental Protocol

Similar to Chapter 3, Section 3.2.3, the experimental protocol was partitioned into two segments: percept mapping and illusion quantification. Percept mapping was used to identify a site on the participant's leg which elicited strong and consistent movement percepts. Illusion quantification was achieved using a motion capture (mocap) system (OptiTrack, OR, USA) and a psychophysical quantification (5-point Likert scale). Mocap plates were attached to the participant's intact limb, and a 5-point Likert scale was used to identify the kinematics and strength of the illusion, respectively. Once a site with strong and consistent movement percepts was determined, the head of the Vibrasense was fixed on that location using clamps in preparation for the limb matching trials. For consistency and repeatability across limb matching trials, the Vibrasense was triggered by the WlBS tracking the single-axis movement of the robotic arm from Chapter 4, Section 4.2.1, for a total duration of 15 seconds. In Chapter 3, the vibratory actuator was manually applied and withdrawn gradually, with this process taking about 5 seconds to perform. Fixing the vibratory actuators on the participant resulted in a full 20 seconds of constant vibration. This duration of constant stimulation produced discomfort for the participant and was therefore reduced to 15 seconds. The robotic arm followed half of a Gaussian trajectory (0 to 90 degrees) for the 15 second duration. However, since only the onset and termination of the robotic arm's movement was used to activate or inactive the Vibrasense respectively, any movement lasting for an equal duration could have been used. Once a location producing a consistent illusion was determined, the site was stimulated for 20 trials. For each trial, the participant was instructed to use their intact limb to match what they felt in configuration, velocity, and duration. This limb matching was performed 20 times, with data from mocap plates (attached proximally and distally of the intact knee) and the strength of illusion recorded for each trial. As in Chapter 3, the participant was fitted with noise-canceling headphones and an eye mask to occlude vision. The participant was also asked to remove his prosthesis for the duration of the trial.

### 5.2.6 Data Processing and Analysis

Data were processed using MATLAB 2016b (MathWorks, Natick, MA, USA). An orthonormal coordinate frame was derived for each mocap plate attached proximally and distally of the participant's intact knee. The local coordinate frames were used to obtain a rotation matrix defining the time-varying orientation of the participant's intact knee. Cardan angles representing the knee

joint angles were then extracted. Full details of this extraction method are outlined in Section 3.2.3 of Chapter 3.

## 5.3 Results

### 5.3.1 System Performance

Both the wireless and wired system were capable of driving the vibratory actuator through detection of the single-axis movement of the robotic arm. Through the entire trial, the frequency dependent threshold-based controller was able to track the state of the robot arm and properly activate or deactivate the vibratory actuator. Since there were no unexpected activations by the vibratory actuator, it can be inferred the real-time filter was able to eliminate any high-frequency noise that might have produced false triggers. Although the wireless system was more ergonomic than its wired counterpart, wireless communication introduced a greater delay. For both systems, signals were transmitted to the PC from the WIbS at 85 Hz (Chapter 4, Section 4.2.1), or approximately every 12 milliseconds (ms). Due to the greater computational demand of the GUI, the signals were transmitted from the paired computer to either the FTDI or Bluetooth radio (attached to the Vibrasense) at 33 Hz (Chapter 4, Section 4.2.1), or approximately every 31 ms, for both systems. The wired system required an additional 5 ms delay to reliably communicate with the Vibrasense, whereas the wireless system required 50 ms of delay for reliable communication. The accumulated delay at the instance when the Vibrasense was triggered was approximately 48 and 93 ms, for the wired and wireless systems, respectively. However, due to the internal transients (inherent delay within electronic systems) of the Vibrasense, there was an additional delay of approximately 700 ms from triggering of the vibration motor to stable actuation. The internal transients of the Vibrasense were estimated by subtracting the total delay of the wireless system (movement of the WIbS to actuation) from the cumulative delay within the system at the onset of triggering. The total delay of the wireless system was determined through the use of an iPhone SE's high-speed camera (Apple Inc., Cupertino, USA, CA) analyzed frame by frame through the Vegas Pro software (MAGIX, Berlin, Germany). The initial frame was chosen to be the first instance of WIbS movement. The final frame was determined by identifying the frame in which the vibration motor stabilized, achieved through visual inspection. Once stabilized the Vibrasense took 2 or 3 frames to complete a cycle which corresponded to 120 and 80 Hz respectively. Taking an average of 10 consecutive sample cycles it was estimated that the

frequency of vibration was 88 Hz which is close to the target frequency of 90 Hz. Through this analysis, the components of the total delay of the Vibrasense (approximately 700 ms) were determined to be roughly 500 ms from triggering until the initial movement of the actuator, and an additional 200 ms until actuation stabilization.

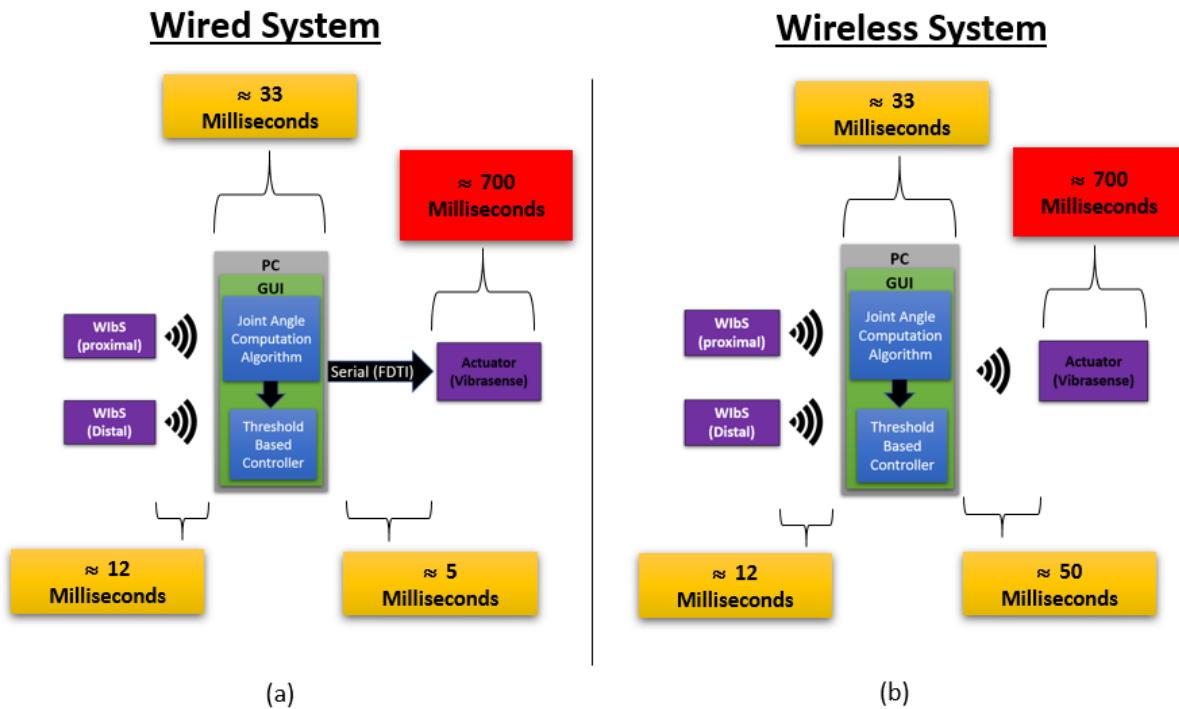


Figure 5.8: (a) and (b) outline the delay introduced by each compartment of the wired and wireless systems, respectively. Both systems impede signal flow from the movement sensor to the Vibrasense by less than 100 milliseconds. However, the internal transients of the Vibrasense introduce a repeatable delay of roughly 700 milliseconds.

### 5.3.2 Mapping and Illusion Quantification

Similar to Chapter 3, participant P1 experienced the KI in multiple sites on the residual limb (Figure 5.9). In contrast to the previous testing, the movement percept was experienced immediately. The participant reported “a pull about the knee”, and the pull was described as a “phantom limb that was moving”. The phantom limb was described as the “entire leg that appears, up to [the] toes” that “[appears] when [vibrated] but is gone when vibration stops”. The site with

the most consistent illusion (Site 3) was located on the anterior segment of the residual limb, similar in location to the site identified in Chapter 3. This site was used for determining the illusion kinematics. Site 3 was consistently reported as a 4 to 5 on the Likert scale. Similar to the findings in Chapter 3, continual stimulation of Site 3 would intermittently result in a stationary phantom limb. As a result, only 16 out of 20 trials evoked the movement percept. Like Chapter 3, the participant's experienced movement percepts can be loosely described as an inverted sigmoidal curve with an initial, middle and terminal phase. The knee flexion angles of the intact limb (captured by mocap plates), which represent the trajectories of the 16 trials that elicited movement percepts, are plotted, with similar trajectories color-coded to aid in visualization (Figure 5.10). In Figure 5.10, blue trajectories represent rapid knee flexion, red trajectories represent minimal and slow knee flexion, and black trajectories are between these extremes. Blue and black movement percept trajectories spanned all the trials; however, blue trajectories tended to concentrate in the middle of the trials and black at the end. Movement percepts represented by red trajectories concentrated near the beginning of the trials and tended to include minor extension within the first 5 seconds of each trial. In contrast to the previous experiment, the participant indicated that they would have continued to experience the illusion of knee flexion if vibration was sustained. The participant indicated trials 1, 4, 5, 8 and 10 experienced a terminal knee flexion angle of the phantom movement.



Figure 5.9: The anterior lateral view of P1's residual limb: The numbers were used as handles to represent the center of areas that, when stimulated, resulted in movement percepts. Site 3 represents the location with the most consistent movement percept; this was the site used for determining the illusion kinematics.

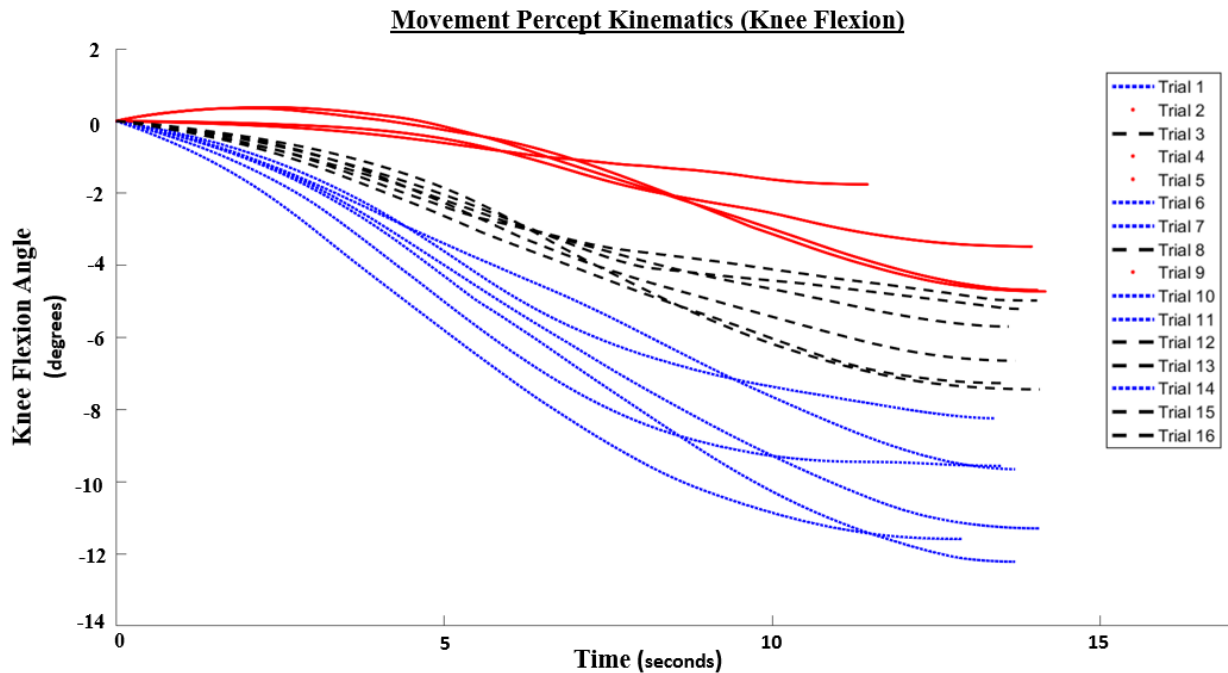


Figure 5.10: The experienced movement percepts (knee flexion) of participant P1, as demonstrated by the participant’s intact limb (captured by mocap plates), are plotted with similar trajectories color-coded. The movement percepts of participant P1 can be generally described as an inverted sigmoidal curve. The blue trajectories represent rapid knee flexion, red trajectories represent minimal and slow knee flexion, and black trajectories are between these extremes. The participant indicated that only five trials (1, 4, 5, 8 and 10) experienced a terminal knee flexion angle; the remainder of trials would have continued to indicate phantom movement if the vibration had not been terminated.

## 5.4 Discussion

In the context of prosthetic applications, practical feedback mechanisms must leverage information regarding the state of the prosthetic device during activities of daily living, e.g., ambulation. Current prosthetic devices are designed to transfer the user’s movement intentions to the movement of the prosthesis. However, information on the actual movement of the prosthesis is not sent back to the user in a functional or intuitive manner. Through a benchtop system, we have developed a method to close this sensory feedback loop.

### 5.4.1 System Performance

Overall, both the wired and wireless systems were able to reliably trigger the vibratory actuator used to elicit movement percepts on the participant; this was expected as both systems are nearly identical. The frequency threshold-based controller in conjunction with the real-time moving average filter was able to reliably detect the movement onset of the single-axis robotic arm and trigger the vibration motor appropriately with no false triggers. As the threshold (0.05 degrees) used for the threshold-based controller is dependent on the sampling frequency of the current system (33 Hz), other systems may require a different threshold value. However, the corresponding triggering velocity of 1.65 degrees/second ( $0.05 \text{ degrees} \times 33 \text{ Hz}$ ) will remain constant across systems. Robustness of the triggering algorithm is vital as false sensory input can be detrimental to reliable prosthetic operation.

Both the triggering systems operated with a delay of roughly 800 ms from triggering to actuation. The majority of the delay within both triggering systems was predominantly caused by the internal transients (inherent delay within electronic systems) of the Vibrasense tactor (700 ms). Practical use of the triggering systems requires a superior vibration actuator with minimal internal transients. Various studies have indicated that delays in feedback can decrease embodiment of the respective device, with a maximum delay of 300 ms resulting in minimal distortion of body ownership [36]. Incorrect activation of the system resulting in movement percepts during stationary activities such as standing can lead to loss of balance and injury [179]. Alternatively, the inability of the system to activate during gait will forfeit any benefits of the sensory feedback system. Therefore, vibratory actuators capable of eliciting movement percepts with shorter transient times must be developed for any practical implementation of this feedback system.

### 5.4.2 System Induced Movement Percepts

Similar to Chapter 3, the participant was able to experience the strongest (4 to 5 on the five-point Likert scale) and most consistent movement percepts in the anterior segment of their residual limb. The stimulation site which produced strong movement percepts (Figure 5.9, Site 3) was identified in a similar location to the site used for quantification of KI kinematics identified in previous testing (Chapter 3, Section 2.3.1). This finding suggests that sites producing movement percepts may remain consistent. Further testing with additional participants is required to determine whether this finding is consistent across users. Compared to previous experimentation (Chapter

3), the participant was able to experience and articulate movement percepts with greater ease. This supports previous discussions suggesting follow-up sessions may improve mental imagery and communication of movement sensations. During mapping, the participant did not experience any sensations characteristic of the isometric tonic vibration reflex (TVR) as they were able to relax and only experienced sensations representative of the KI.

Results of limb matching were similar to those in Chapter 3, with a subtle difference. During the previous testing, 50% of stimulation trials evoked a movement percept compared to 80% in the follow-up session. It is possible that fixing the vibratory actuator with clamps allowed for more consistent and repeatable stimulation. This increase in consistency may correlate to greater success of producing the same movement percepts. Participant P1 also experienced an increased number of movement percepts with no termination flexion angle. This increase in non-terminating movement percepts maybe accounted for by the 5 second decrease in stimulation time when compared to the work in Chapter 3.

Although movement percept trajectories (Figure 5.10) followed similar trends to those in Chapter 3 (Section 3.3.1), differences between groupings are not as distinct. This tighter grouping is consistent with the notion that a consistent and repeatable stimulation results from fixing the vibratory actuator on the participant. Red trajectories, mainly representing early trials, were the most representative of inverted sigmoidal curves as seen in Chapter 3. These red curves demonstrated a positive knee angle correlating to knee extension for half of the trial before changing directions to knee flexion. The experienced knee extension movement percept is most likely a result of the induced isometric TVR, implying the participant was unable to relax for the first half of many early trials when the vibratory actuator was fixed to their residual limb (in comparison to the mapping trials where contact was intermittent). With the exception of the extension in the red curves (isometric TVR), the remaining patterns are consistent with the discussion of muscle thixotropy described in Chapter 3.

In practical implementations of the KI feedback mechanism, discomfort introduced by extended contact of tactors with the residual limb of prosthesis users might be mitigated through the design of retractable tactors embedded within sockets. Augmenting a prosthetic socket with a retractable tactor, capable of eliciting the KI, will offer its own set of challenges. However, such a socket would allow for increased comfort for prosthesis users utilizing the KI feedback mechanism and

also holds potential for reducing the rate of experienced isometric TVR, when compared to a fixed implementation. Although socket design may help improve comfort and allow users to relax while the feedback mechanism is not administered, it does not address the relatively short stimulation time prior to experienced discomfort. A relatively short period of time of continuous vibration (20 seconds) led to experienced discomfort for the participant; gait may involve extended periods of movement. However, this may not be an issue as gait would not require continuous stimulation; an on-off pattern of stimulation would be more viable for the cyclical nature of ambulation. Similar to the solution proposed in Chapter 3, to combat muscle activation, strategic administration of the KI will be required to accommodate various gait patterns and other activities related to ambulation.

### 5.4.3 Practical Use of the Sensory Feedback System

#### 5.4.3.1 Socket Integration

Practical challenges remain before socket integration of this benchtop feedback system is viable. The size of the vibratory actuators presents challenges for socket integration. Locations on the residual limb where both the feedback device and prosthetic socket require strategic contact will present a unique challenge for socket design. Additionally, electrical and mechanical requirements of achieving the desired frequency and amplitude are demanding on miniaturized motors. Furthermore, consistent stimulation of the same anatomical location on the residual limb is required for generating a reliable movement percept. Any displacement of an ill-fitted socket will affect the feedback system's ability to produce consistent and reliable movement percepts. Consequently, prosthetic sockets must not sacrifice socket suspension to integrate the feedback system. In addition to this, a thorough mapping procedure is required to prevent placement of socket-integrated factors in areas evoking painful sensations, e.g., the "electrical shock" sensation experienced by multiple participants in Chapter 3.

As mentioned in Chapter 3, the isometric TVR also has practical implications for socket integration of the KI as a feedback mechanism. Since tissue is generally compressed within a socket, prosthetic users may have greater difficulty relaxing when the feedback mechanism is integrated within sockets, making them more susceptible to the isometric TVR. As previously mentioned, socket-integrated retractable factors might offer a viable solution. Although the design and development of a socket-integrated retractable factor system offer different technical challenges, such a socket will not only allow for increased comfort for prosthesis users utilizing the KI feedback mechanism

but holds potential for reducing the rate of experienced isometric TVR when compared to a fixed implementation.

#### **5.4.3.2 Further Development**

Practical use of the movement feedback system requires strategic administration of the illusion-inducing vibrations. As ambulation may involve varying speeds, a variety of algorithms may need to be developed for users to properly leverage the feedback system. Additionally, pre-stimulation of KI inducing sites (after an extended period of dormancy) may allow users to experience the greatest movement percept sensation when the feedback mechanism is activated. The KI feedback mechanism could also be augmented with simple vibratory substitution at different frequencies. For instance, single steps, rotatory movements (pivots), or other forms of ambulation with minimal duration may benefit from simple vibration, while longer periods of ambulation may benefit from the movement percepts. Algorithms for strategic administration of the illusion must account for fatigue and potential discomfort by participants on top of the varying forms of ambulation. These algorithms must be able to control the socket-integrated retractable system mentioned above, to improve comfort and mitigate the effect of the isometric TVR. Furthermore, users may require training for the most effective use of the movement percepts.

### **5.5 Conclusion**

Current prosthetic devices are designed to transfer the user's movement intentions to the movement of the prosthesis. However, knowledge of the actual movement is not sent back to the user in a functional or intuitive manner. In this chapter, the WIbS was implemented into a benchtop system, allowing us to demonstrate that the device can be used to elicit movement sensations in prosthesis user through the KI. The benchtop system relied on a threshold-based controller, designed to properly activate or deactivate the KI-inducing actuator based on the single-axis movement of a robotic system. An experimental trial with a participant capable of experiencing the KI demonstrated the benchtop system's efficacy in relaying movement feedback. Prior to clinical translation, further testing and development work in socket integration remains.

## 6. Conclusions

The kinesthetic illusion (KI) is a phenomenon that has been documented in both the upper and lower limbs of non-disabled individuals. It has been shown that, with appropriate stimulation, the muscle spindles in the residual limb of individuals with an upper-limb amputation can still evoke a kinesthetic response; even with the anatomical and physiological changes resulting from amputation. The work done for individuals with upper-limb amputations focused solely on individuals who have undergone targeted reinnervation (TR). However, it was not known to date whether similar results may be found for the remainder of individuals with amputation. The present body of work aimed to set up the necessary methodology for exploring the KI for individuals with lower-limb amputations which have not undergone the TR surgery and to take the first steps towards clinical translation of the KI as a feedback mechanism in prosthetic devices.

The first objective of this thesis aimed to perform an exploratory study to determine whether it is possible to provide kinesthetic feedback to individuals using lower-limb prosthesis who have not undergone TR, using the KI. The loss of proprioception and kinesthesia has profound implications for prosthesis users. The inability to distinguish when the lower limbs are moving can be highly disruptive to activities of daily living (e.g., ambulation). Without feedback, prosthesis users must constantly monitor their actions to perform tasks effectively. Chapter 3 described an exploratory study to establish whether individuals with non-TR lower-limb prostheses can experience the KI as related to their missing limbs. While blind to the researchers' intent, 4 out of 9 participants spontaneously reported movement percepts about their phantom knee or ankle. Out of the 4, half the participants experienced movement percepts in the direction characteristic of the KI. The other half experienced a sensation like the patellar reflex (i.e., a singular outward jerk of the knee). The remaining participants experienced a variety of sensations including a stationary phantom limb materializing in the same orientation as their intact limb, tingling, pressure, vibration, a change in temperature, and the sensation of electrical shock. Results from Chapter 3 suggest that the reliability and consistency of the illusion needs to be further investigated in lower-limb prosthesis users capable of experiencing the movement percepts. Practical use of the KI for rehabilitative applications, such as sensory feedback for prosthesis users, may also require user training.

The second objective of this thesis aimed to develop a low-cost wireless sensor, using inertial measurement units, which can track the movement of a single-axis prosthetic knee for the purpose

of bridging the movement of a prosthesis to actuators responsible for administering the KI. Recent technological innovations have produced advanced prostheses to help regain lost motor functionality. However, the majority of commercial lower-limb prosthetic devices to date are incapable of providing movement information such as joint angles. Although lower-limb prosthetic devices capable of measuring joint angles exist, the data is not easily accessible to researchers or prosthesis users. Chapter 4 outlined the design and validation of an inexpensive wireless sensor that is based on inertial measurement units, for the purpose of tracking the single-axis movement of a prosthetic knee. The wireless inertial measurement unit-based system (WibS) was validated through comparison with a commercial inertial measurement unit and a motion capture system. Results of the validation indicate that the WibS is capable of tracking the single-axis movement of lower-limb prostheses in the range of walking speeds commonly performed by prosthesis users. Through the use of the developed sensor, prostheses movement can be quantified and used to provide a functional and intuitive way of activating actuators that close the sensory feedback loop.

In Chapter 5, the WibS was implemented into a benchtop system, allowing us to demonstrate that the device can be used to elicit movement sensations in a prosthesis user through the KI. Both a wired and wireless system capable of driving the vibratory actuator responsible for eliciting the KI through the movement tracking capabilities of the WibS were developed. The two systems relied on a threshold-based controller, designed to properly activate or deactivate the KI-inducing actuator based on the single-axis movement of a robotic system. An experimental trial with a participant capable of experiencing the KI demonstrated the benchtop system's ability to successfully relay kinesthetic feedback.

## 1.1 Future Directions

In moving forward, investigations with a larger participant group will be necessary. Although nine individuals are an adequate sample size for a preliminary study, further investigation into the KI would benefit from a larger sample size. Further study into the KI may also include refinement of the experimental design to include training, visual reinforcement, and the introduction of voluntary muscle activation (as required for prosthesis use), and to proceed with further integration efforts in participants that experienced strong sensations.

As mentioned in Chapter 3, additional exploration of the KI is required to truly understand the illusion's translational capabilities. Chapters 3 and 4 have demonstrated the existence of the KI for individuals with non-TR lower-limb amputations, however this work has only begun to shed light onto the illusion as a potential sensory feedback mechanism. For individuals with TR upper-limb amputations, the KI has been shown to produce perceptions of complex hand grip movements, improve the accuracy of grasp movements, and establish a sense of agency (ownership) of the prosthesis [29]. Moreover, the vibration-induced kinesthetic perceptual feedback has been shown to function within the constraints of a clinical prosthetic socket. Similar investigations, relevant to individuals with lower-limb amputations, are required.

The practical utility of the kinesthetic feedback system developed in this thesis requires implementation and testing with a fully functional prosthesis. However, a variety of technical barriers exist that impede the development of such a system, many of which relate to the proper integration of the feedback device without compromising prosthetic fit or function. For example, the size of the vibratory actuators presents challenges for socket integration. Locations on the residual limb in which both the feedback device and prosthetic socket require strategic contact will present a unique challenge for socket design. Additionally, electrical and mechanical requirements of achieving the desired frequency and amplitude are demanding on miniaturized motors. Furthermore, consistent stimulation of the same anatomical location on the residual limb is required for generating a reliable movement percept. Any displacement of an ill-fitted socket will affect the feedback system's ability to produce consistent and reliable movement percepts. Consequently, prosthetic sockets must not sacrifice socket suspension to integrate the feedback system. Practical use of the movement feedback system will also require strategic administration of the illusion-inducing vibrations. For instance, a variety of algorithms must be developed for users to properly leverage the feedback system. These strategic algorithms must also combat muscle fatigue and discomfort, mitigate the effects of the isometric tonic vibration reflex, and leverage muscle thixotropy. All these pivotal barriers must be addressed prior to the clinical translation of the movement feedback system.

Functional testing of the kinesthetic feedback mechanism, a key component of evaluation, must still be addressed. When the developed sensory feedback system is implemented in a functioning prosthesis, user performance with and without the feedback must be compared. Therefore, the

development of meaningful tests sensitive to changes when sensory information is provided (e.g., walking, perturbation recovery, etc.) will be required to fully evaluate the practicality of the developed feedback system.

In summary, this body of work has confirmed that individuals with non-TR lower-limb amputations can experience the KI. While there are many improvements which need to be made to the developed feedback system, the current work confirms its potential to provide intuitive kinesthetic feedback for individuals using lower-limb prostheses.

## References

- [1] K. Ziegler-Graham, E. J. MacKenzie, P. L. Ephraim, T. G. Travison, and R. Brookmeyer, “Estimating the Prevalence of Limb Loss in the United States: 2005 to 2050,” *Archives of Physical Medicine and Rehabilitation*, vol. 89, no. 3, pp. 422–429, 2008.
- [2] T. C. Agu and M. E. Ojiaku, “The indications for major limb amputations: 8 years retrospective study in a private orthopaedic and trauma centre in the south-east Nigeria,” *Journal of Clinical Orthopaedics and Trauma*, vol. 7, no. 4, pp. 242–247, 2016.
- [3] G. M. Rommers, L. D. W. Vos, J. W. Groothoff, C. H. Schuiling, and W. H. Eisma, “Epidemiology of lower limb amputees in the north of the Netherlands: aetiology, discharge destination and prosthetic use,” *Prosthetics and Orthotics International*, vol. 21, pp. 92–99, 1997.
- [4] H. F. M. Pernot, G. M. M. Winnubst, J. J. M. Cluitmans, and L. P. De Witte, “Amputees in Limburg: Incidence, morbidity and mortality, prosthetic supply, care utilisation and functional level after one year,” *Prosthetics and Orthotics International*, vol. 24, no. 2, pp. 90–96, 2000.
- [5] Y. C. Kim, C. I. Park, D. Y. Kim, T. S. Kim, and J. C. Shin, “Statistical analysis of amputations and trends in Korea,” *Prosthet Orthot Int*, vol. 20, no. 2, pp. 88–95, 1996.
- [6] R. Sinha, W. J. A. Van Den Heuvel, and P. Arokiasamy, “Factors affecting quality of life in lower limb amputees,” *Prosthetics and Orthotics International*, vol. 35, no. 1, pp. 90–96, 2011.
- [7] M. W. Legro, G. D. Reiber, D. G. Smith, M. Del Aguila, J. Larsen, and D. Boone, “Prosthesis evaluation questionnaire for persons with lower limb amputations: Assessing prosthesis-related quality of life,” *Archives of Physical Medicine and Rehabilitation*, vol. 79, no. 8, pp. 931–938, 1998.
- [8] K. A. M. Samuelsson, O. Töytäri, A. L. Salminen, and Å. Brandt, “Effects of lower limb prosthesis on activity, participation, and quality of life: A systematic review,” *Prosthetics and Orthotics International*, vol. 36, no. 2, pp. 145–158, 2012.

- [9] J. M. Van Velzen, C. A. M. Van Bennekom, W. Polomski, J. R. Sloopman, L. H. V Van Der Woude, and H. Houdijk, "Physical capacity and walking ability after lower limb amputation: A systematic review," *Clinical Rehabilitation*, vol. 20, no. 11, pp. 999–1016, 2006.
- [10] D. Manchester, M. Woollacott, N. Zederbauer-Hylton, and O. Marin, "Visual, Vestibular and Somatosensory Contributions to Balance Control in the Older Adult," *Journal of Gerontology*, vol. 44, no. 4, pp. M118–M127, 1989.
- [11] T. Blackburn, K. M. Guskiewicz, M. A. Petschauer, and W. E. Prentice, "Balance and Joint Stability: The Relative Contributions of Proprioception and Muscular Strength," *Journal of Sport Rehabilitation*, vol. 9, no. 4, pp. 315–328, 2000.
- [12] H. Cochrane, K. Orsi, and P. Reilly, "Lower limb amputation Part 3: Prosthetics - A 10 year literature review," *Prosthetics and Orthotics International*, vol. 25, no. 1, pp. 21–28, 2001.
- [13] J. P. Pell, P. T. Donnan, F. G. R. Fowkes, and C. V. Ruckley, "Quality of life following lower limb amputation for peripheral arterial disease," *European Journal of Vascular Surgery*, vol. 7, no. 4, pp. 448–451, 1993.
- [14] J. R. Wingert, H. Burton, R. J. Sinclair, J. E. Brunstrom, and D. L. Damiano, "Joint-Position Sense and Kinesthesia in Cerebral Palsy," *Archives of Physical Medicine and Rehabilitation*, vol. 90, no. 3, pp. 447–453, 2009.
- [15] A. Kavounoudias, C. Tremblay, D. Gravel, A. Iancu, and R. Forget, "Bilateral changes in somatosensory sensibility after unilateral below-knee amputation," *Archives of Physical Medicine and Rehabilitation*, vol. 86, no. 4, pp. 633–640, 2005.
- [16] J. L. Riskowski, A. E. Mikesky, R. E. Bahamonde, T. V. Alvey, and D. B. Burr, "Proprioception, gait kinematics, and rate of loading during walking: Are they related?," *Journal of Musculoskeletal Neuronal Interactions*, vol. 5, no. 4, pp. 379–387, 2005.
- [17] K. R. Schoepp, M. R. Dawson, J. S. Schofield, J. P. Carey, and J. S. Hebert, "Design and Integration of an Inexpensive Wearable Mechanotactile Feedback System for Myoelectric Prostheses," *IEEE Journal of Translational Engineering in Health and Medicine*, vol. 6, no. 1, pp. 1–60, 2018.

- [18] J. S. Schofield, M. R. Dawson, J. P. Carey, and J. S. Hebert, "Characterizing the effects of amplitude, frequency and limb position on vibration induced movement illusions: Implications in sensory-motor rehabilitation," *Technology and Health Care*, vol. 23, no. 2, pp. 129–141, 2015.
- [19] J. Gonzalez, H. Suzuki, N. Natsumi, M. Sekine, and W. Yu, "Auditory display as a prosthetic hand sensory feedback for reaching and grasping tasks," in *Proceedings of the Annual International Conference of the IEEE Engineering in Medicine and Biology Society, EMBS*, 2012, pp. 1789–1792.
- [20] C. Antfolk, M. D'alonzo, B. Rosén, G. Lundborg, F. Sebelius, and C. Cipriani, "Sensory feedback in upper limb prosthetics," *Expert Review of Medical Devices*, vol. 10, no. 1, pp. 45–54, 2013.
- [21] D. J. Tyler and R. Babies, "U . S . Department of Veterans Affairs for sensory stimulation in human amputees," *Journal Neural Engineering*, vol. 12, no. 2, pp. 1–19, 2017.
- [22] T. A. Kuiken, G. A. Dumanian, R. D. Lipshutz, L. A. Miller, K. A. Stubblefield, R. D. Lipschutz, L. A. Miller, and K. A. Stubblefield, "The use of targeted muscle reinnervation for improved myoelectric prosthesis control in a bilateral shoulder disarticulation amputee," *Prosthetics and Orthotics International*, vol. 28, no. February, pp. 245–253, 2004.
- [23] P. Chaubey, T. Rosenbaum-Chou, W. Daly, and D. Boone, "Closed-loop vibratory haptic feedback in upper-limb prosthetic users," *Journal of Prosthetics and Orthotics*, vol. 26, no. 3, pp. 120–127, 2014.
- [24] J. S. Hebert, J. L. Olson, M. J. Morhart, M. R. Dawson, P. D. Marasco, T. A. Kuiken, and K. M. Chan, "Novel targeted sensory reinnervation technique to restore functional hand sensation after transhumeral amputation," *IEEE Transactions on Neural Systems and Rehabilitation Engineering*, vol. 22, no. 4, pp. 765–773, 2014.
- [25] K. Kim and J. E. Colgate, "Haptic feedback enhances grip force control of sEMG-controlled prosthetic hands in targeted reinnervation amputees," *IEEE Transactions on Neural Systems and Rehabilitation Engineering*, vol. 20, no. 6, pp. 798–805, 2012.
- [26] J. D. Brown, A. Paek, M. Syed, M. K. O'Malley, P. A. Shewokis, J. L. Contreras-Vidal, A.

- J. Davis, and R. B. Gillespie, "Understanding the role of haptic feedback in a teleoperated/prosthetic grasp and lift task," in *2013 World Haptics Conference, WHC 2013*, 2013, no. March 2014, pp. 271–276.
- [27] P. D. Marasco, K. Kim, J. E. Colgate, M. A. Peshkin, and T. A. Kuiken, "Robotic touch shifts perception of embodiment to a prosthesis in targeted reinnervation amputees," *Brain*, vol. 134, no. 3, pp. 747–758, 2011.
- [28] J. E. Cheesborough, G. A. Dumanian, L. H. Smith, and T. A. Kuiken, "Targeted Muscle Reinnervation and Advanced Prosthetic Arms," *Seminar in Plastic Surgery*, pp. 62–72, 2015.
- [29] P. D. Marasco, J. S. Hebert, J. W. Sensinger, C. E. Shell, J. S. Schofield, Z. C. Thumser, R. Nataraj, D. T. Beckler, M. R. Dawson, D. H. Blustein, S. Gill, B. D. Mensh, R. Granja-Vazquez, M. D. Newcomb, J. P. Carey, and B. M. Orzell, "Illusory movement perception improves motor control for prosthetic hands," *Science Translational Medicine*, vol. 10, no. 432, pp. 1–13, 2018.
- [30] R. Fitzpatrick and D. I. McCloskey, "Proprioceptive, visual and vestibular thresholds for the perception of sway during standing in humans.," *The Journal of Physiology*, vol. 478, no. 1, pp. 173–186, 1994.
- [31] D. W. Tan, M. A. Schiefer, M. W. Keith, J. R. Anderson, J. Tyler, and D. J. Tyler, "A neural interface provides long-term stable natural touch perception," *Science Translational Medicine*, vol. 6, no. 257, pp. 1–11, 2014.
- [32] A. Cloutier and J. Yang, "Design, Control, and Sensory Feedback of Externally Powered Hand Prostheses: A Literature Review," *Critical Reviews in Biomedical Engineering*, vol. 41, no. 2, pp. 161–181, 2013.
- [33] M. Li, D. Zhang, Y. Chen, X. Chai, L. He, Y. Chen, J. Guo, and X. Sui, "Discrimination and recognition of phantom finger sensation through transcutaneous electrical nerve stimulation," *Frontiers in Neuroscience*, vol. 12, no. APR, pp. 1–15, 2018.
- [34] J. S. Schofield, K. R. Evans, J. P. Carey, and J. S. Hebert, "Applications of sensory feedback in motorized upper extremity prosthesis: A review," *Expert Review of Medical Devices*, vol.

- 11, no. 5. pp. 499–511, 2014.
- [35] J. González and W. Yu, “Multichannel audio aided dynamical perception for prosthetic hand biofeedback,” in *2009 IEEE International Conference on Rehabilitation Robotics, ICORR 2009*, 2009, pp. 240–245.
- [36] B. Stephens-Fripp, G. Alici, and R. Mutlu, “A review of non-invasive sensory feedback methods for transradial prosthetic hands,” *IEEE Access*, vol. 6. pp. 6878–6899, 2018.
- [37] N. Fallahian, H. Saeedi, H. Mokhtarinia, and F. Tabatabai Ghomshe, “Sensory feedback add-on for upper-limb prostheses,” *Prosthetics and Orthotics International*, vol. 41, no. 3, pp. 314–317, 2017.
- [38] K. B. Fite, “Overview of the components used in active and passive lower-limb prosthetic devices,” in *Full Stride: Advancing the State of the Art in Lower Extremity Gait Systems*, V. Tepe and C. M. Peterson, Eds. New York, NY: Springer New York, 2017, pp. 55–74.
- [39] A. Staros, “The SACH ( Solid-Ankle Cushion-Heel ) Foot,” *Orthopedic & Prosthetic Appliance Journal*, vol. June-Augus, pp. 23–31, 1957.
- [40] N. P. Fey, G. K. Klute, and R. R. Neptune, “The influence of energy storage and return foot stiffness on walking mechanics and muscle activity in below-knee amputees,” *Clinical Biomechanics*, vol. 26, no. 10, pp. 1025–1032, 2011.
- [41] T. T. Sowell, “A preliminary clinical evaluation of the Mauch hydraulic foot-ankle system,” *New York*, vol. 5, no. 2, pp. 87–91, 1956.
- [42] I. Sedki and R. Moore, “Patient evaluation of the Echelon foot using the Seattle Prosthesis Evaluation Questionnaire,” *Prosthetics and Orthotics International*, vol. 37, no. 3, pp. 250–254, 2013.
- [43] C. Y. Ko, S. B. Kim, J. K. Kim, Y. Chang, H. Cho, S. Kim, J. Ryu, and M. Mun, “Biomechanical features of level walking by transtibial amputees wearing prosthetic feet with and without adaptive ankles,” *Journal of Mechanical Science and Technology*, vol. 30, no. 6, pp. 2907–2914, 2016.
- [44] L. Fradet, M. Alimusaj, F. Braatz, and S. I. Wolf, “Biomechanical analysis of ramp

- ambulation of transtibial amputees with an adaptive ankle foot system,” *Gait and Posture*, vol. 32, no. 2, pp. 191–198, 2010.
- [45] M. Ernst, B. Altenburg, M. Bellmann, and T. Schmalz, “Standing on slopes - How current microprocessor-controlled prosthetic feet support transtibial and transfemoral amputees in an everyday task,” *Journal of NeuroEngineering and Rehabilitation*, vol. 14, no. 1, pp. 1–16, 2017.
- [46] M. Grimmer, M. Holgate, R. Holgate, A. Boehler, J. Ward, K. Hollander, T. Sugar, and A. Seyfarth, “A powered prosthetic ankle joint for walking and running,” *BioMedical Engineering OnLine*, vol. 15, no. S3, p. 141, 2016.
- [47] P. Z. Feczko, L. M. Jutten, M. J. Van Steyn, P. Deckers, P. J. Emans, and J. J. Arts, “Comparison of fixed and mobile-bearing total knee arthroplasty in terms of patellofemoral pain and function: A prospective, randomised, controlled trial,” *BMC Musculoskeletal Disorders*, vol. 18, no. 1, pp. 1–9, 2017.
- [48] A. M. El-Sayed, N. A. Hamzaid, and N. A. Abu Osman, “Technology Efficacy in Active Prosthetic Knees for Transfemoral Amputees: A Quantitative Evaluation,” *The Scientific World Journal*, vol. 2014, pp. 1–17, 2014.
- [49] C. S. To, R. Kobetic, T. C. Bulea, M. L. Audu, J. R. Schnellenger, G. Pinault, and R. J. Triolo, “Stance control knee mechanism for lower-limb support in hybrid neuroprosthesis,” *The Journal of Rehabilitation Research and Development*, vol. 48, no. 7, p. 839, 2011.
- [50] C. W. Radcliffe and L. Lamoreux, “UC-BL Pneumatic Swing Control Unit for Above-Knee Prostheses,” Manhasset, 1968.
- [51] S. A. Fuenzalida Squella, A. Kannenberg, and Â. Brandão Benetti, “Enhancement of a prosthetic knee with a microprocessor-controlled gait phase switch reduces falls and improves balance confidence and gait speed in community ambulators with unilateral transfemoral amputation,” *Prosthetics and Orthotics International*, vol. 42, no. 2, pp. 228–235, 2018.
- [52] D. Hill and H. Herr, “Effects of a powered ankle-foot prosthesis on kinetic loading of the contralateral limb: A case series,” *IEEE International Conference on Rehabilitation*

*Robotics*, 2013.

- [53] L. Flynn, J. Geeroms, R. Jimenez-Fabian, B. Vanderborght, N. Vitiello, and D. Lefeber, “Ankle-knee prosthesis with active ankle and energy transfer: Development of the CYBERLEGs Alpha-Prosthesis,” *Robotics and Autonomous Systems*, vol. 73, pp. 4–15, 2015.
- [54] F. Sup, H. A. Varol, and M. Goldfarb, “Upslope walking with a powered knee and ankle prosthesis: Initial results with an amputee subject,” *IEEE Transactions on Neural Systems and Rehabilitation Engineering*, vol. 19, no. 1, pp. 71–78, 2011.
- [55] S. K. Au, H. Herr, J. Weber, and E. C. Martinez-Villalpando, “Powered ankle-foot prosthesis for the improvement of amputee ambulation,” *Annual International Conference of the IEEE Engineering in Medicine and Biology - Proceedings*, pp. 3020–3026, 2007.
- [56] M. W. Whittle, “Gait analysis,” in *Soft Tissues: Trauma and Sports Injuries discrepancy*, vol. 4, no. 1, Butterworth-Heinemann Ltd, 1984, pp. 187–199.
- [57] T. M. Kepple, K. L. Siegel, and S. J. Stanhope, “Relative contributions of the lower extremity joint moments to forward progression and support during gait,” *Gait and Posture*, vol. 6, no. 1, pp. 1–8, 1997.
- [58] H. Goujon-Pillet, E. Sapin, P. Fodé, and F. Lavaste, “Three-Dimensional Motions of Trunk and Pelvis During Transfemoral Amputee Gait,” *Archives of Physical Medicine and Rehabilitation*, vol. 89, no. 1, pp. 87–94, 2008.
- [59] A. H. Vette, E. Sanin, A. Bulsen, A. Morris, K. Masani, and M. R. Popovic, “A Portable and Automated Postural Perturbation System for Balance Assessment, Training, and Neuromuscular System Identification,” *Journal of Medical Devices*, vol. 2, no. 4, p. 041007, 2008.
- [60] R. L. Waters and S. Mulroy, “The energy expenditure of normal and pathologic gait,” *Gait and Posture*, vol. 9, no. 3, pp. 207–231, 1999.
- [61] S. H. Cho, J. M. Park, and O. Y. Kwon, “Gender differences in three dimensional gait analysis data from 98 healthy Korean adults,” *Clinical Biomechanics*, vol. 19, no. 2, pp. 145–152, 2004.

- [62] C. Glackin, C. Salge, M. Greaves, D. Polani, S. Slavnić, D. Ristić-Durrant, A. Leu, and Z. Matjačić, “Gait trajectory prediction using Gaussian process ensembles,” in *IEEE-RAS International Conference on Humanoid Robots*, 2015, vol. 2015–Febru, no. April 2016, pp. 628–633.
- [63] J. F. Item-Glatthorn and N. A. Maffiuletti, “Clinical Assessment of Spatiotemporal Gait Parameters in Patients and Older Adults,” *Journal of Visualized experiments*, vol. 93, no. 93, pp. 1–6, 2014.
- [64] P. S. MS, G. A. Steven, R. D. Lipschutz, and T. A. Kuiken, “Differences in Gait Characteristics Between Persons With Bilateral Transtibial Amputations, Due to Peripheral Vascular Disease and Trauma, and Able-Bodied Ambulators,” *Archives of Physical Medicine and Rehabilitation*, vol. 87, no. 7, pp. 1386–1394, 2008.
- [65] J. Sun, S. Wu, and P. A. Voglewede, “Dynamic Simulation of Human Gait Model With Predictive Capability,” in *Journal of Biomechanical Engineering*, 2018, vol. 140, no. 3, p. 031008.
- [66] A. Gefen, M. Megido-Ravid, Y. Itzhak, and M. Arcan, “Biomechanical Analysis of the Three-Dimensional Foot Structure During Gait: A Basic Tool for Clinical Applications,” *Journal of Biomechanical Engineering*, vol. 122, no. 6, p. 630, 2000.
- [67] G. S. Murley, H. B. Menz, and K. B. Landorf, “Foot posture influences the electromyographic activity of selected lower limb muscles during gait,” *Journal of Foot and Ankle Research*, vol. 2, no. 1, pp. 1–9, 2009.
- [68] S. Al-Obaidi, J. C. Wall, A. Al-Yaqoub, and M. Al-Ghanim, “Basic gait parameters: A comparison of reference data for normal subjects 20 to 29 years of age from Kuwait and Scandinavia,” *The Journal of Rehabilitation Research and Development*, vol. 40, no. 4, p. 361, 2003.
- [69] M. D. Latt, H. B. Menz, V. S. Fung, and S. R. Lord, “Walking speed, cadence and step length are selected to optimize the stability of head and pelvis accelerations,” *Experimental Brain Research*, vol. 184, no. 2, pp. 201–209, 2008.
- [70] H. G. Kang and J. B. Dingwell, “Separating the effects of age and walking speed on gait

- variability,” *Gait and Posture*, vol. 27, no. 4, pp. 572–577, 2008.
- [71] J. W. Kwon, S. M. Son, and N. K. Lee, “Changes of kinematic parameters of lower extremities with gait speed: a 3D motion analysis study,” *Journal of Physical Therapy Science*, vol. 27, no. 2, pp. 477–479, 2015.
- [72] J. L. Lelas, G. J. Merriman, P. O. Riley, and D. C. Kerrigan, “Predicting peak kinematic and kinetic parameters from gait speed,” *Gait and Posture*, vol. 17, no. 2, pp. 106–112, 2003.
- [73] F. Farahmand, T. Rezaeian, R. Narimani, and P. H. Dinan, “Kinematic and dynamic analysis of the gait cycle of above-knee amputees,” *Scientia Iranica*, vol. 13, no. 3, pp. 261–271, 2006.
- [74] J. H. Hollman, E. M. McDade, and R. C. Petersen, “Normative spatiotemporal gait parameters in older adults,” *Gait and Posture*, vol. 34, no. 1, pp. 111–118, 2011.
- [75] N. Vanicek, S. Strike, L. McNaughton, and R. Polman, “Gait patterns in transtibial amputee fallers vs. non-fallers: Biomechanical differences during level walking,” *Gait and Posture*, vol. 29, no. 3, pp. 415–420, 2009.
- [76] S. B. Michaud, S. A. Gard, and D. S. Childress, “A preliminary investigation of pelvic obliquity patterns during gait in persons with transtibial and transfemoral amputation,” *J Rehabil Res Dev*, vol. 37, no. 1, pp. 1–10, 2000.
- [77] K. R. Kaufman, J. A. Levine, R. H. Brey, B. K. Iverson, S. K. McCrady, D. J. Padgett, and M. J. Joyner, “Gait and balance of transfemoral amputees using passive mechanical and microprocessor-controlled prosthetic knees,” *Gait and Posture*, vol. 26, no. 4, pp. 489–493, 2007.
- [78] A. D. Segal, M. S. Orendurff, G. K. Klute, M. L. McDowell, J. A. Pecoraro, J. Shofer, and J. M. Czerniecki, “Kinematic and kinetic comparisons of transfemoral amputee gait using C-Leg and Mauch SNS prosthetic knees,” *The Journal of Rehabilitation Research and Development*, vol. 43, no. 7, p. 857, 2006.
- [79] S. M. H. J. Jaegers, J. H. Arendzen, and H. J. de Jongh, “Prosthetic gait of unilateral transfemoral amputees: A kinematic study,” *Archives of Physical Medicine and*

- Rehabilitation*, vol. 76, no. 8, pp. 736–743, 1995.
- [80] T. S. Bae, K. Choi, D. Hong, and M. Mun, “Dynamic analysis of above-knee amputee gait,” *Clinical Biomechanics*, vol. 22, no. 5, pp. 557–566, 2007.
- [81] C. H. Pritham, “Biomechanics and shape of the above-knee socket considered in light of the ischial containment concept,” *Prosthetics and Orthotics International*, vol. 14, no. 1, pp. 9–21, 1990.
- [82] C. W. Radcliffe, “Above-knee prosthetics,” *Prosthetics and orthotics international*, vol. 1, no. 3, pp. 146–160, 1977.
- [83] C. Sjödaahl, G. B. Jarnlo, B. Söderberg, and B. M. Persson, “Pelvic motion in trans-femoral amputees in the frontal and transverse plane before and after special gait re-education,” *Prosthetics and Orthotics International*, vol. 27, no. 3, pp. 227–237, 2003.
- [84] W. S. Marras and K. P. Granata, “Spine loading during trunk lateral bending motions,” *Journal of Biomechanics*, vol. 30, no. 7, pp. 697–703, 1997.
- [85] J. Sullivan, M. Uden, K. P. Robinson, and S. Sooriakumaran, “Rehabilitation of the trans-femoral amputee with an osseointegrated prosthesis: The United Kingdom experience,” *Prosthetics and Orthotics International*, vol. 27, no. 2, pp. 114–120, 2003.
- [86] R. K. Laughman, L. J. Askew, R. R. Bleimeyer, and E. Y. Chao, “Objective clinical evaluation of function: Gait analysis,” *Physical Therapy*, vol. 64, no. 12, pp. 1839–1845, 1984.
- [87] A. H. Vrieling, H. G. van Keeken, T. Schoppen, E. Otten, J. P. K. Halbertsma, A. L. Hof, and K. Postema, “Obstacle crossing in lower limb amputees,” *Gait and Posture*, vol. 26, no. 4, pp. 587–594, 2007.
- [88] X. Drevelle, C. Villa, C. Sauret, P. Fode, N. Martinet, H. Pillet, and F. Lavaste, “Vaulting quantification for transfemoral amputees in different gait situations,” *Computer Methods in Biomechanics and Biomedical Engineering*, vol. 16, no. sup1, pp. 126–127, 2013.
- [89] C. Villa, X. Drevelle, X. Bonnet, F. Lavaste, I. Loiret, P. Fodé, and H. Pillet, “Evolution of vaulting strategy during locomotion of individuals with transfemoral amputation on slopes

- and cross-slopes compared to level walking,” *Clinical Biomechanics*, vol. 30, no. 6, pp. 623–628, 2015.
- [90] X. Drevelle, C. Villa, X. Bonnet, I. Loiret, P. Fodé, and H. Pillet, “Vaulting quantification during level walking of transfemoral amputees,” *Clinical Biomechanics*, vol. 29, no. 6, pp. 679–683, 2014.
- [91] D. J. DiAngelo, D. A. Winter, D. N. Ghista, and W. R. Newcombe, “Performance assessment of the Terry Fox jogging prosthesis for above-knee amputees,” *Journal of Biomechanics*, vol. 22, no. 6–7, 1989.
- [92] S. S. Rao, L. A. Boyd, S. J. Mulroy, E. L. Bontrager, J. K. Gronley, and J. Perry, “Segment velocities in normal and transtibial amputees: Prosthetic design implications,” *IEEE Transactions on Rehabilitation Engineering*, vol. 6, no. 2, pp. 219–226, 1998.
- [93] B. Kitabayashi, “The Physical Therapist’s Responsibility to the Lower Extremity Child Amputee,” *Physical Therapy*, vol. 41, no. 10, pp. 722–727, 1961.
- [94] C. A. Cohen, “Scapulocostal syndrome: diagnosis and treatment,” *South Med J*, vol. 73, no. 4, p. 433–4, 437 ST–Scapulocostal syndrome: diagnosis, 1980.
- [95] R. Morotti, C. Rizzi, D. Regazzoni, and G. Colombo, “Digital Human Modelling to Analyse Virtual Amputee’s Interaction With the Prosthesis,” in *Volume 1A: 34th Computers and Information in Engineering Conference*, 2014, p. V01AT02A074.
- [96] L. Nolan, A. Wit, K. Dudziński, A. Lees, M. Lake, and M. Wychowański, “Adjustments in gait symmetry with walking speed in trans-femoral and trans-tibial amputees,” *Gait and Posture*, vol. 17, no. 2, pp. 142–151, 2003.
- [97] C. M. Powers, S. Rao, and J. Perry, “Knee kinetics in trans-tibial amputee gait,” *Gait and Posture*, vol. 8, no. 1, pp. 1–7, 1998.
- [98] H. Nadollek, S. Brauer, and R. Isles, “Outcomes after trans-tibial amputation: the relationship between quiet stance ability, strength of hip abductor muscles and gait,” *Physiotherapy research international: the journal for researchers and clinicians in physical therapy*, vol. 7, no. 4, pp. 203–214, 2002.

- [99] E. Isakov, O. Keren, and N. Benjuya, "Trans-tibial amputee gait: Time-distance parameters and EMG activity," *Prosthetics and Orthotics International*, vol. 24, no. 3, pp. 216–220, 2000.
- [100] S. Bakhshi, M. H. Mahoor, and B. S. Davidson, "Development of a body joint angle measurement system using IMU sensors," in *Proceedings of the Annual International Conference of the IEEE Engineering in Medicine and Biology Society, EMBS*, 2011, vol. 2011, pp. 6923–6926.
- [101] Z. Lin, M. Zecca, S. Sessa, L. Bartolomeo, H. Ishii, K. Itoh, and A. Takanishi, "Development of an ultra-miniaturized inertial measurement unit WB-3 for human body motion tracking," *2010 IEEE/SICE International Symposium on System Integration: SI International 2010 - The 3rd Symposium on System Integration, SII 2010, Proceedings*, pp. 414–419, 2010.
- [102] H. J. Luinge and P. H. Veltink, "Measuring orientation of human body segments using miniature gyroscopes and accelerometers," *Medical and Biological Engineering and Computing*, vol. 43, no. 2, pp. 273–282, 2005.
- [103] D. Roetenberg, H. Luinge, and P. Slycke, "Xsens MVN: full 6DOF human motion tracking using miniature inertial sensors," 2013.
- [104] T. Seel, J. Raisch, and T. Schauer, "IMU-based joint angle measurement for gait analysis," *Sensors (Switzerland)*, vol. 14, no. 4, pp. 6891–6909, 2014.
- [105] R. V. Vitali, S. M. Cain, R. S. McGinnis, A. M. Zaferiou, L. V. Ojeda, S. P. Davidson, and N. C. Perkins, "Method for estimating three-dimensional knee rotations using two inertial measurement units: Validation with a coordinate measurement machine," *Sensors (Switzerland)*, vol. 17, no. 9, 2017.
- [106] R. Zhang, H. Yang, F. Höflinger, and L. M. Reindl, "Adaptive Zero Velocity Update Based on Velocity Classification for Pedestrian Tracking," *IEEE Sensors Journal*, vol. 17, no. 7, pp. 2137–2145, 2017.
- [107] S. Han and J. Wang, "A novel method to integrate IMU and magnetometers in attitude and heading reference systems," *Journal of Navigation*, vol. 64, no. 4, pp. 727–738, 2011.

- [108] W. Li and J. Wang, "Effective adaptive kalman filter for MEMS-IMU/magnetometers integrated attitude and heading reference systems," *Journal of Navigation*, vol. 66, no. 1, pp. 99–113, 2013.
- [109] S. O. H. Madgwick, A. J. L. Harrison, and R. Vaidyanathan, "Estimation of IMU and MARG orientation using a gradient descent algorithm," in *IEEE International Conference on Rehabilitation Robotics*, 2011, pp. 1–7.
- [110] T. Sun, H. Li, Q. Liu, L. Duan, M. Li, C. Wang, Q. Liu, W. Li, W. Shang, Z. Wu, and Y. Wang, "Inertial Sensor-Based Motion Analysis of Lower Limbs for Rehabilitation Treatments," *Journal of Healthcare Engineering*, vol. 2017, 2017.
- [111] L. Derafa, A. Benallegue, and L. Fridman, "Super twisting control algorithm for the attitude tracking of a four rotors UAV," *Journal of the Franklin Institute*, vol. 349, no. 2, pp. 685–699, 2012.
- [112] M. Šenk and L. Chèze, "Rotation sequence as an important factor in shoulder kinematics," in *Clinical Biomechanics*, 2006, vol. 21, no. SUPPL. 1, pp. 3–8.
- [113] J. W. Wilson, "Four-gimbal systems for simulation display," *Simulation*, vol. 12, no. 3, pp. 115–120, 1969.
- [114] B. K. P. Horn, "Closed-form solution of absolute orientation using unit quaternions," *Journal of the Optical Society of America A*, vol. 4, no. 4, p. 629, 1987.
- [115] H. Tannous, D. Istrate, A. Benlarbi-Delai, J. Sarrazin, D. Gamet, M. C. Ho Ba Tho, and T. T. Dao, "A new multi-sensor fusion scheme to improve the accuracy of knee flexion kinematics for functional rehabilitation movements," *Sensors (Switzerland)*, vol. 16, no. 11, 2016.
- [116] F. Gırrbach, J. Hol, G. Bellusci, and M. Diehl, "Optimization-Based Sensor Fusion of GNSS and IMU Using a Moving Horizon Approach," *Sensors*, vol. 17, no. 6, p. 1159, 2017.
- [117] Y. Ren and X. Ke, "Particle Filter Data Fusion Enhancements for MEMS-IMU/GPS," *Intelligent Information Management*, vol. 02, no. 07, pp. 417–421, 2010.
- [118] R. E. Kalman, "A New Approach to Linear Filtering and Prediction Problems," *Journal of*

*Basic Engineering*, vol. 82, no. 1, p. 35, 1960.

- [119] R. Zhu and Z. Zhou, “A real-time articulated human motion tracking using tri-axis inertial/magnetic sensors package,” *IEEE Transactions on Neural Systems and Rehabilitation Engineering*, vol. 12, no. 2, pp. 295–302, 2004.
- [120] G. Cooper, I. Sheret, L. McMillian, K. Siliverdis, N. Sha, D. Hodgins, L. Kenney, and D. Howard, “Inertial sensor-based knee flexion/extension angle estimation,” *Journal of Biomechanics*, vol. 42, no. 16, pp. 2678–2685, 2009.
- [121] Z. Lin, M. Zecca, S. Sessa, L. Bartolomeo, H. Ishii, and A. Takanishi, “Development of the wireless ultra-miniaturized inertial measurement unit WB-4: Preliminary performance evaluation,” in *Proceedings of the Annual International Conference of the IEEE Engineering in Medicine and Biology Society, EMBS*, 2011, pp. 6927–6930.
- [122] A. M. Sabatini, “Quaternion-based extended Kalman filter for determining orientation by inertial and magnetic sensing,” *IEEE Transactions on Biomedical Engineering*, vol. 53, no. 7, pp. 1346–1356, 2006.
- [123] Y. Jung, D. Kang, and J. Kim, “Upper body motion tracking with inertial sensors,” in *2010 IEEE International Conference on Robotics and Biomimetics, ROBIO 2010*, 2010, no. 3, pp. 1746–1751.
- [124] M. Miezal, G. Bleser, N. Schmitz, and D. Stricker, “A generic approach to inertial tracking of arbitrary kinematic chains,” in *Proceedings of the 8th International Conference on Body Area Networks*, 2013, no. October 2013, pp. 2–6.
- [125] E. Ruffaldi, L. Peppoloni, A. Filippeschi, and C. A. Avizzano, “A novel approach to motion tracking with wearable sensors based on Probabilistic Graphical Models,” *Proceedings - IEEE International Conference on Robotics and Automation*, no. May, pp. 1247–1252, 2014.
- [126] Z. Q. Zhang, W. C. Wong, and J. K. Wu, “Ubiquitous human upper-limb motion estimation using wearable sensors,” *IEEE Transactions on Information Technology in Biomedicine*, vol. 15, no. 4, pp. 513–521, 2011.
- [127] M. El-Gohary, L. Holmstrom, J. Huisinga, E. King, J. McNamers, and F. Horak, “Upper

- limb joint angle tracking with inertial sensors,” in *Proceedings of the Annual International Conference of the IEEE Engineering in Medicine and Biology Society, EMBS*, 2011, pp. 5629–5632.
- [128] L. Peppoloni, A. Filippeschi, E. Ruffaldi, and C. A. Avizzano, “A novel 7 degrees of freedom model for upper limb kinematic reconstruction based on wearable sensors,” in *SISY 2013 - IEEE 11th International Symposium on Intelligent Systems and Informatics, Proceedings*, 2013, no. October 2015, pp. 105–110.
- [129] A. Giannitrapani, N. Ceccarelli, F. Scortecci, and A. Garulli, “Comparison of EKF and UKF for spacecraft localization via angle measurements,” *IEEE Transactions on Aerospace and Electronic Systems*, vol. 47, no. 1, pp. 75–84, 2011.
- [130] J. J. LaViola, “A comparison of unscented and extended Kalman filtering for estimating quaternion motion,” in *Proceedings of the 2003 American Control Conference, 2003.*, 2003, vol. 3, pp. 2435–2440.
- [131] M. Rhudy, Y. Gu, J. Gross, S. Gururajan, and M. R. Napolitano, “Sensitivity Analysis of Extended and Unscented Kalman Filters for Attitude Estimation,” *Journal of Aerospace Information Systems*, vol. 10, no. 3, pp. 131–143, 2013.
- [132] D. Hong-de, D. Shao-wu, C. Yuan-cai, and W. Guang-bin, “Performance Comparison of EKF / UKF / CKF for the,” *Telkomnika*, vol. 10, no. 7, pp. 1692–1699, 2012.
- [133] M. Euston, P. Coote, R. Mahony, J. Kim, and T. Hamel, “A complementary filter for attitude estimation of a fixed-wing UAV,” *2008 IEEE/RSJ International Conference on Intelligent Robots and Systems, IROS*, pp. 340–345, 2008.
- [134] T. Islam, M. S. Islam, M. Shajid-Ul-Mahmud, and M. Hossam-E-Haider, “Comparison of complementary and Kalman filter based data fusion for attitude heading reference system,” *AIP Conference Proceedings*, vol. 1919, 2017.
- [135] Y. Tian, H. Wei, and J. Tan, “An adaptive-gain complementary filter for real-time human motion tracking with MARG sensors in free-living environments,” *IEEE Transactions on Neural Systems and Rehabilitation Engineering*, vol. 21, no. 2, pp. 254–264, 2013.
- [136] H. Zhou and H. Hu, “Reducing drifts in the inertial measurements of wrist and elbow

- positions,” *IEEE Transactions on Instrumentation and Measurement*, vol. 59, no. 3, pp. 575–585, 2010.
- [137] M. Mihelj, “Inverse kinematics of human arm based on multisensor data integration,” *Journal of Intelligent and Robotic Systems: Theory and Applications*, vol. 47, no. 2, pp. 139–153, 2006.
- [138] H. J. Luinge, P. H. Veltink, and C. T. M. Baten, “Ambulatory measurement of arm orientation,” *Journal of Biomechanics*, vol. 40, no. 1, pp. 78–85, 2007.
- [139] H. Dejnabadi, B. M. Jolles, E. Casanova, P. Fua, and K. Aminian, “Estimation and visualization of sagittal kinematics of lower limbs orientation using body-fixed sensors,” *IEEE Transactions on Biomedical Engineering*, vol. 53, no. 7, pp. 1385–1393, 2006.
- [140] E. Palermo, S. Rossi, F. Marini, F. Patanè, and P. Cappa, “Experimental evaluation of accuracy and repeatability of a novel body-to-sensor calibration procedure for inertial sensor-based gait analysis,” *Measurement: Journal of the International Measurement Confederation*, vol. 52, no. 1, pp. 145–155, 2014.
- [141] Z. Zhang, Z. Huang, J. Wu, Zhiqiang Zhang, Zhipei Huang, and Jiankang Wu, “Hierarchical information fusion for human upper limb motion capture,” *12th International Conference on Information Fusion, 2009. FUSION '09*, pp. 1704–1711, 2009.
- [142] G. Bleser, G. Hendeby, and M. Miezal, “Using egocentric vision to achieve robust inertial body tracking under magnetic disturbances,” in *2011 10th IEEE International Symposium on Mixed and Augmented Reality, ISMAR 2011*, 2011, no. October, pp. 103–109.
- [143] T. Taunyazov, B. Omarali, and A. Shintemirov, “A novel low-cost 4-DOF wireless human arm motion tracker,” in *Proceedings of the IEEE RAS and EMBS International Conference on Biomedical Robotics and Biomechatronics*, 2016, vol. 2016–July, no. June, pp. 157–162.
- [144] X. Robert-Lachaine, H. Mecheri, C. Larue, and A. Plamondon, “Validation of inertial measurement units with an optoelectronic system for whole-body motion analysis,” *Medical and Biological Engineering and Computing*, vol. 55, no. 4, pp. 609–619, 2017.
- [145] J. Favre, B. M. Jolles, R. Aissaoui, and K. Aminian, “Ambulatory measurement of 3D knee joint angle,” *Journal of Biomechanics*, vol. 41, no. 5, pp. 1029–1035, 2008.

- [146] M. Robert, H. Tarek, and P. Jean-Michel, “Nonlinear Complementary Filters on the Special Orthogonal Group,” *Ieee Transactions on Automatic Control*, vol. 53, no. 5, pp. 1203–1218, 2008.
- [147] M. El-Gohary and J. McNames, “Shoulder and elbow joint angle tracking with inertial sensors,” *IEEE Transactions on Biomedical Engineering*, vol. 59, no. 9, pp. 2635–2641, 2012.
- [148] M. El-Gohary and J. McNames, “Human Joint Angle Estimation with Inertial Sensors and Validation with A Robot Arm,” *IEEE Transactions on Biomedical Engineering*, vol. 62, no. 7, pp. 1759–1767, 2015.
- [149] A. D. Young, “Use of body model constraints to improve accuracy of inertial motion capture,” in *2010 International Conference on Body Sensor Networks, BSN 2010*, 2010, pp. 180–186.
- [150] V. Joukov, M. Karg, and D. Kulic, “Online tracking of the lower body joint angles using IMUs for gait rehabilitation,” in *2014 36th Annual International Conference of the IEEE Engineering in Medicine and Biology Society, EMBC 2014*, 2014, pp. 2310–2313.
- [151] G. Pons-Moll, A. Baak, J. Gall, L. Leal-Taixé, M. Müller, H. P. Seidel, and B. Rosenhahn, “Outdoor human motion capture using inverse kinematics and von mises-fisher sampling,” in *Proceedings of the IEEE International Conference on Computer Vision*, 2011, no. November, pp. 1243–1250.
- [152] S. K. Park and Y. S. Suh, “A zero velocity detection algorithm using inertial sensors for pedestrian navigation systems,” *Sensors (Switzerland)*, vol. 10, no. 10, pp. 9163–9178, 2010.
- [153] A. D. Young, “From posture to motion,” *Proceedings of the Fifth International Conference on Body Area Networks - BodyNets '10*, p. 131, 2010.
- [154] S. Salehi, N. Mostofi, and G. Bleser, “A practical in-field magnetometer calibration method for IMUs,” in *Proceedings of the IROS Workshop on Cognitive Assistive Systems: Closing the Action-Perception Loop*, 2012, no. May 2014, pp. 39–44.
- [155] P. Picerno, A. Cereatti, and A. Cappozzo, “Joint kinematics estimate using wearable inertial

- and magnetic sensing modules,” *Gait and Posture*, vol. 28, no. 4, pp. 588–595, 2008.
- [156] J. Favre, F. Luthi, B. M. Jolles, O. Siegrist, B. Najafi, and K. Aminian, “A new ambulatory system for comparative evaluation of the three-dimensional knee kinematics, applied to anterior cruciate ligament injuries,” *Knee Surgery, Sports Traumatology, Arthroscopy*, vol. 14, no. 7, pp. 592–604, 2006.
- [157] A. G. Cutti, A. Ferrari, P. Garofalo, M. Raggi, A. Cappello, and A. Ferrari, “‘Outwalk’: A protocol for clinical gait analysis based on inertial and magnetic sensors,” *Medical and Biological Engineering and Computing*, vol. 48, no. 1, pp. 17–25, 2010.
- [158] G. X. Lee and K. S. Low, “A factorized quaternion approach to determine the arm motions using triaxial accelerometers with anatomical and sensor constraints,” *IEEE Transactions on Instrumentation and Measurement*, vol. 61, no. 6, pp. 1793–1802, 2012.
- [159] T. Liu, Y. Inoue, and S. Kyoko, “Development of a wearable sensor system for quantitative gait analysis,” *Elsevier*, vol. 42, no. 2, pp. 978–988, 2007.
- [160] Q. Yuan, I. M. Chen, and A. Caus, “Human velocity tracking and localization using 3 IMU sensors,” in *IEEE Conference on Robotics, Automation and Mechatronics, RAM - Proceedings*, 2013, pp. 25–30.
- [161] X. Meng, Z. Q. Zhang, J. K. Wu, and W. C. Wong, “Hierarchical information fusion for global displacement estimation in microsensor motion capture,” *IEEE Transactions on Biomedical Engineering*, vol. 60, no. 7, pp. 2052–2063, 2013.
- [162] S. Zihajehzadeh and E. J. Park, “A Novel Biomechanical Model-Aided IMU/UWB Fusion for Magnetometer-Free Lower Body Motion Capture,” *IEEE Transactions on Systems, Man, and Cybernetics: Systems*, vol. 47, no. 6, pp. 927–938, 2017.
- [163] J. A. Corrales, F. A. Candelas, and F. Torres, “Hybrid tracking of human operators using IMU/UWB data fusion by a Kalman filter,” in *Proceedings of the 3rd international conference on Human robot interaction - HRI '08*, 2008, p. 193.
- [164] A. Tognetti, F. Lorussi, N. Carbonaro, and D. de Rossi, “Wearable goniometer and accelerometer sensory fusion for knee joint angle measurement in daily life,” *Sensors (Switzerland)*, vol. 15, no. 11, pp. 28435–28455, 2015.

- [165] C. R. Noback, N. L. Strominger, R. J. Demarest, and D. A. Ruggiero, “The human nervous system: Structure and function: Sixth edition,” *The Human Nervous System: Structure and Function: Sixth Edition*, pp. 1–477, 2005.
- [166] C. K. Barha, L. S. Nagamatsu, and T. Liu-Ambrose, *Basics of neuroanatomy and neurophysiology*, 1st ed., vol. 138. Elsevier B.V., 2016.
- [167] K. O. Johnson, “The roles and functions of cutaneous mechanoreceptors,” *Current Opinion in Neurobiology*, vol. 11, no. 4, pp. 455–461, 2001.
- [168] H. Kajimoto, N. Kawakami, and S. Tachi, “Psychophysical evaluation of receptor selectivity in electro-tactile display,” *13th Int. Sympo. on Measurement and Control in Robotics (ISMCR)*, no. January, pp. 3–6, 2003.
- [169] K. M. Gottschaldt and C. Vahle-Hinz, “Merkel cell receptors: Structure and transducer function,” *Science*, vol. 214, no. 4517, pp. 183–186, 1981.
- [170] J. Fradette, D. Larouche, C. Fugère, R. Guignard, A. Beauparlant, V. Couture, L. Caouette-Laberge, A. Roy, and L. Germain, “Normal human Merkel cells are present in epidermal cell populations isolated and cultured from glabrous and hairy skin sites,” *Journal of Investigative Dermatology*, vol. 120, no. 2, pp. 313–317, 2003.
- [171] N. Cauna, “Fine morphological changes in the penicillate nerve endings of human hairy skin during prolonged itching,” *The Anatomical Record*, vol. 188, no. 1, pp. 1–11, 1977.
- [172] A. B. Vallbo and R. S. Johansson, “Properties of cutaneous mechanoreceptors in the human hand related to touch sensation,” *Human Neurobiology*, vol. 3, no. 1, pp. 3–14, 1984.
- [173] B. F. Goldby, L. R. Robinson, F. Goldby, and L. R. Robinson, “The central connexions of dorsal spin nerve roots and the ascending tract,” *Journal of anatomy*, vol. 96, no. 2, pp. 153–170, 1962.
- [174] C. J. Hodge and A. V. Apkarian, “The Spinothalamic Tract,” *Critical Reviews in Neurobiology*, vol. 5, no. 4, pp. 363–397, 1990.
- [175] C. Watson and M. Harrison, “The Location of the Major Ascending and Descending Spinal Cord Tracts in all Spinal Cord Segments in the Mouse: Actual and Extrapolated,”

- Anatomical Record*, vol. 295, no. 10, pp. 1692–1697, 2012.
- [176] K. A. Kaczmarek, J. G. Webster, P. Bach-y-Rita, and W. J. Tompkins, “Electrotactile and Vibrotactile Displays for Sensory Substitution Systems,” *IEEE Transactions on Biomedical Engineering*, vol. 38, no. 1, pp. 1–16, 1991.
- [177] P. Bach-Y-Rita, “Tactile Sensory Substitution Studies,” *Annals of the New York Academy of Sciences*, vol. 1013, no. 1, pp. 83–91, 2006.
- [178] C. E. Stepp and Y. Matsuoka, “Relative to direct haptic feedback, remote vibrotactile feedback improves but slows object manipulation,” in *2010 Annual International Conference of the IEEE Engineering in Medicine and Biology Society, EMBC’10*, 2010, pp. 2089–2092.
- [179] P. Marayong, I. H. Khoo, K. Nguyen, N. Bharti, B. Ruhe, D. Craig, and W. Wu, “Vibrotactile device for rehabilitative training of persons with lower-limb amputation,” in *2014 IEEE Healthcare Innovation Conference, HIC 2014*, 2014, vol. 90840, pp. 157–160.
- [180] B. Chen, Y. Feng, and Q. Wang, “Combining vibrotactile feedback with volitional myoelectric control for robotic transtibial prostheses,” *Frontiers in Neurorobotics*, vol. 10, no. AUG, pp. 1–14, 2016.
- [181] D. G. Buma, J. R. Buitenweg, and P. H. Veltink, “Intermittent stimulation delays adaptation to electrocutaneous sensory feedback,” *IEEE Transactions on Neural Systems and Rehabilitation Engineering*, vol. 15, no. 3, pp. 435–441, 2007.
- [182] M. Markovic, M. A. Schweisfurth, L. F. Engels, T. Bentz, D. Wüstefeld, D. Farina, and S. Dosen, “The clinical relevance of advanced artificial feedback in the control of a multi-functional myoelectric prosthesis,” *Journal of NeuroEngineering and Rehabilitation*, vol. 15, no. 1, pp. 1–15, 2018.
- [183] R. S. Armiger, F. V. Tenore, K. D. Katyal, M. S. Johannes, A. Makhlin, M. L. Natter, J. E. Colgate, S. J. Bensmaia, and R. J. Vogelstein, “Enabling closed-loop control of the Modular Prosthetic Limb through haptic feedback,” *Johns Hopkins APL Technical Digest (Applied Physics Laboratory)*, vol. 31, no. 4, pp. 345–353, 2013.
- [184] S. G. Meek, S. C. Jacobsen, and P. P. Goulding, “Extended physiologic taction: Design and

- evaluation of a proportional force feedback system,” *Journal of Rehabilitation Research and Development*, vol. 26, no. 3, pp. 53–62, 1989.
- [185] M. Isaković, M. Belić, M. Štrbac, I. Popović, and S. Došen, “Electrotactile feedback improves performance and facilitates learning in the routine grasping task,” *European Journal of Translational Myology*, vol. 26, no. 3, pp. 197–202, 2016.
- [186] A. W. Shehata, L. F. Engels, M. Controzzi, C. Cipriani, E. J. Scheme, and J. W. Sensinger, “Improving internal model strength and performance of prosthetic hands using augmented feedback,” *Journal of NeuroEngineering and Rehabilitation*, vol. 15, no. 1, pp. 1–12, 2018.
- [187] P. H. Chappell, “Making sense of artificial hands,” *Journal of Medical Engineering and Technology*, vol. 35, no. 1, pp. 1–18, 2011.
- [188] C. Antfolk, M. D’Alonzo, M. Controzzi, G. Lundborg, B. Rosen, F. Sebelius, and C. Cipriani, “Artificial redirection of sensation from prosthetic fingers to the phantom hand map on transradial amputees: Vibrotactile versus mechanotactile sensory feedback,” *IEEE Transactions on Neural Systems and Rehabilitation Engineering*, vol. 21, no. 1, pp. 112–120, 2013.
- [189] A. Benvenuto, S. Raspopovic, K. P. Hoffmann, J. Carpaneto, G. Cavallo, G. Di Pino, E. Guglielmelli, L. Rossini, P. M. Rossini, M. Tombini, and S. Micera, “Intrafascicular thin-film multichannel electrodes for sensory feedback: Evidences on a human amputee,” in *2010 Annual International Conference of the IEEE Engineering in Medicine and Biology Society, EMBC’10*, 2010, pp. 1800–1803.
- [190] T. S. Davis, H. A. C. Wark, D. T. Hutchinson, D. J. Warren, K. O’Neill, T. Scheinblum, G. A. Clark, R. A. Normann, and B. Greger, “Restoring motor control and sensory feedback in people with upper extremity amputations using arrays of 96 microelectrodes implanted in the median and ulnar nerves,” *Journal of Neural Engineering*, vol. 13, no. 3, 2016.
- [191] D. J. Tyler, “Neural interfaces for somatosensory feedback: bringing life to a prosthesis,” *Current Opinion in Neurology*, vol. 28, no. 6, pp. 574–581, 2017.
- [192] P. M. Rossini, S. Micera, A. Benvenuto, J. Carpaneto, G. Cavallo, L. Citi, C. Cipriani, L. Denaro, V. Denaro, G. Di Pino, F. Ferreri, E. Guglielmelli, K. P. Hoffmann, S. Raspopovic,

- J. Rigosa, L. Rossini, M. Tombini, and P. Dario, "Double nerve intraneural interface implant on a human amputee for robotic hand control," *Clinical Neurophysiology*, vol. 121, no. 5, pp. 777–783, 2010.
- [193] G. S. Dhillon, "Effects of Short-Term Training on Sensory and Motor Function in Severed Nerves of Long-Term Human Amputees," *Journal of Neurophysiology*, vol. 93, no. 5, pp. 2625–2633, 2005.
- [194] R. L. Rauck, L. Kapural, S. P. Cohen, J. M. North, C. A. Gilmore, R. H. Zang, and J. W. Boggs, "Peripheral Nerve Stimulation for the Treatment of Postamputation Pain-A Case Report," *Pain Practice*, vol. 12, no. 8, pp. 649–655, 2012.
- [195] G. Macefield, S. C. Gandevia, and D. Burke, "Perceptual responses to microstimulation of single afferents innervating joints, muscles and skin of the human hand.," *The Journal of Physiology*, vol. 429, no. 1, pp. 113–129, 1990.
- [196] S. Micera, P. M. Rossini, J. Rigosa, L. Citi, J. Carpaneto, S. Raspopovic, M. Tombini, C. Cipriani, G. Assenza, M. C. Carrozza, K. P. Hoffmann, K. Yoshida, X. Navarro, and P. Dario, "Decoding of grasping information from neural signals recorded using peripheral intrafascicular interfaces," *Journal of NeuroEngineering and Rehabilitation*, vol. 8, no. 1, pp. 2–11, 2011.
- [197] K. Horch, S. Meek, T. G. Taylor, and D. T. Hutchinson, "Object discrimination with an artificial hand using electrical stimulation of peripheral tactile and proprioceptive pathways with intrafascicular electrodes," *IEEE Transactions on Neural Systems and Rehabilitation Engineering*, vol. 19, no. 5, pp. 483–489, 2011.
- [198] T. A. Kuiken, P. D. Marasco, B. A. Lock, R. N. Harden, and J. P. A. Dewald, "Redirection of cutaneous sensation from the hand to the chest skin of human amputees with targeted reinnervation," *Proceedings of the National Academy of Sciences*, vol. 104, no. 50, pp. 20061–20066, 2007.
- [199] G. A. Dumanian, J. H. Ko, K. D. O'Shaughnessy, P. S. Kim, C. J. Wilson, and T. A. Kuiken, "Targeted reinnervation for transhumeral amputees: Current surgical technique and update on results," *Plastic and Reconstructive Surgery*, vol. 124, no. 3, pp. 863–869, 2009.

- [200] J. S. Hebert, K. Elzinga, K. M. Chan, J. Olson, and M. Morhart, “Updates in Targeted Sensory Reinnervation for Upper Limb Amputation,” *Current Surgery Reports*, vol. 2, no. 3, p. 45, 2014.
- [201] T. A. Kuiken, L. A. Miller, R. D. Lipschutz, B. A. Lock, K. Stubblefi, P. D. Marasco, P. Zhou, and G. A. Dumanian, “Targeted reinnervation for enhanced prosthetic arm function in a woman with a proximal amputation: a case study,” *The Lancet*, vol. 369, no. 9559, pp. 371–380, 2007.
- [202] G. M. Goodwin, D. I. Mccloskey, and P. B. C. Matthews, “The contribution of muscle afferents to kinesthesia shown by vibration induced illusions of movement and by the effects of paralysing joint afferents,” *Brain*, vol. 95, no. 4, pp. 705–748, 1972.
- [203] U. Proske and S. C. Gandevia, “The Proprioceptive Senses: Their Roles in Signaling Body Shape, Body Position and Movement, and Muscle Force,” *Physiological Reviews*, vol. 92, no. 4, pp. 1651–1697, 2012.
- [204] J. P. Roll and J. P. Vedel, “Kinaesthetic role of muscle afferents in man, studied by tendon vibration and microneurography,” *Experimental Brain Research*, vol. 47, no. 2, pp. 177–190, 1982.
- [205] J. P. Roll, J. P. Vedel, and E. Ribot, “Alteration of proprioceptive messages induced by tendon vibration in man: a microneurographic study,” *Experimental Brain Research*, vol. 76, no. 1, pp. 213–222, 1989.
- [206] U. Proske, “What is the role of muscle receptors in proprioception?,” *Muscle and Nerve*, vol. 31, no. 6, pp. 780–787, 2005.
- [207] J. Kucera, “Histochemical study of long nuclear chain fibers in the cat muscle spindle,” *The Anatomical Record*, vol. 198, no. 4, pp. 567–580, 1980.
- [208] D. Fritz-Ritson, “The anatomy and physiology of the muscle spindle, and its role in posture and movement a review,” *The Journal of the CCA*, vol. 26, no. 4, pp. 144–150, 1982.
- [209] G. M. Goodwin, D. I. Mccloskey, and P. B. C. Matthews, “The contribution of muscle afferents to kinesthesia shown by vibration induced illusions of movement and by the effects of paralysing joint afferents,” *Brain*, vol. 95, no. 4, pp. 705–748, 1972.

- [210] C. Blanchard, R. Roll, J. P. Roll, and A. Kavounoudias, “Combined contribution of tactile and proprioceptive feedback to hand movement perception,” *Brain Research*, vol. 1382, pp. 219–229, 2011.
- [211] G. Eklund, “Position sense and state of contraction; the effects of vibration,” *Journal of Neurology, Neurosurgery and Psychiatry*, vol. 35, no. 5, pp. 606–611, 1972.
- [212] B. Y. F. J. Clark, P. B. C. Matthews, and R. B. Muir, “Response of soleus Ia afferents to vibration in the presence of the tonic vibration reflex in the decerebrate cat,” *Journal of Physiology*, vol. 311, pp. 97–112, 1981.
- [213] S. Calvin-Figuière, P. Romaguère, and J. P. Roll, “Relations between the directions of vibration-induced kinesthetic illusions and the pattern of activation of antagonist muscles,” *Brain Research*, vol. 881, no. 2, pp. 128–138, 2000.
- [214] T. Kito, T. Hashimoto, T. Yoneda, S. Katamoto, and E. Naito, “Sensory processing during kinesthetic aftereffect following illusory hand movement elicited by tendon vibration,” *Brain Research*, vol. 1114, no. 1, pp. 75–84, 2006.
- [215] G. Eklund, “General Features of Vibration-Induced Effects on Balance,” *Uppsala Journal of Medical Sciences*, vol. 77, no. 2, pp. 112–124, 1972.
- [216] M. Metral, B. Blettery, J. P. Bresciani, M. Luyat, and M. Guerraz, “Trying to move your unseen static arm modulates visually-evoked kinesthetic illusion,” *PLoS ONE*, vol. 8, no. 11, pp. 1–9, 2013.
- [217] B. Craske, “Perception of impossible limb positions induced by tendon vibration,” *Science*, vol. 196, no. 4285, pp. 71–73, 1977.
- [218] M. Guerraz, S. Provost, R. Narison, A. Brugnion, S. Virolle, and J. P. Bresciani, “Integration of visual and proprioceptive afferents in kinesthesia,” *Neuroscience*, vol. 223, pp. 258–268, 2012.
- [219] T. Seizova-Cajic and R. Azzi, “Conflict with vision diminishes proprioceptive adaptation to muscle vibration,” *Experimental Brain Research*, vol. 211, no. 2, pp. 169–175, 2011.
- [220] M. Izumizaki, M. Tsuge, L. Akai, U. Proske, and I. Homma, “The illusion of changed

- position and movement from vibrating one arm is altered by vision or movement of the other arm,” *Journal of Physiology*, vol. 588, no. 15, pp. 2789–2800, 2010.
- [221] J. R. Lackner and A. B. Taublieb, “Influence of vision on vibration-induced illusions of limb movement,” *Experimental Neurology*, vol. 85, no. 1, pp. 97–106, 1984.
- [222] E. Rabin and A. M. Gordon, “Prior experience and current goals affect muscle-spindle and tactile integration,” *Experimental Brain Research*, vol. 169, no. 3, pp. 407–416, 2006.
- [223] C. Fromm and J. Noth, “Reflex responses of gamma motoneurons to vibration of the muscle they innervate.,” *The Journal of Physiology*, vol. 256, no. 1, pp. 117–136, 1976.
- [224] K. E. Hagbarth, G. Hellsing, and L. Löfstedt, “TVR and vibration-induced timing of motor impulses in the human jaw elevator muscles,” *Journal of Neurology, Neurosurgery and Psychiatry*, vol. 39, no. 8, pp. 719–728, 1976.
- [225] V. B. Issurin, “Vibrations and their applications in sport: A review,” *Journal of Sports Medicine and Physical Fitness*, vol. 45, no. 3, pp. 324–336, 2005.
- [226] J. C. Gilhodes, V. S. Gurfinkel, and J. P. Roll, “Role of ia muscle spindle afferents in post-contraction and post-vibration motor effect genesis,” *Neuroscience Letters*, vol. 135, no. 2, pp. 247–251, 1992.
- [227] M. Schieppati and P. Crenna, “From activity to rest: gating of excitatory autogenetic afferences from the relaxing muscle in man,” *Experimental Brain Research*, vol. 56, no. 3, pp. 448–457, 1984.
- [228] P. Romaiquère, J. P. Vedel, and S. Pagni, “Effects of tonic vibration reflex on motor unit recruitment in human wrist extensor muscles,” *Brain Research*, vol. 602, no. 1, pp. 32–40, 1993.
- [229] V. B. Issurin, D. G. Liebermann, and G. Tenenbaum, “Effect of vibratory stimulation training on maximal force and flexibility,” *Journal of Sports Sciences*, vol. 12, no. 6, pp. 561–566, 1994.
- [230] H. S. Park and B. J. Martin, “Contribution of the tonic vibration reflex to muscle stress and muscle fatigue,” *Scandinavian Journal of Work, Environment and Health*, vol. 19, no. 1,

pp. 35–42, 1993.

- [231] A. G. Feldman and M. L. Latash, “Afferent and efferent components of joint position sense; interpretation of kinaesthetic illusion,” *Biological Cybernetics*, vol. 42, no. 3, pp. 205–214, 1982.
- [232] P. Romaguère, J. L. Anton, M. Roth, L. Casini, and J. P. Roll, “Motor and parietal cortical areas both underlie kinaesthesia,” *Cognitive Brain Research*, vol. 16, no. 1, pp. 74–82, 2003.
- [233] S. Radovanovic, A. Korotkov, M. Ljubisavljevic, E. Lyskov, J. Thunberg, G. Kataeva, S. Danko, M. Roudas, S. Pakhomov, S. Medvedev, and H. Johansson, “Comparison of brain activity during different types of proprioceptive inputs: A positron emission tomography study,” *Experimental Brain Research*, vol. 143, no. 3, pp. 276–285, 2002.
- [234] L. Casini, P. Romaguère, A. Ducorps, D. Schwartz, J. L. Anton, and J. P. Roll, “Cortical correlates of illusory hand movement perception in humans: A MEG study,” *Brain Research*, vol. 1121, no. 1, pp. 200–206, 2006.
- [235] B. C. Stillman, “Vibratory Motor Stimulation: A Preliminary Report,” *Australian Journal of Physiotherapy*, vol. 16, no. 3, pp. 118–123, 1970.
- [236] L. G. Bongiovanni, K. E. Hagbarth, and L. Stjernberg, “Prolonged muscle vibration reducing motor output in maximal voluntary contractions in man.,” *The Journal of Physiology*, vol. 423, no. 1, pp. 15–26, 1990.
- [237] K. Honda and K. Kiguchi, “A study on the effect of vibration stimulation phase to knee joint extension motion change for perception-assist,” in *IEEE International Conference on Advanced Intelligent Mechatronics (AIM)*, Munich, 2018, pp. 957–962.
- [238] Y. P. Ivanenko, R. Grasso, and F. Lacquaniti, “Influence of Leg Muscle Vibration on Human Walking,” *Journal of Neurophysiology*, vol. 84, no. 4, pp. 1737–1747, 2000.
- [239] U. Proske and S. C. Gandevia, “The kinaesthetic senses,” *Journal of Physiology*, vol. 587, no. 17, pp. 4139–4146, 2009.
- [240] D. Robertson, G. Caldwell, J. Hamill, G. Kamen, and S. Whittlesey, “Three-Dimensional Kinematics,” in *Research methods in biomechanics*, vol. 2, Human Kinetics, 2004, pp. 35–

- [241] G. Wu, S. Siegler, P. Allard, C. Kirtley, A. Leardini, D. Rosenbaum, M. Whittle, D. D. D’Lima, L. Cristofolini, H. Witte, O. Schmid, and I. Stokes, “ISB recommendation on definitions of joint coordinate system of various joints for the reporting of human joint motion—part I: ankle, hip, and spine,” *Journal of Biomechanics*, vol. 35, no. 4, pp. 543–548, 2002.
- [242] G. Wu, F. C. T. Van Der Helm, H. E. J. Veeger, M. Makhsous, P. Van Roy, C. Anglin, J. Nagels, A. R. Karduna, K. McQuade, X. Wang, F. W. Werner, and B. Buchholz, “ISB recommendation on definitions of joint coordinate systems of various joints for the reporting of human joint motion - Part II: Shoulder, elbow, wrist and hand,” *Journal of Biomechanics*, vol. 38, no. 5, pp. 981–992, 2005.
- [243] D. A. Winter and S. E. Sienko, “Biomechanics of below-knee amputee gait,” *Journal of Biomechanics*, vol. 21, no. 5, pp. 361–367, 1988.
- [244] Y. Sagawa, K. Turcot, S. Armand, A. Thevenon, N. Vuillerme, and E. Watelain, “Biomechanics and physiological parameters during gait in lower-limb amputees: A systematic review,” *Gait and Posture*, vol. 33, no. 4, pp. 511–526, 2011.
- [245] B. J. Martin and H. S. Park, “Analysis of the tonic vibration reflex: Influence of vibration variables on motor unit synchronization and fatigue,” *European Journal of Applied Physiology and Occupational Physiology*, vol. 75, no. 6, pp. 504–511, 1997.
- [246] L. N. Zaidell, K. N. Mileva, D. P. Sumners, and J. L. Bowtell, “Experimental evidence of the tonic vibration reflex during whole-body vibration of the loaded and unloaded leg,” *PLoS ONE*, vol. 8, no. 12, pp. 1–9, 2013.
- [247] D. Burke, C. J. Andrews, J. W. Lance, and D. Gail, “Tonic vibration reflex in spasticity , Parkinson ’ s disease , and normal subjects,” pp. 477–486, 1972.
- [248] C. Oatis, “Biomechanics of Skeletal Muscles,” in *Medicine & Science in Sports & Exercise*, vol. 45, no. 5, Oregon, 2013, p. 1020.
- [249] P. Krstrup, K. Söderlund, M. Mohr, J. González-Alonso, and J. Bangsbo, “Recruitment of fibre types and quadriceps muscle portions during repeated, intense knee-extensor exercise

- in humans,” *Pflugers Archiv European Journal of Physiology*, vol. 449, no. 1, pp. 56–65, 2004.
- [250] U. Bogacka, D. Dziedzic, I. Komarnitki, and B. Cizek, “Anatomy of the long peroneal muscle of the leg,” *Folia Morphologica (Poland)*, vol. 76, no. 2, pp. 284–288, 2017.
- [251] S. S. Blemker and S. L. Delp, “Rectus femoris and vastus intermedius fiber excursions predicted by three-dimensional muscle models,” *Journal of Biomechanics*, vol. 39, no. 8, pp. 1383–1391, 2006.
- [252] J. P. Charles, O. Cappellari, A. J. Spence, J. R. Hutchinson, and D. J. Wells, “Musculoskeletal geometry, muscle architecture and functional specialisations of the mouse hindlimb,” *PLoS ONE*, vol. 11, no. 4, pp. 1–21, 2016.
- [253] Y. Xiao, J. S. Williams, and I. Brownell, “Merkel cells and touch domes: More than mechanosensory functions?,” *Experimental Dermatology*, vol. 23, no. 10, pp. 692–695, 2014.
- [254] A. E. Dubin and A. Patapoutian, “Nociceptors: The sensors of the pain pathway,” *Journal of Clinical Investigation*, vol. 120, no. 11, pp. 3760–3772, 2010.
- [255] A. Entinger, “Arduino based I / O-system for rapid prototyping of robotic systems,” pp. 1–5.
- [256] P. Jonsson, P. W. Johnson, and M. Hagberg, “Accuracy and feasibility of using an electrogoniometer for measuring simple thumb movements,” *Ergonomics*, vol. 50, no. 5, pp. 647–659, 2007.
- [257] M. R. Dawson, “The Development of a Myoelectric Training Tool for Above-Elbow Amputees,” *The Open Biomedical Engineering Journal*, vol. 6, no. 1, pp. 5–15, 2012.
- [258] M. W. Legro, G. E. Reiber, J. M. Czerniecki, and B. J. Sangeorzan, “Recreational activities of lower-limb amputees with prostheses,” vol. 38, no. 3, pp. 319–325, 2010.
- [259] H. Ferdinando, H. Khoswanto, and D. Purwanto, “Embedded Kalman filter for inertial measurement unit (IMU) on the ATmega8535,” *INISTA 2012 - International Symposium on INnovations in Intelligent SysTems and Applications*, pp. 1–5, 2012.

- [260] A. Filippeschi, N. Schmitz, M. Miezal, G. Bleser, E. Ruffaldi, and D. Stricker, “Survey of motion tracking methods based on inertial sensors: A focus on upper limb human motion,” *Sensors (Switzerland)*, vol. 17, no. 6, p. 1257, 2017.
- [261] X. Robert-Lachaine, H. Mecheri, C. Larue, and A. Plamondon, “Accuracy and repeatability of single-pose calibration of inertial measurement units for whole-body motion analysis,” *Gait and Posture*, vol. 54, pp. 80–86, 2017.
- [262] L. A. Jones, “Motor Illusions: What Do They Reveal About Proprioception?,” *Psychological Bulletin*, vol. 103, no. 1, pp. 72–86, 1988.
- [263] T. R. Makin, F. de Vignemont, and A. A. Faisal, “Neurocognitive barriers to the embodiment of technology,” *Nature Biomedical Engineering*, vol. 1, no. 1, p. 0014, 2017.
- [264] P. V. K. Et.al, “A Review Paper on I2C Communication Protocol,” *International Journal of Advance Research, Ideas and Innovations in Technology*, vol. 4, no. 2, pp. 340–343, 2018.
- [265] N. Y. Feng Li, *Digital Techniques and Systems*, 5th ed. China: Springer, 1973.

# Appendix A [Ethics]

## A.1. Consent for Release of Contact Information

Jacqueline S Hebert, MD FRCPC  
Associate Professor, Division of Physical Medicine and Rehabilitation  
Faculty of Medicine & Dentistry, University of Alberta  
5005 Katz Group Centre University of Alberta

### Consent for Release of Contact Information

**Study Title:** Physiologically Relevant Prosthetic Limb Movement Feedback for Upper and Lower Extremity Amputees.

**Sponsor:** Department of Defense (DOD), Congressionally Directed Medical Research Programs

**University of Alberta Health Research Ethics Board Protocol number:** Pro00063695

**Principal Investigator:** Jacqueline S. Hebert MD, FRCPS phone: 780-248-5767

This form is for you to provide consent for a member of the study team to contact you to tell you more about the research study and see if you might be interested in taking part in the research.

#### Study Summary:

We are doing this study because we are studying different ways to provide sensation or feeling from a prosthetic limb. In order to do this we must understand how persons with limb amputation feel their phantom limb when we apply various types of pressure to the limb. We will apply the knowledge we gain from this study to develop methods to provide sensation from an artificial limb. We would like to study persons with any level of major amputation (above the wrist or ankle). After learning about the study, if you agree to participate, the study will take place at the University of Alberta. You will participate in at least 3 study visits.

**Completing this form does not provide consent to participate in the study.** You do not need to provide your contact information at all. There are no risks or benefits to providing consent for release of your contact information, other than a research study staff will contact you to provide more information on the study. This consent expires one year after the date of signing. The individual signing the consent, by contacting the study staff, can revoke this consent at any time.

#### CONSENT:

By signing this consent, I give permission to the study team to contact me in order to give me more information about this study and to be asked to participate in the study.

Name: \_\_\_\_\_

Phone number: \_\_\_\_\_ and/or email: \_\_\_\_\_

Signature: \_\_\_\_\_ Date: \_\_\_\_\_

#### *Person obtaining consent:*

Name: \_\_\_\_\_ Signature: \_\_\_\_\_

Date: \_\_\_\_\_

University of Alberta Health Research Ethics Board.  
Pro00063695; Version 1: March 4, 2016

## A.2. Participant Information Letter and Consent Form

Jacqueline S Hebert, MD FRCPC  
Associate Professor, Division of Physical Medicine and Rehabilitation  
Faculty of Medicine & Dentistry, University of Alberta  
5005 Katz Group Centre University of Alberta

### **PARTICIPANT INFORMATION LETTER AND CONSENT FORM (AMPUTEE PARTICIPANTS)**

**Title of Study:** Physiologically Relevant Prosthetic Limb Movement Feedback for Upper and Lower Extremity Amputees.

**Sponsor:** Department of Defense (DOD), Congressionally Directed Medical Research Programs (CDMRP)

**University of Alberta Health Research Ethics Board Protocol number:** Pro00063695

**Principal Investigator:** Jacqueline S. Hebert MD, FRCPS phone: 780-248-5767

---

#### **Why am I being asked to take part in this research study?**

You are being asked to participate in this research study because you have a limb amputation and have expressed interest in participating in a research study that investigates how to provide prosthetic users with feedback from their prosthesis. The purpose of this information sheet is to provide you with the information needed to decide if you wish to participate in this study. Before you make a decision, one of the researchers will go over this form with you. You are encouraged to ask questions if you feel anything needs to be made clearer. You will be given a copy of this form for your records.

#### **What is the reason for doing the study?**

We are doing this study because we are studying different ways to provide sensation or feeling from a prosthetic limb. In order to do this we must understand how persons with limb amputation feel their phantom limb when we apply various types of pressure and vibration to the limb. We will apply the knowledge we gain from this study to develop methods to provide sensation from an artificial limb. The University of Alberta is working with the Cleveland Clinic and the Louis Stokes Cleveland Department of Veterans Affairs Medical Center (Ohio, Cleveland US) to conduct this study. The device being studied is experimental, which means that it is not an approved device that can be purchased.

#### **What will I be asked to do?**

If you agree to participate, the study will take place at the University of Alberta, and possibly one visit to the Glenrose Rehabilitation Hospital. You will be asked to participate in at least 3 and up to 5 study visits. You will be required to wear a short sleeve shirt and shorts for the testing sessions.

During the first study visit, we will place a vibrating device against your muscles and the skin on your amputated limb and ask different questions about how it feels to you. The vibrating device should not be painful or uncomfortable. We will place the vibration in several locations on your limb (up to 10 spots) for 2-3 minutes each spot, and ask you if you feel any sensations other than simple vibration. You will be asked to describe the feeling, and demonstrate what you feel by showing us with your other limb. We will also have some recording devices on your skin, such as a surface muscle recording device, which is held on using tape and

adhesive. This study visit will take about 3 hours total, with breaks throughout the testing session.

For the next study visit, we will place against your skin and muscles small robots that vibrate your muscles and push on your skin. When the robots are running you will tell in words and show us with the other side of your body what you feel. Some times during your visit the small robots will also be connected to prosthetic hands or feet, which are moving. While this is happening sometimes the small robots will be on and sometimes they will be off. During the sessions you will be telling us and showing us how things feel to you. This study visit may take more than one 3 hour session to complete. If you agree, we will schedule a couple of visits based on your availability. Each session of testing will last for no more than 3 hours.

For the last session, we will attach these robotic devices to experimental sockets with prosthetic hands or feet attached, and see how you feel and move while wearing the socket. You will answer questions about what you feel on questionnaires and you will do specific types of occupational therapy and physical therapy tasks like moving blocks to different bins or walking on a treadmill. If you are fit with a lower limb prosthetic socket, you will need to attend the Glenrose Rehabilitation Hospital to be tested on the Computer Assisted Rehabilitation Environment, a treadmill with a virtual reality surround screen. This study portion may take up to 3 visits for 2 to 4 hours each, as we will need to fit the socket to your limb comfortably and then do the testing.

We will take photos and videos of you during the study visit. We will use the photos and videos to collect data about your movement and responses. We will store the photos and video on a secure hard drive that is password protected and accessible only to the study staff in a restricted access locked room. There is a possibility that we will ask to use information collected during the research study, including photographs or videos that identify you, in presentations, publications, marketing materials, and other media. If you agree to us using information like this, we will ask you to sign a separate authorization form.

#### **What are the risks and discomforts?**

*Bruising/Pain:* There is a possibility of pain or bruising from the touch and vibration robots pushing into your limbs. The study staff can change how the robots push on you to minimize any discomfort.

*Electrical Hazards:* There is a possibility of an electrical shock whenever electricity is used to power instruments. The vibration and touch robots run on a battery pack that is similar to the battery pack that is in your current myoelectric (motorized) prosthesis. The risk of electrical shock from the touch and vibration robots is no greater than what would be expected with your current device.

*Skin irritation:* If you are allergic to tape or to some metals your skin may react, so we will ask you if you have any skin allergies before proceeding.

*Tiredness/Fatigue:* if you feel tired or uncomfortable at any time, we can take a break or stop the study and data collection with no impact on you.

It is not possible to know all of the risks that may happen in a study, but the researchers have taken all reasonable safeguards to minimize any known risks to a study participant. If you become ill or injured as a result of being in this study, you will receive necessary medical

treatment, at no additional cost to you. By signing this consent form you are not releasing the investigator(s), institution(s) and/or sponsor(s) from their legal and professional responsibilities.

**What are the benefits to me?**

You are not expected to get any benefit from being in this research study. The information gained however, will guide the development of a new type of prostheses that provides sensory feedback.

**Do I have to take part in the study?**

Being in this study is your choice. If you decide to be in the study, you can change your mind and stop being in the study at any time, and it will in no way affect you. If you decide to end your participation in the study, you can tell the researchers at any time. If the data collection has been completed, we will still use your information anonymously. If you withdraw before the data collection is completed, you can withdraw all of your data.

**Will I be paid to be in the research?**

You will be reimbursed \$15 for the cost of parking at the facility (receipt required) and provided a compensation of \$25 for each testing session. If you have to travel by vehicle from out of town, you will also be reimbursed for mileage at a rate of 50 cents per km. You will be reimbursed either by cash or by mailing a cheque. Your name and address will be needed to process these payments. If you do not live in the vicinity of Edmonton, the study will provide travel and lodging for the sessions that you are required to be at the study site.

**Voluntary Participation:**

Being in this study is your choice. If you decide to be in the study, you can change your mind and stop being in the study at any time, and it will in no way affect the care or treatment that you are entitled to.

**Will my information be kept private?**

During the study we will be collecting data about you, such as your age, sex, amputation and the location on your limb that we have tested. We will also be keeping a video file and photographs of your testing to verify the data that we collect. You can choose to allow us to use this video for presentation and publications of the data, or you can choose to have us keep this video data confidential. At the University of Alberta, we keep data stored for a minimum of 5 years after the end of the study, at which time we destroy identifying data. However the raw (unidentified) data and the video and photographic images may be kept indefinitely.

We will do everything we can to make sure that this data is kept private. No data relating to this study that includes your name will be released outside of the researcher's office or published by the researchers. Sometimes, by law, we may have to release your information with your name so we cannot guarantee absolute privacy. However, we will make every legal effort to make sure that your information is kept private.

People outside the University of Alberta may need to see your information for this study. Examples include other institutions in the study (the Louis Stokes Cleveland VA Medical Center and the Cleveland Clinic), safety monitors at the University of Alberta, and the sponsor of the research and their agents. The study is being conducted/sponsored by the Cleveland

Clinic Learner School of Medicine and the Department of Defense (DOD) through a Congressionally Directed Medical Research Program (CDMRP). This is a Department of Defense Funded effort, and as such, protocol information including information about participant health, especially in case of injury or reports of non-compliance, will be shared with representatives of the Department of Defense. The Department of Defense has regulatory oversight responsibilities that require it to ensure that funded research is being conducted in accordance with Federal/Department of Defense policy and that rights of the subject are being protected, and as such, the PI will share information with these entities, if requested. The research data may also be subject to any United States privacy legislation such as the Freedom Act, which would allow the US government to survey any stored electronic data within the United States.

You do not have to give this permission to use and give out your information; however you will not be able to participate in this research study without providing this permission by signing this consent form. The use and disclosure of your information has no expiration date.

You may cancel your permission to use and disclose your information at any time by notifying the Principal Investigator in writing: Jacqueline Hebert, 5005 Katz Group Centre, University of Alberta, T6G 2E1. If you do cancel your permission to use and disclose your information, your participation in this study will end and no further information about you will be collected. Your cancellation would not affect information already collected in the study.

The University of Alberta is getting money from the study sponsor to cover the costs of doing this study. You are entitled to request any details concerning this compensation from the Principal Investigator.

**What if I have questions?**

If you have any questions about the research now or later, please contact Dr. Jacqueline Hebert at 780-248-5767 or at [BLINC.lab.UofA@gmail.com](mailto:BLINC.lab.UofA@gmail.com).

If you have any questions regarding your rights as a research participant, you may contact the Health Research Ethics Board at 780-492-2615. This office has no affiliation with the study investigators.

**PARTICIPANT CONSENT (AMPUTEE)**

**Title of Study:** Physiologically Relevant Prosthetic Limb Movement Feedback for Upper and Lower Extremity Amputees.

**HREB Protocol number:** Pro00063695

**Principal Investigator:** Dr. Jacqueline Hebert

**Phone Number:** 780-248-5767

	<u>Yes</u>	<u>No</u>
Do you understand that you have been asked to be in a research study?	<input type="checkbox"/>	<input type="checkbox"/>
Have you read and received a copy of the attached Information Sheet?	<input type="checkbox"/>	<input type="checkbox"/>
Do you understand the benefits and risks involved in taking part in this research study?	<input type="checkbox"/>	<input type="checkbox"/>
Have you had an opportunity to ask questions and discuss this study?	<input type="checkbox"/>	<input type="checkbox"/>
Do you understand that you are free to leave the study at any time without having to give a reason and without penalty?	<input type="checkbox"/>	<input type="checkbox"/>
Has the issue of confidentiality been explained to you?	<input type="checkbox"/>	<input type="checkbox"/>
Do you understand who will have access to your study records?	<input type="checkbox"/>	<input type="checkbox"/>
Do you consent to the researchers taking video and audio recordings of your testing?	<input type="checkbox"/>	<input type="checkbox"/>
Do you consent to the researchers using your video recordings for scientific presentation and/or publication?	<input type="checkbox"/>	<input type="checkbox"/>
Who explained this study to you? _____		
I agree to take part in this study:		
Signature of Research Participant _____		
Printed Name: _____		
Date: _____		
I believe that the person signing this form understands what is involved in the study and voluntarily agrees to participate.		
Signature of Investigator or Designee _____ Date _____		
<b>THE INFORMATION SHEET MUST BE ATTACHED TO THIS CONSENT FORM AND A COPY GIVEN TO THE RESEARCH PARTICIPANT</b>		

### A.3. Participant Information Sheet

DIVISION OF PHYSICAL MEDICINE & REHABILITATION  
FACULTY OF MEDICINE & DENTISTRY

---

#### Participant Information Sheet

**Project name:** *Physiologically Relevant Prosthetic Limb Movement Feedback for Upper and Lower Extremity Amputees*

**Project number:** Pro00063695

**Participant ID:** 00063695 – \_\_\_ – \_\_\_ – \_\_\_

**Date of visit (dd/mm/yyyy):** \_\_\_\_\_

**Exclusion Criteria Screen:**  Able to tolerate pressure on residual limb  
 Not on blood thinners  
 No Cognitive or language barrier

*Please complete the rest of this sheet only if all of the responses above have been selected.*

**Level(s) of Amputation ( R / L ): \_\_\_\_\_**

**Date of Amputation (month/year): \_\_\_\_\_**

**Date of Birth (month/year): \_\_\_\_\_**

**Residual Limb Length (in cm) from bony prominence to bone end:**

Body landmark used: (knee medial joint line / greater trochanter / acromion / medial epicondyle)

**Phantom limb sensation:**  Yes  No

**Phantom limb Pain:**  Yes  No

Comments on phantom:

**Visit comments (do not identify the participant by name):**

# Appendix B [Motion Capture Joint Angle Calculations]

## B.1. MATLAB Code for Determining Illusion Kinematics

```
calibrationFile = 'File Location'; % Path to calibration file
trialFile = 'File Location'; % Path to trial file
saveFolder = 'File Location'; % save file path

% Load marker data from calibration file
[~, ~, calMarkerData, calMarkerHeader] = ...
    loadReformatOptiTrackData(calibrationFile);
% Reformat marker data into data struct - a bit easier to work with
calMarkerDataStruct = makeMarkerDataStruct(calMarkerHeader, calMarkerData);

% Get calibration matrices
calRUPA1 = calMarkerDataStruct.RULRUL1;
calRUPA2 = calMarkerDataStruct.RULRUL2;
calRUPA3 = calMarkerDataStruct.RULRUL3;
rupaCalRTM = calClusterToGlobCS(calRUPA1, calRUPA2, calRUPA3);
calRFRM1 = calMarkerDataStruct.RLLRLL1;
calRFRM2 = calMarkerDataStruct.RLLRLL2;
calRFRM3 = calMarkerDataStruct.RLLRLL3;
rfrmCalRTM = calClusterToGlobCS(calRFRM1, calRFRM2, calRFRM3);

% Load marker data from trial file
[optiFrame, optiTime, trialMarkerData, trialMarkerHeader] = ...
    loadReformatOptiTrackData(trialFile);
% Reformat marker data into data struct - a bit easier to work with
trialMarkerDataStruct = makeMarkerDataStruct...
    (trialMarkerHeader, trialMarkerData);
trialLength = length(optiFrame);

% Extract trial marker data
RUPA1 = trialMarkerDataStruct.RULRUL1;
RUPA2 = trialMarkerDataStruct.RULRUL2;
RUPA3 = trialMarkerDataStruct.RULRUL3;
RFRM1 = trialMarkerDataStruct.RLLRLL1;
RFRM2 = trialMarkerDataStruct.RLLRLL2;
RFRM3 = trialMarkerDataStruct.RLLRLL3;

% Calculate angles between two plates:
% Make coordiante system for upper plate over trial data
[rupaX, rupaY, rupaZ] = defCS(RUPA1, RUPA2, RUPA3, RUPA1, 1);
% Create array of vector components of provisional coordinate system
rupaPCS = cat(3, rupaX, rupaY, rupaZ);
rupaPCS = permute(rupaPCS, [2 3 1]);
% Calibrate coordinate system relative to global
rupa = zeros(3, 3, trialLength);
for i=1:trialLength
    rupa(:, :, i) = rupaPCS(:, :, i) * rupaCalRTM;
end

% Make coordiante system for lower plate over trial data
[rfrmX, rfrmY, rfrmZ] = defCS(RFRM1, RFRM2, RFRM3, RFRM1, 1);
% Create array of vector components of provisional coordinate system
rfrmPCS = cat(3, rfrmX, rfrmY, rfrmZ);
% [3 2 1] for Robertson, [2 3 1] for Goldenberg
rfrmPCS = permute(rfrmPCS, [2 3 1]);
% Calibrate coordinate system relative to global
rfrm = zeros(3, 3, trialLength);
for i=1:trialLength
    rfrm(:, :, i) = rfrmPCS(:, :, i) * rfrmCalRTM;
end

% Compute YXZ moving axes euler angles of lower cluster relative to upper
[RY, RX, RZ] = calcKinAngles_ZXYmoving(rfrm, rupa);
saveData = [optiTime, RZ];
trialFileSplit = strsplit(trialFile, '\');
trialNameWithExt = trialFileSplit(end);
trialName = strtok(trialNameWithExt, '.');
saveName = [fullfile(saveFolder, trialName), '_ZXYangles.mat'];
save(saveName, 'saveData');
```

## Function: loadReformatOptiTrackData

```
function [optiFrame, optiTime, optiMarkerData, optiMarkerHeader] = ...
    loadReformatOptiTrackData(optiFile)

% Initialize some outputs
optiMarkerHeader = {};
optiMarkerData = [];
% Import data from OptiTrack file
optiFileData = importdata(optiFile);
numData = optiFileData.data; % numeric rigid body & marker data from Motive
headerData = optiFileData.textdata; % cell array containing header text
% Output OptiTrack frame number and time
optiFrame = numData(:,1);
optiTime = numData(:,2);
% Get info about column type (Rigid Body or Marker):
% row containing 'Rigid Body' or 'Marker' ends up here, as one string
colType = headerData(2,1);
colType = strrep(colType, ',', ' '); % replace first two commas - kind
% of hacky way to make string split
% work correctly with first two columns empty
colType = strsplit(colType, ','); % split string into column headers

if length(colType) ~= size(numData,2)
    warning('Warning: header vs. data size mismatch')
end
% Get info about RB or Marker name:
% row containing RB/Marker name ends up here, as one string
colID = headerData(3,1);
colID = strrep(colID, ',', ' '); % replace first two commas
colID = strsplit(colID, ',');
% Find first and last Marker columns (ignore Rigid Bodies for now)
firstMarker = find(strcmp(colType, 'Marker'), 1, 'first');
lastMarker = find(strcmp(colType, 'Marker'), 1, 'last');
% Loop through Marker columns
for i = firstMarker:3:lastMarker
    % Get current column ID
    curColID = colID{i};
    % Ignore unlabeled markers for now
    if strfind(curColID, 'Unlabeled')
        continue
    end
    % Reformat column header for output
    rbName = strtok(curColID, ':');
    % replace 'Marker#' with [rbName]# so kinematics will work
    curColID = strrep(curColID, 'Marker', rbName);
    markerHeader = {'M:', curColID, ':X'}, ['M:', curColID, ':Y'], ...
        ['M:', curColID, ':Z'];
    optiMarkerHeader = [optiMarkerHeader, markerHeader];
    % Add marker position to output data
    optiMarkerData = [optiMarkerData, numData(:,i:i+2)];
end
```

## Function: makeMarkerDataStruct

```
function markerDataStruct = makeMarkerDataStruct(header, data)
colons = repmat(':', 1, length(header));
headerID = cellfun(@strtok, header, colons, 'UniformOutput', 0);
firstMocap = find(strcmp(headerID, 'M'), 1, 'first');
lastMocap = find(strcmp(headerID, 'M'), 1, 'last');
for i = firstMocap:3:lastMocap
    marker = header{i};
    markerSplit = strsplit(marker, ':');
    markerName = strcat(markerSplit{2}, markerSplit{3});
    markerName = markerName(find(~isspace(markerName)));
    markerDataStruct.(markerName) = data(:,i:i+2);
end
end
```

## Function: calClusterToGlobCS

```
function calRTM = calClusterToGlobCS(M1, M2, M3)
% Define coordinate system in calibration position
[rbX, rbY, rbZ] = defCS(M1, M2, M3, M1, 1);
% Create array of vector components of coordinate system
rb = cat(3, rbX, rbY, rbZ);
rb = permute(rb, [2 3 1]); % [3 2 1] for Robertson, [2 3 1] for Goldenberg
% Create average calibration coordinate system
rbAvg = nanmean(rb,3);
```

```
% Create rotational transformation matrix (RTM)
calRTM = rbAvg\eye(3);
```

## Function: defCS

```
function [unit1, unit2, unit3] = defCS(M1, M2, M3, M4, crossCoeff)
vect1 = M1 - M2;
vect2 = cross(vect1, M3-M4);
vect3 = crossCoeff * cross(vect1, vect2);
mag1 = sqrt(sum(vect1.*vect1,2));
unit1 = vect1./[mag1,mag1,mag1];
mag2 = sqrt(sum(vect2.*vect2,2));
unit2 = vect2./[mag2,mag2,mag2];
mag3 = sqrt(sum(vect3.*vect3,2));
unit3 = vect3./[mag3,mag3,mag3];
end
```

## Function: calcKinAngles\_ZXYmoving

```
function [x_angle, y_angle, z_angle] = calcKinAngles_ZXYmoving(distSeg, proxSeg)
distRTM = zeros(3,3,length(distSeg));
for i=1:length(distSeg)
    distRTM(:,:,i) = proxSeg(:,:,i)' * distSeg(:,:,i);
end
% ZXY Moving Axes From Goldenberg:
if (distRTM(3, 2,:) < 1)
    if (distRTM(3, 2,:) > -1)
        x_angle(:,1) = asin(distRTM(3, 2,:));
        z_angle(:,1) = atan2(-distRTM(1, 2,:), distRTM(2, 2,:));
        y_angle(:,1) = atan2(-distRTM(3, 1,:), distRTM(3, 3,:));
    else % r32 = -1
        % Not a unique solution : thetaY - thetaZ = atan2(r02,r00)
        x_angle(:,1) = -pi / 2;
        z_angle(:,1) = -atan2(distRTM(1, 3,:), distRTM(1, 1,:));
        y_angle(:,1) = 0;
    end
end
else % r32 = 1
    % Not a unique solution: thetaY + thetaZ = atan2(r13, r11)
    x_angle(:,1) = pi / 2;
    z_angle(:,1) = atan2(distRTM(1, 3, :), distRTM(1, 1,:));
    y_angle(:,1) = 0;
end
end
x_angle(:,1) = (180/pi) * x_angle(:,1);
y_angle(:,1) = (180/pi) * y_angle(:,1);
z_angle(:,1) = (180/pi) * z_angle(:,1);
end
```

## Appendix C [Movement Sensor Development]

### C.1. Hardware

#### Arduino Pro Mini

The Wireless inertial measurement unit-based system (WiBS) uses the Arduino microcontroller. Arduino is an open-source microcontroller popular for its capacity in rapid prototyping [255]. Arduino consists of both a microcontroller and an IDE (Integrated Development Environment) that runs on your computer, used to write and upload computer code to the physical board. Additionally, the Arduino IDE uses a simplified version of C++, making it easier to program. Unlike other Arduino development boards which rely on a universal serial bus (USB) to upload code, the Pro Mini requires a separate piece of hardware (a programmer) in order to load new code onto the board (Figure C1). The USB circuitry was eliminated to make the Pro Mini as small as possible. The absence of this circuit means an external component, the FTDI Basic Breakout (SparkFun, CO, USA), is required to upload code to the Arduino Pro Mini (Figure C2).



Figure C1: Universal serial bus (USB) circuitry was removed from the Arduino Pro Mini microcontroller to make the device as small as possible. As a result, the Arduino Pro Mini requires a programmer (FTDI basic) to upload code onto the microcontroller.

#### Bosch BNO05

Similar to the OptiTrack motion capture system, the Bosch BNO05 inertial measurement unit (IMU) allows users to set the global coordinate frame to any orthonormal basis. The global coordinate frame of the IMU can be altered by writing the appropriate bits to the device's `AXIS_MAP_SIGN` address. However, the device will periodically boot into the default frame (Figure C1).

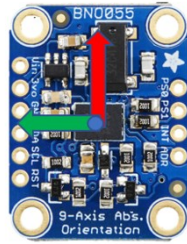


Figure C2: The default global frame for the BNO05 IMU module is shown in the figure. The device will periodically boot into its default frame even if the appropriate bits are written to the `AXIS_MAP_SIGN` address.

Therefore, keeping the default coordinate frame and using a rotation matrix to transform the default frame to the desired basis, i.e., the joint coordinate system outlined by the international society of biomechanics, improves reliability.

### **Arduino Pro Mini and BNO05 Communication**

The Arduino Pro Mini talks to the BNO05 through I2C communication. I2C is a protocol utilizing two wires, called SCL and SDA: SCL is the clock line used to synchronize all data transfers over the I2C bus, SDA is the data line. The SCL & SDA lines are connected to all devices on the I2C bus [264]. Both SCL and SDA lines are open-drain drivers, meaning the controller can drive its output low but it cannot drive it high. Pull-up resistors to the power supply are required to drive the line high. These pull-up resistors are connected from the SCL line to the 5 voltage line and another from the SDA line to the 5 voltage line; only one set of pull-up resistors is required for the whole I2C bus. The devices on the I2C bus are either masters or slaves. The master (Arduino Pro Mini) drives the SCL clock line; the slaves respond to the master. There can be multiple slaves on the I2C bus, however, there is normally only one master (Figure C3). Each slave must have a unique address. I2C addresses are commonly 7 bits long, this means that you can have up to 128 devices on the I2C bus [42]. Data is transferred in sequences of 8 bits with a standard clock (SCL) speed of about 100 kiloHertz (kHz) [40]. Arduino provides a wire library to simplify I2C communication [43].

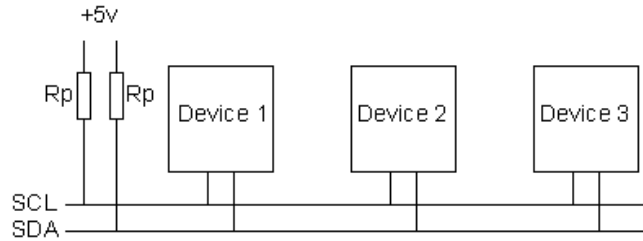


Figure C3: The Arduino Pro Mini communicates with the BNO05 IMU module through I2C communication. I2C is a protocol utilizing two wires, called SCL (clock line) and SDA (data line). Both lines require pull up resistors since the controller is only capable of driving the lines low, the figure demonstrates three peripheral devices connected to the data and clock line.

### Solid Model for Movement Sensor Enclosure

The hardware enclosure was designed in SolidWorks 2016 (Figure C4) to secure all the electronics. The IMU board is screwed tightly to the base of the enclosure; this is important for obtaining reliable and consistent readings. The design also provides for a removable top, providing access to the battery for recharging. There is also an on/off switch to conserve battery when the module is not in use.

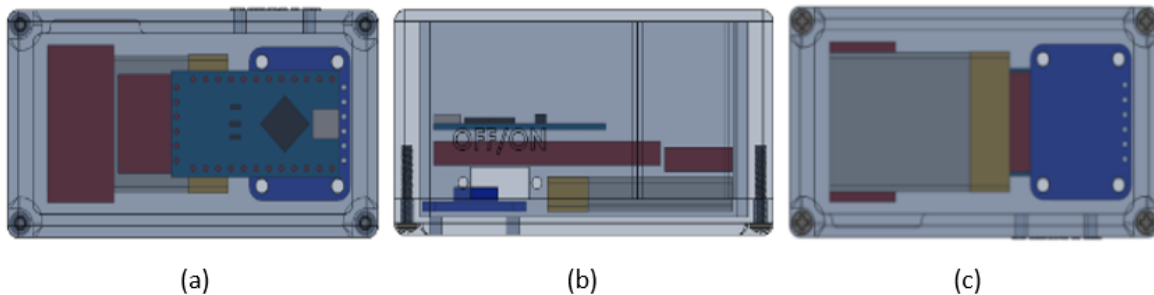


Figure C4: The top (a), side (b) and bottom (c) view of the SolidWorks 2016 model for the enclosure of the WbS. The design allows for a removable top for battery removal and recharging. An on/off switch allows for battery conservation.

## C.2. Arduino Code for Sensor Acquisition and RN42 Bluetooth Radio

### Transmission

```
#include <Wire.h>
#include <Adafruit_Sensor.h>
#include <Adafruit_BNO055.h>
#include <utility/imumaths.h>

Adafruit_BNO055 bno = Adafruit_BNO055(55, BNO055_ADDRESS_A);

// Send buffer
// Flag used to identify stream start
byte const FLAG = 0x2E;
// Sendbuffer
byte sendBuffer[22];

// Initialize IMU calibration values
uint8_t system_cal = 5;
uint8_t gyro_cal = 5;
uint8_t accel_cal = 5;
uint8_t mag_cal = 5;

// Quaternion outputs
double quaternion_X = 0;
double quaternion_Y = 0;
double quaternion_Z = 0;
double quaternion_W = 0;

byte * quaternion_X_Pointer = (byte *) &quaternion_X;
byte * quaternion_Y_Pointer = (byte *) &quaternion_Y;
byte * quaternion_Z_Pointer = (byte *) &quaternion_Z;
byte * quaternion_W_Pointer = (byte *) &quaternion_W;

void setup(void)
{
  Serial.begin(9600);
  Serial.println("Orientation Sensor Test");

  /* Initialise the sensor */
  if (!bno.begin())
  {
    /* There was a problem detecting the BNO055 ... check your connections */
    Serial.print("Ooops, no BNO055 1111 detected ... Check your wiring or I2C ADDR!");
    while (1);
  }

  delay(1000);

  bno.setExtCrystalUse(true);
  pinMode(LED_BUILTIN, OUTPUT);
  digitalWrite(LED_BUILTIN, HIGH);
}

void loop(void)
{
  sensors_event_t event;
  bno.getEvent(&event);

  imu::Quaternion quat = bno.getQuat();

  quaternion_X = quat.x();
  quaternion_Y = quat.y();
  quaternion_Z = quat.z();
  quaternion_W = quat.w();

  // displayCalStatus(bno2);
  bno.getCalibration(&system_cal, &gyro_cal, &accel_cal, &mag_cal);

  sendInfo();}
```

## Function: sendInfo

```
// transmits information to the computer via Bluetooth
void sendInfo()
{
    // Load flags
    sendBuffer[0] = FLAG;
    sendBuffer[1] = FLAG;

    // Quaternions 1
    sendBuffer[2]= quaternion_X_Pointer[0];    // quaternion_x Byte 1
    sendBuffer[3]= quaternion_X_Pointer[1];    // quaternion_x Byte 2
    sendBuffer[4]= quaternion_X_Pointer[2];    // quaternion_x Byte 3
    sendBuffer[5]= quaternion_X_Pointer[3];    // quaternion_x Byte 4

    sendBuffer[6]= quaternion_Y_Pointer[0];    // quaternion_y Byte 1
    sendBuffer[7]= quaternion_Y_Pointer[1];    // quaternion_y Byte 2
    sendBuffer[8]= quaternion_Y_Pointer[2];    // quaternion_y Byte 3
    sendBuffer[9]= quaternion_Y_Pointer[3];    // quaternion_y Byte 4

    sendBuffer[10]= quaternion_Z_Pointer[0];   // quaternion_z Byte 1
    sendBuffer[11]= quaternion_Z_Pointer[1];   // quaternion_z Byte 2
    sendBuffer[12]= quaternion_Z_Pointer[2];   // quaternion_z Byte 3
    sendBuffer[13]= quaternion_Z_Pointer[3];   // quaternion_z Byte 4

    sendBuffer[14]= quaternion_W_Pointer[0];   // quaternion_w Byte 1
    sendBuffer[15]= quaternion_W_Pointer[1];   // quaternion_w Byte 2
    sendBuffer[16]= quaternion_W_Pointer[2];   // quaternion_w Byte 3
    sendBuffer[17]= quaternion_W_Pointer[3];   // quaternion_w Byte 4

    // Calibration of IMU data (unsigned int)
    sendBuffer[18] = system_cal;    //calibration for IMU1
    sendBuffer[19] = gyro_cal;
    sendBuffer[20] = accel_cal;
    sendBuffer[21] = mag_cal;

    // Send data over bluetooth
    Serial.write(sendBuffer, sizeof(sendBuffer));

    delay(50);
}
```

## Function: displaySensorDetails

```
void displaySensorDetails(Adafruit_BNO055 IMU)
{
    sensor_t sensor;
    IMU.getSensor(&sensor);
    Serial.println("-----");
    Serial.print ("Sensor:      "); Serial.println(sensor.name);
    Serial.print ("Driver Ver:  "); Serial.println(sensor.version);
    Serial.print ("Unique ID:   "); Serial.println(sensor.sensor_id);
    Serial.print ("Max Value:   "); Serial.print(sensor.max_value); Serial.println(" xxx");
    Serial.print ("Min Value:   "); Serial.print(sensor.min_value); Serial.println(" xxx");
    Serial.print ("Resolution:  "); Serial.print(sensor.resolution); Serial.println(" xxx");
    Serial.println("-----");
    Serial.println("");
    delay(500);
}
```

## Function: displaySensorStatus

```
void displaySensorStatus(Adafruit_BNO055 IMU)
{
  /* Get the system status values (mostly for debugging purposes) */
  uint8_t system_status, self_test_results, system_error;
  system_status = self_test_results = system_error = 0;
  IMU.getSystemStatus(&system_status, &self_test_results, &system_error);

  /* Display the results in the Serial Monitor */
  Serial.println("");
  Serial.print("System Status: 0x");
  Serial.println(system_status, HEX);
  Serial.print("Self Test:    0x");
  Serial.println(self_test_results, HEX);
  Serial.print("System Error: 0x");
  Serial.println(system_error, HEX);
  Serial.println("");
  delay(500);
}
```

## Function: displayCalStatus

```
void displayCalStatus(Adafruit_BNO055 IMU)
{
  /* Get the four calibration values (0..3) */
  /* Any sensor data reporting 0 should be ignored, */
  /* 3 means 'fully calibrated' */
  uint8_t system, gyro, accel, mag;
  system = gyro = accel = mag = 0;
  IMU.getCalibration(&system, &gyro, &accel, &mag);

  /* The data should be ignored until the system calibration is > 0 */
  Serial.print("\t");
  if (!system)
  {
    Serial.print("! ");
  }

  /* Display the individual values */
  Serial.print("Sys:");
  Serial.print(system, DEC);
  Serial.print(" G:");
  Serial.print(gyro, DEC);
  Serial.print(" A:");
  Serial.print(accel, DEC);
  Serial.print(" M:");
  Serial.print(mag, DEC);
}
```

### C.3. Software

The movement sensors graphical user interface (GUI) is comprised of two pages. The initial interface allows entry of the trail information (IMU type and trial number) and establishes virtual serial connections to the WiBS (Figure C5). All the information entered can be altered in the second GUI except for the IMU type.

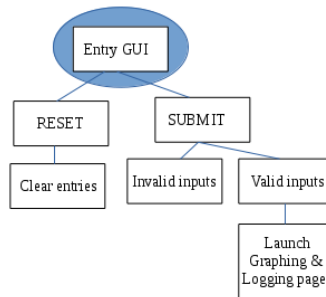


Figure C5: The first page of the graphical user interface is predominately used to input participant information and establish connections to the WiBS; this figure outlines the class diagram for the first page of the user interface.

The second page is mainly responsible for displaying and logging the transmitted data (Figure C6).

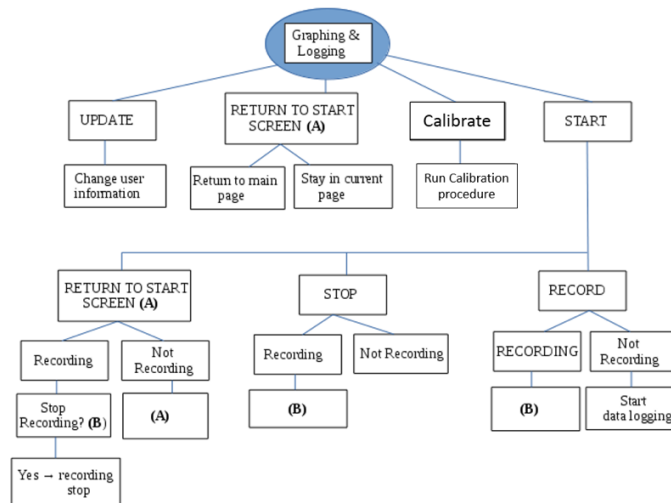


Figure C6: The second page of the graphical user interface is used to display and log data; this figure outlines the class diagram for the second page of the user interface.

## C.4. C# Code for the Movement Sensors Graphical User Interface

### Entry Graphical User Interface

```
public Form1()
{
    //initialize GUI
    InitializeComponent();
    trialNotificationLabel.Hide();
    weightNotificationLabel.Hide();
    //find potential COM Port and fill dropdown list with all the Ports available
    fillCOMPortDropDownList();
}
```

### Function: fillCOMPortDropDownList

```
public void fillCOMPortDropDownList()
{
    var ports = SerialPort.GetPortNames();
    manualComPort1Selection.Items.Clear();
    manualComPort1Selection.Items.AddRange(ports);
    manualComPort2Selection.Items.Clear();
    manualComPort2Selection.Items.AddRange(ports);
    manualComPort3Selection.Items.Clear();
    manualComPort3Selection.Items.AddRange(ports);
    int potentialComPort1Index = manualComPort1Selection.FindString(COMPort1);
    int potentialComPort2Index = manualComPort2Selection.FindString(COMPort2);

    if (!(potentialComPort1Index == -1)) //if index not found, set the index to zero
    {
        manualComPort1Selection.SelectedIndex = potentialComPort1Index; //choose presumed port index
        manualComPort2Selection.SelectedIndex = potentialComPort2Index; //choose presumed port index
    }
    else {}
    isCOMPortConnected = true;
}
```

### Function: saveFilePath

```
public void saveFilePath()
{
    MessageBox.Show("Choose location to save file\n-default location will be the current users desktop\n-the file will be saved as: participantCode.txt\n-naming the file is optional",
        "File Path",
        MessageBoxButtons.OK,
        MessageBoxIcon.Information);
    SaveFileDialog sf = new SaveFileDialog();
    // Feed the dummy name to the save dialog
    sf.FileName = Code + ".txt";
    if (sf.ShowDialog() == DialogResult.OK)
    {
        // Now here's our save folder
        filePath = Path.GetDirectoryName(sf.FileName);
    }
}
```

### Function: update\_csv\_header

```
public void update_csv_header(string joint, string trialnumber, string velocity, string start_stop)
{
    //if so, save everything to csv file
    var csv = new StringBuilder();
    var newLine = string.Format("Joint: {0}, Velocity: {1}, Trial#: {2} (g), DateTime: {4}, {3}",
        joint, velocity, trialnumber, start_stop, DateTime.Now.ToString("yyyy/M/d/--HH:mm:ss"));
    csv.AppendLine(newLine);
    try
    {
        updatedfilePath = filePath + '\\' + Code + '_' + joint + ".txt";
        File.AppendAllText(updatedfilePath, csv.ToString());
    }
    catch
    {
    }
}
```

```

        updatedfilePath = filePathDefault + '\\\' + Code + ' \' + joint + ".txt";
        File.AppendAllText(updatedfilePath, csv.ToString());
    }
}

```

## Function: submitButton

```

private void submitButton(object sender, EventArgs e)
{
    inSubmit = true;
    try
    {
        saveFilePath();
        //check to see if all entries are filled
        if (!string.IsNullOrEmpty(participantCodeInput.Text) &&
            !string.IsNullOrEmpty(trialNumberInput.Text) &&
            !string.IsNullOrEmpty(weightInput.Text) && (isCOMPortConnected) /* &&
            (correctComPort)*/)
        {
            //pop up gui that will ask if sure to submit
            switch (MessageBox.Show("Are you sure you want to submit?",
                "Submit information",
                MessageBoxButtons.YesNo,
                MessageBoxIcon.Question))
            {
                case DialogResult.Yes:
                    //update csv
                    Code = participantCodeInput.Text;
                    trial = trialNumberInput.Text;
                    weightGrams = weightInput.Text;

                    update_csv_header(Code, trial, weightGrams, "Program Start");
                    //close current gui and open second gui
                    this.Hide();
                    var form2 = new Form2(this);
                    form2.Closed += (s, args) => this.Close();
                    form2.Show();
                    break;

                case DialogResult.No:
                    // "No" processing
                    inSubmit = false;
                    break;
            }
        }
        else
        {
            if (!isCOMPortConnected)
            {
                MessageBox.Show("Please fill all fields appropriately",
                    "Empty fields",
                    MessageBoxButtons.OK,
                    MessageBoxIcon.Error);
                inSubmit = false;
            }
            else
            {
                MessageBox.Show("COM Port Failed to connect : " + COMPortInfoFound,
                    "COM Port failure",
                    MessageBoxButtons.OK,
                    MessageBoxIcon.Error);
                inSubmit = false;
            }
        }
    }
    catch
    {
        if (!returnFromSecondPage)
        {
            MessageBox.Show("Trial and Weight must be numerical",
                "Invalid Entry",
                MessageBoxButtons.OK,
                MessageBoxIcon.Error);
            inSubmit = false;
        }
        else
        {

```

```

        returnFromSecondPage = false;
        inSubmit = false;
    }
}

```

## Plotting and Logging Graphical User Interface

```

public Form2(Form1 fm1)
{
    InitializeComponent();
    this.form1 = fm1;
    counter = 0;
    //set up user information
    setUserInformation();
    //initialize serial
    initializeSerial();
    //initialize layout
    initializeLayout();
    //set up graphs and layout
    initializeGraphs();
}

```

### Function: initializeLayout

```

void initializeLayout()
{
    //recording initally false
    isRecording = false;
    //set up button layout
    stopButton.Hide();
    recordButton.Enabled = false;
    vibrasenseTriggeringButton.Enabled = false;
}

```

### Function: initializeSerial

```

void initializeSerial()
{
    try
    {
        //set up serial information
        myport1 = new SerialPort(form1.COMPort1, 9600, Parity.None, 8, StopBits.One);
        myport1.Open();
        myport1.DataReceived += new SerialDataReceivedEventHandler(DataReceivedHandler1);
    }
    catch
    {
        myport1.Close();
        comPortErrorReturnToMainPage(1);
    }

    try
    {
        myport2 = new SerialPort(form1.COMPort2, 9600, Parity.None, 8, StopBits.One);
        myport2.Open();
        myport2.DataReceived += new SerialDataReceivedEventHandler(DataReceivedHandler2);
    }
    catch
    {
        myport2.Close();
        comPortErrorReturnToMainPage(2);
    }

    try
    {
        myport3 = new SerialPort(form1.COMPort3, 9600, Parity.None, 8, StopBits.One);
        myport3.Open();
    }
    catch
    {
        myport3.Close();
        comPortErrorReturnToMainPage(3);
    }
}

```

```
}
```

## Function: setTrialInformation

```
void setTrialInformation()
{
    jointTypeInput.Text = jointTypeInput.Text;
    velocityInput.Text = velocityInput.Text;
    if (counter == 0)
    {
        //set trail number to the number set on the opening GUI
        trialNumberInput.Text = form1.trial;
        velocityInput.Text = form1.weightGrams;
        //dont allow input until program starts
        trialNumberInput.Enabled = false;
        velocityInput.Enabled = false;
    }
    else
    {
        //trail number should match with the trail text input
        trialNumberInput.Text = trialNumberInput.Text;
        velocityInput.Text = velocityInput.Text;
    }
}
```

## Function: startButton

```
private void startButton(object sender, EventArgs e)
{
    if (counter == 0)
    { swatch.Start(); }
    else
    { swatch.Restart(); }

    this.GraphTimer.Start();
    if (counter == 1)
    {
        // allow input program starts
        trialNumberInput.Enabled = true;
        velocityInput.Enabled = true;
        jointTypeInput.Enabled = true;
    }
    //hide start button and show stop, and record button
    startButton.Hide();
    updateTrialButton.Hide();
    trialNumberInput.Enabled = false;
    jointTypeInput.Enabled = false;
    velocityInput.Enabled = false;
    stopButton.Show();
    recordButton.Enabled = true;
    vibrasenseTriggeringButton.Enabled = true;
    atStaticMenu = false;
    //indicate start clicked
    form1.update_csv_header(jointTypeInput.Text, trialNumberInput.Text, velocityInput.Text, "trial Start");
}
```

## Function: stopButton

```
void stopButton ()
{
    //stop timer
    this.GraphTimer.Stop();
    swatch.Stop();
    //show start button ,remove stop and record
    startButton.Show();
    startButton.Enabled = true;
    updateTrialButton.Show();
    trialNumberInput.Enabled = true;
    velocityInput.Enabled = true;
    jointTypeInput.Enabled = true;
    stopButton.Hide();
    recordButton.Enabled = false;
    vibrasenseTriggeringButton.Enabled = false;
    atStaticMenu = true;
    //update output file header with new trail number
}
```

```

form1.update_csv_header(jointTypeInput.Text, trialNumberInput.Text, velocityInput.Text, "Trial End");
//Auto increment trial number
incrementTrailNumber();
}

```

## Function: startRecording

```

void startRecording()
{
    switch (MessageBox.Show("Start recording?",
        "record",
        MessageBoxButtons.YesNo,
        MessageBoxIcon.Question))
    {
        case DialogResult.Yes:
            this.isRecording = true;
            recordButton.ForeColor = Color.Red;
            //start timer
            recordingTime.Start();
            //start logging to csv
            isLogging = true;
            break;
        case DialogResult.No:
            // "No" processing
            break;
    }
}

```

## Function: calibrate

```

private void calibrate(object sender, EventArgs e)
{
    if (calibrationFinished == 0)
    { // calibration started
        DialogResult res = MessageBox.Show("Calibration initiated.", "Initiate Calibration", MessageBoxButtons.OKCancel);
        if (res == DialogResult.OK)
        {
            calibrationButton.Text = "Stop";
        }
        calibrationFinished = 1;
    }
    else
    {
        //Generate rotation Matrix
        float[,] R1_UC = Moperator.quaternionsToRotationMatrix(q1);
        float[,] R2_UC = Moperator.quaternionsToRotationMatrix(q2);
        //generate Calibration matrix for both IMU's
        R1_calibrationMatrix = Moperator.generateCalibrationMatrix(R1_UC); // now calibration matrices are defined
        R2_calibrationMatrix = Moperator.generateCalibrationMatrix(R2_UC);
        calibrationButton.Enabled = false;
        Thread.Sleep(5);
        calibrationButton.Enabled = true;
        MessageBox.Show("Calibration Complete!", "Calibration", MessageBoxButtons.OK);
        calibrationButton.Text = "Start";
        calibrationFinished = 0;
    }
}

```

## Function: comPortErrorReturnToMainPage

```

public void comPortErrorReturnToMainPage(int portNumber)
{
    DialogResult res = MessageBox.Show("Unable to open COM Port:\n" + portNumber.ToString() + "\nyou will be returned to
the previous page",
    "COM Port Connected Failed",
    MessageBoxButtons.OK,
    MessageBoxIcon.Error);
    if (res == DialogResult.OK)
    {
        //close this form and open the first one
        form1.returnFromSecondPage = true;
        form1.correctComPort = false;
    }
}

```

```

        form1.Show();
        this.Close();
    }
}

```

## Function: DataReceivedHandler

```

private void DataReceivedHandler(
    object sender,
    SerialDataReceivedEventArgs e)
{
    try
    {
        int dataKey = 0;
        while (true)
        {
            dataKey = myport.ReadByte() + myport.ReadByte() * 256;
            if (dataKey == 0x2E + 256 * 0x2E)
            {
                dataKey = 0;
                break;
            }
        }
        //Quaternions
        byte[] quaternion_X_ByteArray = new byte[] { (byte)myport1.ReadByte(), (byte)myport1.ReadByte(),
            (byte)myport1.ReadByte(), (byte)myport1.ReadByte() };
        byte[] quaternion_Y_ByteArray = new byte[] { (byte)myport1.ReadByte(), (byte)myport1.ReadByte(),
            (byte)myport1.ReadByte(), (byte)myport1.ReadByte() };
        byte[] quaternion_Z_ByteArray = new byte[] { (byte)myport1.ReadByte(), (byte)myport1.ReadByte(),
            (byte)myport1.ReadByte(), (byte)myport1.ReadByte() };
        byte[] quaternion_W_ByteArray = new byte[] { (byte)myport1.ReadByte(), (byte)myport1.ReadByte(),
            (byte)myport1.ReadByte(), (byte)myport1.ReadByte() };

        //convert bytes to floats
        quaternion_W = BitConverter.ToSingle(quaternion_W_ByteArray, 0);
        quaternion_X = BitConverter.ToSingle(quaternion_X_ByteArray, 0);
        quaternion_Y = BitConverter.ToSingle(quaternion_Y_ByteArray, 0);
        quaternion_Z = BitConverter.ToSingle(quaternion_Z_ByteArray, 0);

        q = new float[] { quaternion_W, quaternion_X, quaternion_Y, quaternion_Z };

        //IMU calibration status 1
        byte systemCalibration = (byte)myport.ReadByte();
        byte gyroCalibration = (byte)myport.ReadByte();
        byte accelCalibration = (byte)myport.ReadByte();
        byte magCalibration = (byte)myport.ReadByte();
        statusArrayIMU_sgam = new float[] { systemCalibration, gyroCalibration, accelCalibration, magCalibration };
    }
    catch (Exception ex)
    {
        //if packets fail, all values will be -1
        statusArrayIMU1_sgam = new float[] { -12, -12, -12, -12 };
    }
}

```

## Function: updateAxis

```

void updateAxis(Chart chart1, Chart chart2, Chart chart3)
{
    chart1.ChartAreas[0].AxisX.CustomLabels.Clear();
    chart2.ChartAreas[0].AxisX.CustomLabels.Clear();
    chart3.ChartAreas[0].AxisX.CustomLabels.Clear();
    for (int i = 0; i < ((MAX_X_VALUES)); i++)
    {
        long elapsed_time = swatch.ElapsedMilliseconds;
        int seconds = (int)(elapsed_time / 1000) % 60;
        int minutes = (int)((elapsed_time / (1000 * 60)) % 60);
        int hours = (int)((elapsed_time / (1000 * 60 * 60)) % 24);
        string timeStamp = Convert.ToString(hours) + ":" + Convert.ToString(minutes) + ":" + Convert.ToString(seconds +
i);
        if (i % 2 == 0)
        {
            chart1.ChartAreas[0].AxisX.CustomLabels.Add(i, i + 1, Convert.ToString(timeStamp));
            chart2.ChartAreas[0].AxisX.CustomLabels.Add(i, i + 1, Convert.ToString(timeStamp));
            chart3.ChartAreas[0].AxisX.CustomLabels.Add(i, i + 1, Convert.ToString(timeStamp));
        }
    }
}

```

```

    }
    else
    {
        chart1.ChartAreas[0].AxisX.CustomLabels.Add(i, i + 1, Convert.ToString(""));
        chart2.ChartAreas[0].AxisX.CustomLabels.Add(i, i + 1, Convert.ToString(""));
        chart3.ChartAreas[0].AxisX.CustomLabels.Add(i, i + 1, Convert.ToString(""));
    }
}
}

```

## Function: GraphTimer

```

private void GraphTimer(object sender, EventArgs e)
{
    //Generate rotation Matrix
    float[,] R1_UC = Moperator.quaternionsToRotationMatrix(q1);
    float[,] R2_UC = Moperator.quaternionsToRotationMatrix(q2);
    //Use Calibration to determine appropriate orientation
    float[,] R1_C = Moperator.multiplyTwoRotationMatrices(R1_UC, R1_calibrationMatrix);
    float[,] R2_C = Moperator.multiplyTwoRotationMatrices(R2_UC, R2_calibrationMatrix);
    //find relative transformation of IMU1 to IMU2
    float[,] R1_C_Transpose = Moperator.generateTransposeOfRotationMatrix(R1_C);
    float[,] R2_C_Transpose = Moperator.generateTransposeOfRotationMatrix(R2_C);
    float[,] R1to2 = Moperator.multiplyTwoRotationMatrices(R1_C_Transpose, R2_C);
    float[] ZYX = Moperator.extractEulerAnglesFromZYXRotationMatrix(R1to2);
    currentRollAngleValue = ZYX[0];
    currentPitchAngleValue = ZYX[1];
    currentYawAngleValue = ZYX[2];
    //clearing previous series points
    rollAngleSeries.Points.Clear();
    pitchAngleSeries.Points.Clear();
    yawAngleSeries.Points.Clear();

    for (int i = 0; i < MAX_X_VALUES - 1; i++)
    {
        //updating force data series
        rollAngledataArray[i] = rollAngledataArray[i + 1];
        rollAngleSeries.Points.AddXY(i, rollAngledataArray[i]);
        //updating acceleration data series
        pitchAngledataArray[i] = pitchAngledataArray[i + 1];
        pitchAngleSeries.Points.AddXY(i, pitchAngledataArray[i]);
        //updating tilt angle data series
        yawAngledataArray[i] = yawAngledataArray[i + 1];
        yawAngleSeries.Points.AddXY(i, yawAngledataArray[i]);
    }
    //enter current force value to array -> series
    rollAngledataArray[MAX_X_VALUES - 1] = currentRollAngleValue;
    rollAngleSeries.Points.AddXY(MAX_X_VALUES, currentRollAngleValue);
    //enter current force value to array -> series
    pitchAngledataArray[MAX_X_VALUES - 1] = currentPitchAngleValue;
    pitchAngleSeries.Points.AddXY(MAX_X_VALUES, currentPitchAngleValue);
    //enter current force value to array -> series
    yawAngledataArray[MAX_X_VALUES - 1] = currentYawAngleValue;
    yawAngleSeries.Points.AddXY(MAX_X_VALUES, currentYawAngleValue);
    //update graphs with new data
    rollGraph.Update();
    pitchGraph.Update();
    yawGraph.Update();

    if (isLogging)
    {
        //string roll, pitch, yaw, IMU1 status , IMU2 status
        update_csv_data(Quaternion_W1.ToString(), Quaternion_X1.ToString(), Quaternion_Y1.ToString(),
            Quaternion_Z1.ToString(), Quaternion_W2.ToString(), Quaternion_X2.ToString(), Quaternion_Y2.ToString(),
            Quaternion_Z2.ToString(), XYZ, XZY, YXZ, YZX, ZXY, ZYX, statusArrayIMU1_sgam[0].ToString(),
            statusArrayIMU1_sgam[1].ToString(), statusArrayIMU1_sgam[2].ToString(), statusArrayIMU1_sgam[3].ToString(),
            statusArrayIMU2_sgam[0].ToString(), statusArrayIMU2_sgam[1].ToString(), statusArrayIMU2_sgam[2].ToString(),
            statusArrayIMU2_sgam[3].ToString());
    }
    //reset user information incase trial number has been changed
    setUserInformation();
    //update calibration info
    updateCalibration();
    //update x axis
    updateAxis(rollGraph, pitchGraph, yawGraph);
    counter++;
}

```

```
}
```

## Function: quaternionsToRotationMatrix

```
public float[,] quaternionsToRotationMatrix(float[] q)
{
    float[,] RotationMatrix = { { 0, 0, 0 }, { 0, 0, 0 }, { 0, 0, 0 } };
    RotationMatrix[0, 0] = 1 - 2 * (q[2] * q[2] + q[3] * q[3]);
    RotationMatrix[0, 1] = 2 * (q[1] * q[2] - q[0] * q[3]);
    RotationMatrix[0, 2] = 2 * (q[1] * q[3] + q[0] * q[2]);
    RotationMatrix[1, 0] = 2 * (q[1] * q[2] + q[0] * q[3]);
    RotationMatrix[1, 1] = 1 - 2 * (q[1] * q[1] + q[3] * q[3]);
    RotationMatrix[1, 2] = 2 * (q[2] * q[3] - q[0] * q[1]);
    RotationMatrix[2, 0] = 2 * (q[1] * q[3] - q[0] * q[2]);
    RotationMatrix[2, 1] = 2 * (q[2] * q[3] + q[0] * q[1]);
    RotationMatrix[2, 2] = 1 - 2 * (q[1] * q[1] + q[2] * q[2]);
    return RotationMatrix;
}
```

## Function: generateZXYRotationMatrixFromEuler

```
public float[,] generateZXYRotationMatrixFromEuler(float roll, float pitch, float yaw)
{
    float[,] RotationMatrix = { { 0, 0, 0 }, { 0, 0, 0 }, { 0, 0, 0 } };
    RotationMatrix[0, 0] = (float)(Math.Cos(pitch) * Math.Cos(yaw) - Math.Sin(roll) * Math.Sin(pitch) * Math.Sin(yaw));
    RotationMatrix[0, 1] = (float)(-Math.Cos(roll) * Math.Sin(yaw));
    RotationMatrix[0, 2] = (float)(Math.Cos(yaw) * Math.Sin(pitch) + Math.Cos(pitch) * Math.Sin(roll) * Math.Sin(yaw));
    RotationMatrix[1, 0] = (float)(Math.Cos(yaw) * Math.Sin(roll) * Math.Sin(pitch) + Math.Cos(pitch) * Math.Sin(yaw));
    RotationMatrix[1, 1] = (float)(Math.Cos(roll) * Math.Cos(yaw));
    RotationMatrix[1, 2] = (float)(-Math.Cos(pitch) * Math.Cos(yaw) * Math.Sin(roll) + Math.Sin(pitch) * Math.Sin(yaw));
    RotationMatrix[2, 0] = (float)(-Math.Cos(roll) * Math.Sin(pitch));
    RotationMatrix[2, 1] = (float)(Math.Sin(roll));
    RotationMatrix[2, 2] = (float)(Math.Cos(roll) * Math.Cos(pitch));
    return RotationMatrix;
}
```

## Function: generateTransposeOfRotationMatrix

```
public float[,] generateTransposeOfRotationMatrix(float[,] RotationMatrix)
{
    float[,] Rout = { { 0, 0, 0 }, { 0, 0, 0 }, { 0, 0, 0 } };
    int m = 3; //row
    int n = 3; //col
    for (int x = 0; x < n; x++)
    {
        for (int y = 0; y < m; y++)
        {
            Rout[x, y] = RotationMatrix[y, x];
        }
    }
    return Rout;
}
```

## Function: multiplyTwoRotationMatrices

```
public float[,] multiplyTwoRotationMatrices(float[,] R1, float[,] R2)
{
    float[,] Rout = { { 0, 0, 0 }, { 0, 0, 0 }, { 0, 0, 0 } };
    int m = 3; //row
    int n = 3; //col
    /* Loop through each and get product, then sum up and store the value */
    for (int i = 0; i < m; i++)
    {
        for (int j = 0; j < n; j++)
        {
            Rout[i, j] = 0;
            for (int k = 0; k < m; k++)
            {
                Rout[i, j] = Rout[i, j] + R1[i, k] * R2[k, j];
            }
        }
    }
    return Rout;
}
```

## Function: generateCalibrationMatrix

```
public float[,] generateCalibrationMatrix(float[,] R1)
{
    //multiply R1 transpose with the identity matrix to get calibration matrix
    float[,] R1_transpose = generateTransposeOfRotationMatrix(R1);
    float[,] CalMatrix = multiplyTwoRotationMatrices(R1_transpose, zLeftxUpyOutOfKneeMatrix);//identityMatrix);
    return CalMatrix;
}
```

## Function: extractEulerAnglesFromZXYRotationMatrix

```
public float[] extractEulerAnglesFromZXYRotationMatrix(float[,] R)
{
    //https://www.geometrictools.com/Documentation/EulerAngles.pdf
    float[] output = { 0, 0, 0 };
    float x_angle = 0;
    float y_angle = 0;
    float z_angle = 0;
    if (R[2, 1] < 1)
    {
        if (R[2, 1] > -1)
        {
            x_angle = (float)Math.Asin(R[2, 1]);
            z_angle = (float)Math.Atan2(-R[0, 1], R[1, 1]);
            y_angle = (float)Math.Atan2(-R[2, 0], R[2, 2]);
        }
        else // r21 = -1
        {
            // Not a unique solution : thetaY - thetaZ = atan2(r02,r00)
            x_angle = (float)(-Math.PI / 2);
            z_angle = (float)(-Math.Atan2(R[0, 2], R[0, 0]));
            y_angle = 0;
        }
    }
    else // r21 = 1
    {
        // Not a unique solution : thetaY + thetaZ = atan2(r02,r00)
        x_angle = (float)(Math.PI / 2);
        z_angle = (float)(Math.Atan2(R[0, 2], R[0, 0]));
        y_angle = 0;
    }
    output[0] = 57.2958f * x_angle;
    output[1] = 57.2958f * y_angle;
    output[2] = 57.2958f * z_angle;
    return output;
}
```

## Appendix D [Movement Sensor Validation]

### D.1. Delsys Trigno

The Trigno (Delsys, MA, USA) was the commercial IMU system used in the validation study of the WbS (Figure D1). Delsys' Trigno offers EMG, accelerometer, gyroscope and magnetometer data with a 16-bit resolution with a sampling rate of 2 kHz for EMG and roughly 150 Hz for other measurements. Delsys also offers a GUI to view orientation and EMG data from the Trigno and a software development kit (SDK) for direct access to real-time data of the system. The Trigno SDK was used to extract unit quaternions for the joint angle calculations outline in Chapter 4 Section 4.2.1.

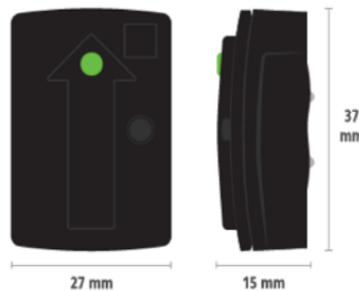


Figure D1: The Delsys Trigno inertial measurement unit was one of the devices used in the movement sensor validation study. The Trigno offers EMG, accelerometer, gyroscope and magnetometer data with a 16-bit resolution with a sampling rate of 2 kHz for EMG and roughly 150 Hz for other measurements.

An adaption of the GUI for the WbS was developed to convert the unit quaternion of the Trigno to joint angles of the robotic system used in validating the movement sensor (Figure D2). The Trigno system communicates with a computer through the Internet protocol suite, commonly known as TCP/IP [265]. TCP/IP is an end-to-end data communication system which specifies how data should be packetized, addressed, transmitted, routed, and received; this functionality is organized into four abstraction layers. In ascending order, the layers are the link layer, which contains communication methods for data that remains within a single network segment; the internet layer, providing internetworking between independent networks; the transport layer

handling host-to-host communication; and the application layer, which provides process-to-process data exchange for applications.



Figure D2: The graphical interface developed for the Trigno system is very similar to that of the Wlbs. The initial interface (a) still allows entry of the trail information (IMU type and trial number) but establishes a TCP/IP connection, rather than a virtual serial connection, to the Trigno system. The second page (b) of the graphical user interface is still used to display and log data.

## D.2. C# Code for Delsys Trigno TCP/IP Communication

### Function: connectTCP\_IP

```
//TCP/IP connection
private void connectTCP_IP()
{
    try
    {
        //Establish TCP/IP connection to server using URL entered
        commandSocket = new TcpClient(serverURL, commandPort);
        commandStream = commandSocket.GetStream();//Set up communication streams
        commandReader = new StreamReader(commandStream, Encoding.ASCII);
        commandWriter = new StreamWriter(commandStream, Encoding.ASCII);
        //Get initial response from server and display
        commandReader.ReadLine(); //get extra line terminator
        connected = true; //indicate that we are connected
    }
    catch (Exception connectException)
    {
        //connection failed, display error message
        MessageBox.Show("Could not connect.\n" + connectException.Message);
    }
    //build a list of connected sensor types
    _sensors = new List<SensorTypes>();
    for (int i = 1; i <= 16; i++)
    {
        string query = "SENSOR " + i + " " + COMMAND_SENSOR_TYPE;
```

```

        string response = SendCommand(query);
        _sensors.Add(response.Contains("INVALID")? SensorTypes.NoSensor : sensorList[response]);
    }
    SendCommand("UPSAMPLE OFF");
}

```

### Function: SendCommand

```

//Send a command to the server and get the response
public string SendCommand(string command)
{
    string response = "";
    //Check if connected
    if (connected)
    {
        commandWriter.WriteLine(command); //Send the command
        commandWriter.WriteLine(); //terminate command
        commandWriter.Flush(); //make sure command is sent immediately
        //Read the response line and display
        response = commandReader.ReadLine();
        response = commandReader.ReadLine();//get extra line terminator
    }
    else
        MessageBox.Show("Not connected.");return response; //return the response we got
}

```

### Function: closeTCP\_IP

```

public void closeTCP_IP()
{//Check if running and display error message if not
    if (running)
    {
        MessageBox.Show("Can't quit while acquiring data!");return;
    }
    SendCommand(COMMAND_QUIT); connected = false; //send QUIT command
    //Close all streams and connections
    commandReader.Close(); commandWriter.Close();commandStream.Close();
    commandSocket.Close();imuAuxStream.Close();imuAuxSocket.Close();
}

```

## D.3. C# Code for Three Degree of Freedom Robotic Arm

### Function: performSingleAxisMovement

```

public void performSingleAxisMovement(int minPosition, int maxPosition, int maxVelocity, bool
                                     movementDirection, string joint, int jointID)
{
    double[] jointRate = { 0, 0 };
    if (sinusoid == true)
    {
        fileHeaderSetup(joint, jointID, robotObj, "Sinusoid");
        period = Math.PI * (double)((maxPosition - minPosition) / (maxVelocity)) * 1000; //period in milliseconds
        if (motionTime.ElapsedMilliseconds < period * numberOfCycles)
        {
            robotObj.Motor[jointID].p = Convert.ToInt32(generateSineWave(minPosition, maxPosition, maxVelocity,
                                                                           motionTime.ElapsedMilliseconds));
            jointRate = generateCosineWave(minPosition, maxPosition, maxVelocity, motionTime.ElapsedMilliseconds);
            robotObj.Motor[jointID].w = (int)jointRate[1];
        }
        else
        {
            returnToHomePosition();
        }
    }
    else if (gussian == true)
    {
        fileHeaderSetup(joint, jointID, robotObj, "Gussian");
        if (motionTime.ElapsedMilliseconds < timeToPerformGussainMotionINms)
        {
            robotObj.Motor[jointID].p = Convert.ToInt32(generateGussian(maxPosition, minPosition, (double)maxVelocity,

```

```

        timeToPerformGussainMotionINms, motionTime.ElapsedMilliseconds));
    jointRate = gaussianDerivative(maxPosition, (double)maxVelocity, timeToPerformGussainMotionINms,
        motionTime.ElapsedMilliseconds);
    robotObj.Motor[jointID].w = (int)jointRate[1];
}
else
{
    if (joint == "elbow")
    {
        robotObj.Motor[jointID].p = 2063; // return to the center
        robotObj.Motor[jointID].w = maxVelocity;
    }
    else
    {
        robotObj.Motor[jointID].p = 0; // return to the end corner
        robotObj.Motor[jointID].w = maxVelocity;
    }
    returnToHomePosition();
}
}
else if (movementDirection == true)
{
    robotObj.Motor[jointID].p = maxPosition;
    robotObj.Motor[jointID].w = maxVelocity;
}
else if (movementDirection == false)
{
    robotObj.Motor[jointID].p = minPosition;
    robotObj.Motor[jointID].w = maxVelocity;
}
if (jointID == 0)
{
    update_csv_data_all(ID1_present_position, ID2_present_position, ID3_present_position, (int)jointRate[0],
        robotObj.Motor[1].w, robotObj.Motor[2].w, period.ToString(), logFilesCount);
}
else if (jointID == 1)
{
    update_csv_data_all(ID1_present_position, ID2_present_position, ID3_present_position, robotObj.Motor[0].w,
        (int)jointRate[0], robotObj.Motor[2].w, period.ToString(), logFilesCount);
}
else
{
    update_csv_data_all(ID1_present_position, ID2_present_position, ID3_present_position, robotObj.Motor[0].w,
        robotObj.Motor[1].w, (int)jointRate[0], period.ToString(), logFilesCount);
}
}
}

```

## Function: fileHeaderSetup

```

public void fileHeaderSetup(String task, int ServoID, Robot robotObj, string motion)
{
    if (movementInitiated)
    {
        validationTrialNumberArray_SEW[ServoID] = validationTrialNumberArray_SEW[ServoID] + 1;
        if (ServoID == 3)
        {
            update_csv_header(task, robotObj.Motor[ServoID-1].w.ToString(), motion,
                validationTrialNumberArray_SEW[ServoID].ToString());
        }
        else
        {
            update_csv_header(task, robotObj.Motor[ServoID].w.ToString(), motion,
                validationTrialNumberArray_SEW[ServoID].ToString());
        }
        movementInitiated = false;
    }
}
}

```

## Function: generateSineWave

```

public double generateSineWave(int minValue, int maxValue, int maxVelocity, long time)
{
    double A = (maxValue - minValue)/2;
    double w = maxVelocity / A;
    double output = A * Math.Sin(w*time/1000)
    return output;
}

```

## Function: generateCosineWave

```
public double[] generateCosineWave(int minValue, int maxValue, int maxVelocity, long time)
{
    double[] output = { 0, 0 };
    double A = (maxValue - minValue)/2;
    double w = maxVelocity / A;
    output[0] = A * w * Math.Cos(w * time / 1000);
    output[1] = Math.Abs(output[0]);
    return output;
}
```

## Function: generateGussian

```
public double generateGussian(int maxValue, int minValue, double maxVel, int timeToPerformAction_ms, long time)
{
    double mean = (double)timeToPerformAction_ms / 2;
    double timeToPeak = mean + (mean / 2);
    double A = (maxValue - minValue)/2;
    double sigmaSquared = Math.Sqrt(A * (timeToPeak - mean) / (maxVel/gussianSigmaScaleFactor));
    double powerOfexponent = -Math.Pow((time - mean), 2) / (2 * sigmaSquared);
    double output = A * Math.Pow(Math.E, powerOfexponent) + minValue;
    return output;
}
```

## Function: gaussianDerivative

```
public double[] gaussianDerivative(int maxValue, double maxVel, int timeToPerformAction_ms, long time)
{ //http://www.cedar.buffalo.edu/~srihari/CSE555/Normal12.pdf
    double[] output = { 0, 0 };
    double mean = (double)timeToPerformAction_ms / 2;
    double timeToPeak = mean + (mean / 2);
    double A = maxValue;
    double sigmaSquared = Math.Sqrt(A * (timeToPeak - mean) / (maxVel/ gaussianSigmaScaleFactor));
    double powerOfexponent = -Math.Pow(((time-242) - mean), 2) / (2 * sigmaSquared);
    output[0] = A * (((time - 242) - mean) / sigmaSquared) * Math.Pow(Math.E, powerOfexponent);
    output[1] = Math.Abs(output[0]);
    return output; // any higher thank 263 => 180deg/s keep as is
}
```

## Function: motorPositionToRadsDegrees

```
private double motorPositionToRadsDegrees(double Position)
{
    return ((Position - 2048.0) / 4096.0) * 360;
}
```

## Appendix E [Movement Sensor Integration]

### E.1. Hardware

Similar to the WbS, the wireless triggering system used in Chapter 5 Section 5.2.2 is composed of the RN42 Bluetooth module (Microchip technology, AZ, USA), a lithium-ion battery with a boost converter (SparkFun, CO, USA) and an Arduino Pro Mini microcontroller (Arduino, MA, USA) (Figure E1 (b)). The wireless systems use's the Arduino's digital pin 2 to trigger the Vibrasense when appropriate signals are received from the threshold-based controller running on the paired computer (Figure E1).

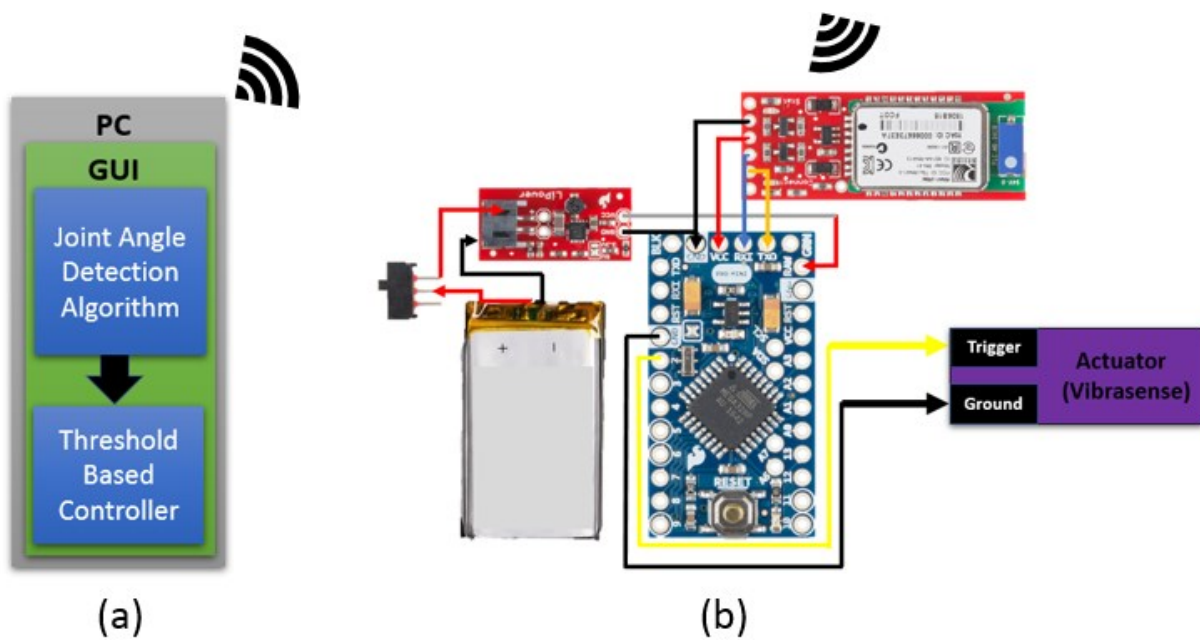


Figure E1: The wireless triggering system using the Arduino to trigger the Vibrasense when signals are received from the threshold-based controller. The system is comprised of an Arduino Pro Mini microcontroller, RN42 Bluetooth module, a lithium-ion battery, and a boost converter.

## E.2. Software

The user interface of the movement sensor was adapted to pair with the triggering module (Figure E2 (a)) and indicate when the system was operational (Figure E2 (b)).

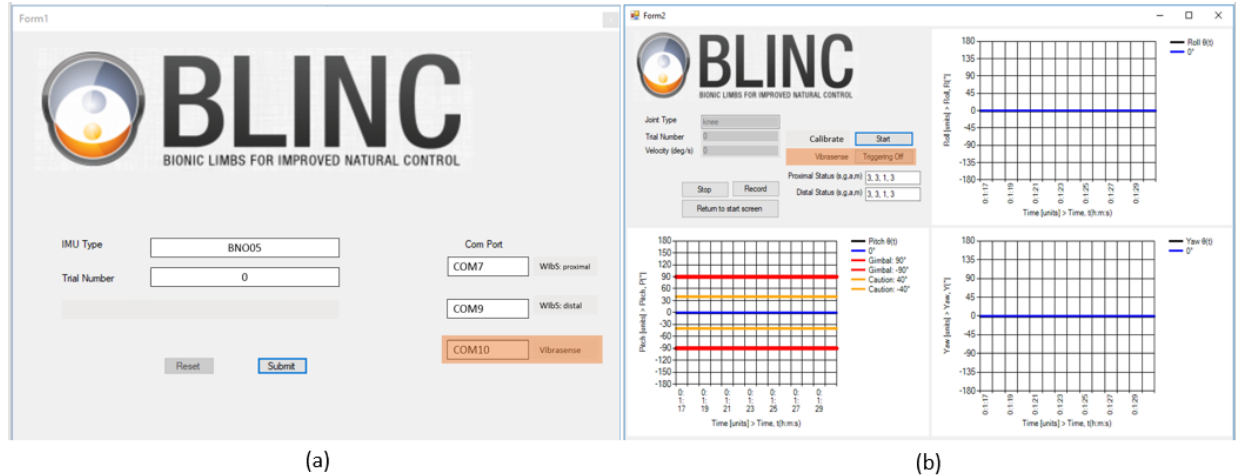


Figure E2: The graphical user interface of the movement sensor was modified to accommodate the trigger system. The entry user interface (a) can establish a connection with the triggering system whereas, the second user interface (b) indicates whether the system is functional, modifications are highlighted in orange.

## E.3. C# Code for Vibratory Actuator Triggering System

### Function: GraphTimer

```
private void GraphTimer(object sender, EventArgs e)
{
    //Generate rotation Matrix
    float[,] R1_UC = Moperator.quaternionsToRotationMatrix(q1);
    float[,] R2_UC = Moperator.quaternionsToRotationMatrix(q2);
    //Use Calibration to determine appropriate orientation
    float[,] R1_C = Moperator.multiplyTwoRotationMatrices(R1_UC, R1_calibrationMatrix);
    float[,] R2_C = Moperator.multiplyTwoRotationMatrices(R2_UC, R2_calibrationMatrix);
    //find relative transformation of IMU1 to IMU2
    float[,] R1_C_Transpose = Moperator.generateTransposeOfRotationMatrix(R1_C);
    float[,] R2_C_Transpose = Moperator.generateTransposeOfRotationMatrix(R2_C);
    float[,] R1to2 = Moperator.multiplyTwoRotationMatrices(R1_C_Transpose, R2_C);
    float[] ZXY = Moperator.extractEulerAnglesFromZXYRotationMatrix(R1to2);
    currentRollAngleValue = ZXY[0];
    currentPitchAngleValue = ZXY[1];
    currentYawAngleValue = ZXY[2];

    float changeInXAxis = Math.Abs(Math.Abs(currentYawAngleValue) - Math.Abs(yawAngledataArray[0]));
    if (vibrasenseIsTurnedON)
    {
        //(float angleThreshold, int delay, float changeInAngle)
        triggerVibrasenseWirelesslyWithArudino((float)threshold, delay, changeInXAxis);
        //*****//or *****
        //(float angleThreshold, int delay, float changeInAngle) -> connect DTR and ground
    }
}
```

```

        triggerVibrasenseWiredFTDI((float)threshold, delay, changeInXAxis);
    }

    //clearing previous series points
    rollAngleSeries.Points.Clear();
    pitchAngleSeries.Points.Clear();
    yawAngleSeries.Points.Clear();
    for (int i = 0; i < MAX_X_VALUES - 1; i++)
    {
        //updating force data series
        rollAngleDataArray[i] = rollAngleDataArray[i + 1];
        rollAngleSeries.Points.AddXY(i, rollAngleDataArray[i]);
        //updating acceleration data series
        pitchAngleDataArray[i] = pitchAngleDataArray[i + 1];
        pitchAngleSeries.Points.AddXY(i, pitchAngleDataArray[i]);
        //updating tilt angle data series
        yawAngleDataArray[i] = yawAngleDataArray[i + 1];
        yawAngleSeries.Points.AddXY(i, yawAngleDataArray[i]);
    }
    //enter current force value to array -> series
    rollAngleDataArray[MAX_X_VALUES - 1] = currentRollAngleValue;
    rollAngleSeries.Points.AddXY(MAX_X_VALUES, currentRollAngleValue);
    //enter current force value to array -> series
    pitchAngleDataArray[MAX_X_VALUES - 1] = currentPitchAngleValue;
    pitchAngleSeries.Points.AddXY(MAX_X_VALUES, currentPitchAngleValue);
    //enter current force value to array -> series
    yawAngleDataArray[MAX_X_VALUES - 1] = currentYawAngleValue;
    yawAngleSeries.Points.AddXY(MAX_X_VALUES, currentYawAngleValue);
    //update graphs with new data
    rollGraph.Update();
    pitchGraph.Update();
    yawGraph.Update();
    if (isLogging)
    {
        //string roll, pitch, yaw, IMU1 status , IMU2 status
        update_csv_data(quaternion_W1.ToString(), quaternion_X1.ToString(), quaternion_Y1.ToString(),
            quaternion_Z1.ToString(), quaternion_W2.ToString(), quaternion_X2.ToString(), quaternion_Y2.ToString(),
            quaternion_Z2.ToString(), XYZ, XZY, YXZ, YZX, ZXY, ZYX, statusArrayIMU1_sgam[0].ToString(),
            statusArrayIMU1_sgam[1].ToString(), statusArrayIMU1_sgam[2].ToString(), statusArrayIMU1_sgam[3].ToString(),
            statusArrayIMU2_sgam[0].ToString(), statusArrayIMU2_sgam[1].ToString(), statusArrayIMU2_sgam[2].ToString(),
            statusArrayIMU2_sgam[3].ToString());
    }
    //reset user information incase trial number has been changed
    setUserInformation();
    //update calibration info
    updateCalibration();
    //update x axis
    updateXAxis(rollGraph, pitchGraph, yawGraph);
    counter++;
}

```

## Function: triggerVibrasenseWithWiredFTDI

```

public void triggerVibrasenseWithWiredFTDI(float angleThreshold, int delay, float changeInAngle)
{ //connect DTR and ground of the FTDI chip

    //Set comport high if angles pass threshold 5 degrees
    try
    {
        if (!Ftdi1.IsOpen)
        {
            ftdiDeviceCount = 0;
            Ftdi1.ResetPort();
            // Determine the number of FTDI devices connected to the machine
            ftStatus = Ftdi1.GetNumberOfDevices(ref ftdiDeviceCount);
            // Check status
            if (ftStatus == FTDI.FT_STATUS.FT_OK)
            {
                string numberOfDevice = ftdiDeviceCount.ToString();
            }
            if (ftdiDeviceCount == 0)
            {
                Console.WriteLine("No FTDI device found!");
            }
            // Allocate storage for device info list
            FTDI.FT_DEVICE_INFO_NODE[] ftdiDeviceList = new
                FTDI.FT_DEVICE_INFO_NODE[ftdiDeviceCount];

```

```

        // Populate our device list
        ftStatus = Ftdi1.GetDeviceList(ftdiDeviceList);
        // Open first device in our list by serial number
        ftStatus = Ftdi1.OpenBySerialNumber(ftdiDeviceList[0].SerialNumber);
        //Ftdi1.GetCOMPort(out comstr);
    }
    if (changeInAngle >= angleThreshold && (vibrasenseTriggered == true))
    {
        Ftdi1.SetDTR(false); //high
        Thread.Sleep(delay);
        Ftdi1.SetDTR(true); //low
        vibrasenseTriggered = false;
    }
    if (changeInAngle < angleThreshold && (vibrasenseTriggered == false))
    {
        Ftdi1.SetDTR(false); //high
        Thread.Sleep(delay);
        Ftdi1.SetDTR(true); //low
        vibrasenseTriggered = true;
    }
}
}
catch
{
    Console.WriteLine("There is an issue");
}
}
}

```

## Function: triggerVibrasenseWirelesslyWithArudino

```

public void triggerVibrasenseWirelesslyWithArudino(float angleThreshold, int delay, float changeInAngle)
{
    byte[] sendBytes = new byte[3];
    if (changeInAngle >= angleThreshold && (vibrasenseTriggered == true))
    {
        //load the buffer
        sendBytes = loadByteBuffer(sendBytes, 1);
        //send buffer
        myport3.Write(sendBytes, 0, 3); // transmit to arduino
        Thread.Sleep(delay);
        vibrasenseTriggered = false;
    }
    else if (changeInAngle < angleThreshold && (vibrasenseTriggered == false))
    {
        //load the buffer
        sendBytes = loadByteBuffer(sendBytes, 1);
        //send buffer
        myport3.Write(sendBytes, 0, 3); // transmit to arduino
        Thread.Sleep(delay);
        vibrasenseTriggered = true;
    }
}
}
}

```